理學博士學位論文

효모에서 Vps34의 인산화를 통한 자가포식 활성 조절

Regulation of autophagic activity by Vps34 phosphorylation in *Saccharomyces cerevisiae*

2023年 2月

서울大學校 大學院

生命科學部

이 용 욱

효모에서 Vps34의 인산화를 통한 자가포식 활성 조절

指導敎授 許 元 琦

이 論文을 理學博士學位論文으로 제출함

2022 年 12 月

서울大學校 大學院

生命科學部

李 鎔 旭

李鎔旭의 理學博士學位論文을 認准함

2022 年 12 月

委 員 長	석 영 재 (인)
副 委 員 長	허 원 기 (인)
委 員	김 현 아 (인)
委 員	강 찬 희 (인)
委 員	정 우 현 (인)

Regulation of autophagic activity by Vps34 phosphorylation in *Saccharomyces cerevisiae*

by

Yongook Lee

Adviser:

Professor Won-Ki Huh, Ph. D.

A Thesis Submitted in Partial Fulfillment of the Requirements for the Degree of Doctor of Philosophy

School of Biological Sciences

Seoul National University

Date Approved

Dec 26/2022

Yeong-Jae Seok _____

Won-Ki Huh _____

Joy Kim _____

Chanhee Kang _____

Woo-Hyun Chung _____

ABSTRACT

Regulation of autophagic activity by Vps34 phosphorylation in *Saccharomyces cerevisiae*

Yongook Lee
School of Biological Sciences
The Graduate School
Seoul National University

Macroautophagy/autophagy is a key catabolic pathway in which double-membrane autophagosomes sequester various substrates destined for degradation, allowing cells to maintain homeostasis and survive under stressful conditions. Several autophagy-related (Atg) proteins are recruited to the phagophore assembly site (PAS) and orchestrate to manage autophagosome biogenesis. Vps34 is a class III phosphatidylinositol 3-kinase, and Atg14-containing Vps34 complex I plays essential roles in the initial steps of autophagy induction. However, the regulatory mechanisms of yeast Vps34 complex I are still poorly understood. Here, I report that Atg1-dependent phosphorylation of Vps34 is required for robust autophagy activity in *Saccharomyces cerevisiae*. Following nitrogen starvation, Vps34 in complex I is selectively phosphorylated on multiple serine/threonine residues in its helical domain. This phosphorylation promotes full autophagy

activation and cell survival. In vivo phosphorylation of Vps34 was completely disrupted in the absence of Atg1 or its kinase activity, and Atg1 directly phosphorylated Vps34 in vitro, regardless of its complex association type. I also revealed that localization of Vps34 complex I to the PAS provides molecular basis for complex I-specific phosphorylation. This phosphorylation is required for the normal dynamics of Atg18 and Atg8 at the PAS. Together, this study reveals a novel regulatory mechanism of yeast Vps34 complex I and provides new insights into the Atg1-dependent dynamic regulation of the PAS.

Key words: Vps34, Atg1, autophagy, nitrogen starvation, *Saccharomyces cerevisiae*, Atg8, Atg18

Student Number: 2016-24695

CONTENTS

LIST OF FIGURES

LIST OF TABLES

ABBREVIATIONS

ATG	Autophagy-related
BARA	Chronological lifespan
CCD	Ribosomal DNA
CPY	Extrachromosomal ribosomal DNA circles
GFP	Non-transcribed spacer
IP-MS	immunoprecipitation followed by tandem mass spectrometry
NTD	the N-terminal domain
PAS	phagophore assembly site
PtdIns	phosphatidylinositol
PtdIns3P	phosphatidylinositol 3-phosphate
PtdIns3K	phosphatidylinositol 3-kinase
SUR	Structurally uncharacterized region
$Vps34^{KD}$	$Vps34^{D731N}$

1. INTRODUCTION

1.1 Autophagy: Self-eating process for self-renewal

Eukaryotic cells are forced to adopt a variety of strategies to cope with constantly fluctuating environmental conditions. One of those strategies that cells can employ is 'to eliminate' something to recycle fundamental materials and remove cytotoxic constituents. Macroautophagy, hereafter referred to as autophagy, is a major cellular catabolic process that can degrade a wide range of cellular components such as dysfunctional proteins or organelles, thereby recycling multiple building blocks for macromolecules and getting rid of harmful components (Feng et al., 2014; Reggiori and Klionsky, 2013; Yang and Klionsky, 2009). In response to autophagy-inducing stimuli such as nutrient starvation, a double membrane vesicle called autophagosome sequesters autophagic cargo destined for degradation, and then the cargo-containing autophagosome finally fuses with the vacuole or lysosomes for degradation (Nishimura and Tooze, 2020). Depending on its cargo selectivity, autophagy can be divided into two types, namely bulk and selective autophagy (Figure 1). In bulk autophagy, the autophagosome non-selectively encapsulates bulk cytoplasm while selective autophagy can exclusively eliminate specific cargoes including mitochondria (mitophagy), peroxisome (pexophagy), and endoplasmic reticulum (ER-phagy) (Farre and Subramani, 2016). Accumulating evidence highlights the fundamental importance of autophagy in human pathophysiology. Defective autophagy is closely associated not only with various human diseases including neurodegenerative disease, inflammation, and cancer but also with aging and

longevity (Deng et al., 2022; Dou et al., 2022; Ichimiya et al., 2020; Ruocco et al., 2016).

1.2 Autophagy process from a molecular perspective

Autophagy occurs in five major steps: initiation, nucleation, elongation, maturation, and fusion with the vacuole (Figure 2). When autophagy begins, a cup-shaped membrane called the phagophore is formed at the perivacuolar punctate structure known as phagophore assembly site (PAS). At the PAS, autophagy-related (Atg) proteins orchestrate expansion of the phagophore to complete mature autophagosome (Ktistakis and Tooze, 2016; Mizushima et al., 2011; Rubinsztein et al., 2012). The autophagosome then finally engulfs desirable cargo and fuses with the vacuole. About 40 *ATG* genes have been identified so far, and among them, Atg proteins that play an essential role in all known types of autophagy are called the core autophagy machinery. These core Atg proteins can be classified into five multifunctional groups that are recruited to the PAS in a hierarchical manner: Atg1 initiating complex, Atg9, PtdIns3K complex, Atg2-Atg18 complex, and Ubiquitin-like conjugating system (Ariosa and Klionsky, 2016; Licheva et al., 2022; Suzuki et al., 2017).

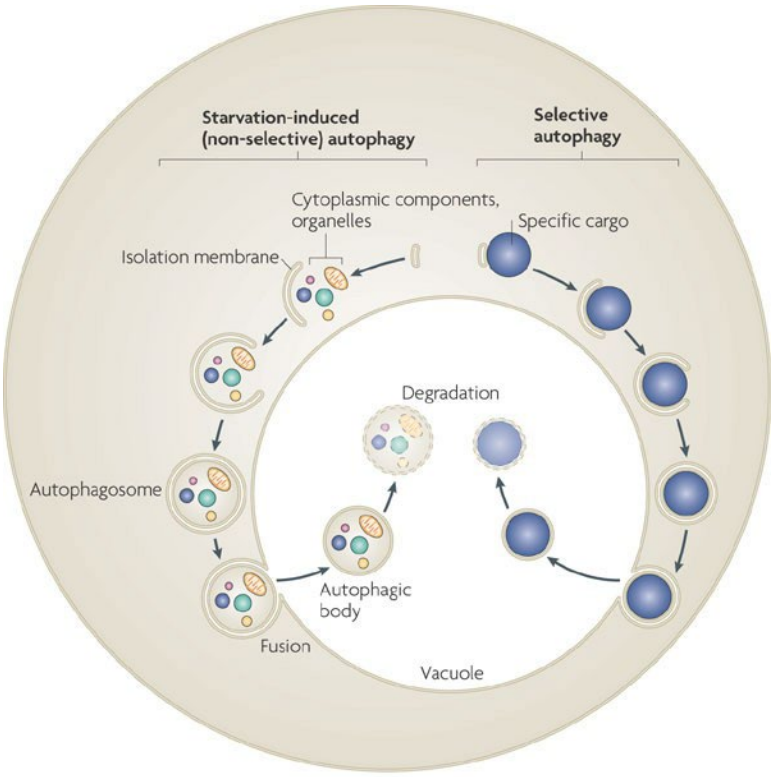

(Nakatogawa et al., 2009)

Figure 1. Two types of autophagy.

Autophagy can be divided into two types: Non-selective (bulk) autophagy and selective autophagy. In bulk autophagy, the isolation membrane (phagophore) non-selectively sequesters bulk cytoplasm including protein aggregates and organelles. The sequestered cargoes are released into the lumen of the vacuole, where the cargoes are degraded. In selective autophagy, the phagophore engulfs autophagy substrates with specific interaction between desired autophagic substrates and various autophagic receptor proteins, thereby degrading specific cellular constituents as required.

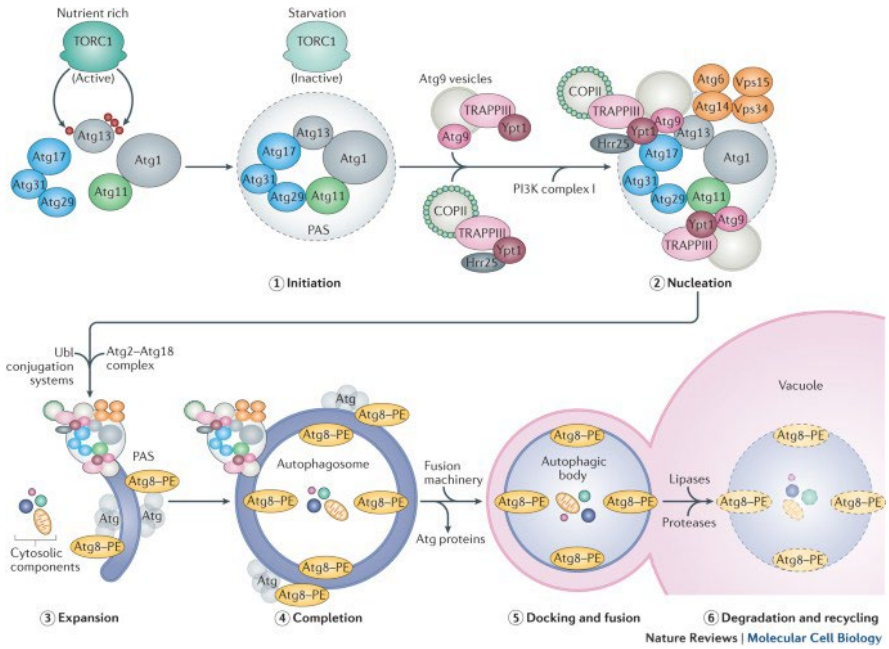

(Farre and Subramani, 2016)

Figure 2. Autophagy process and Atg machinery.

Target of rapamycin complex 1 (TORC1) inhibits autophagy under nutrient-rich condition by phosphorylating Atg13. Autophagy is initiated when TORC1 is inhibited in response to nutrient starvation and this allows Atg13 dephosphorylation and Atg1 kinase complex assembly. The assembled Atg1 complex promotes the Atg proteins nucleation by recruiting downstream Atg proteins including PtdIns3K complex to the phagophore assembly site (PAS). PtdIns3K complex then synthesize PtdIns3P at the PAS, which promotes the expansion of phagophore and completion of autophagosome. Completed autophagosome finally fuses with the vacuole, inside which the sequestered substrates are degraded.

1.2.1 Autophagy initiation: Atg1/ULK1 kinase complex

Atg1/ULK1 kinase is the sole kinase among the Atg machinery and is an essential regulator of autophagy that acts most upstream of autophagy signaling (Figure 3) (Noda and Fujioka, 2015). Under growing conditions, Atg13 is hyperphosphorylated by the target of rapamycin complex 1 (TORC1), which inhibits autophagy initiation. Upon starvation, Atg13 is dephosphorylated in response to the inactivation of the TORC1 and this allows the formation of the heteropentameric Atg1 complex which consists of Atg1, Atg13, Atg17, Atg29, and Atg31 (Fujioka et al., 2014; Kamada et al., 2010). Consequently, these pentameric Atg1 complexes bind each other to form an inter-complex, supramolecular structure that serves as a scaffold for the PAS assembly, and then Atg1 is fully activated (Yamamoto et al., 2016). This higher-order PAS assembly has been shown to be crucial for the recruitment of nearly all downstream Atg effectors including Atg9, PtdIns3K complex I, and Atg18 (Jao et al., 2013; Suzuki et al., 2007; Suzuki et al., 2015). Active Atg1 kinase promotes the subsequent steps of autophagy by phosphorylating several Atg proteins, such as Atg4, Atg9, and Atg13, at the PAS (Hu et al., 2019; Kira et al., 2021; Papinski et al., 2014; Sanchez-Wandelmer et al., 2017).

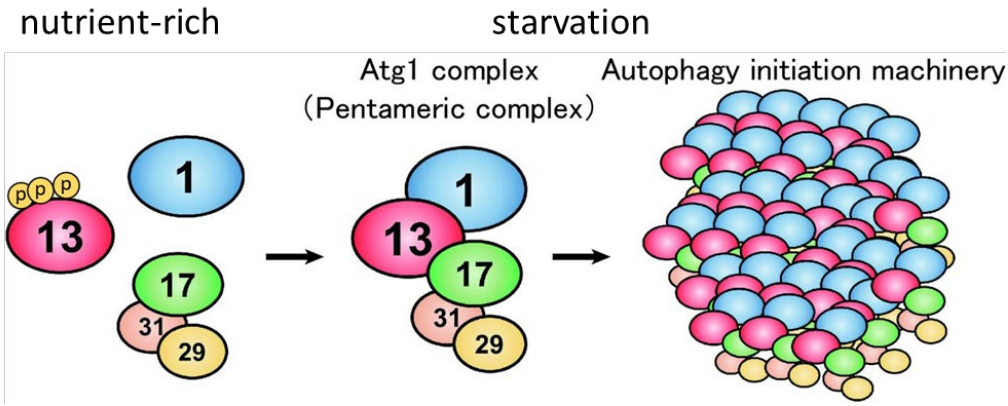

(Yamamoto *et al.*, 2016)

Figure 3. Supramolecular assembly of Atg1 kinase complex.

Under nutrient-rich condition, Atg13 is phosphorylated by TORC1. Atg13 dephosphorylation under starvation allows the assembly of pentameric Atg1 complex, which consists of Atg1, Atg13, Atg17, Atg29, and Atg31. The pentameric Atg1 complexes further bind each other, forming supramolecular structure which serves as an interaction platform to recruits downstream Atg proteins and then Atg1 is fully activated. Active Atg1 kinase phosphorylates multiple substrates such as Atg4 and Atg9 at the PAS.

1.2.2 PAS nucleation: Atg9 vesicle

Atg9 is the only integral membrane protein among the core Atg machinery. Atg9 is contained in a cytoplasmic vesicle called Atg9 vesicle (Noda, 2021). While most of the core Atg proteins localize at the PAS, Atg9 vesicle cycles between the PAS and the peripheral sites which are adjacent to mitochondria. This translocation provides membrane lipids for initial phagophore expansion (Mari et al., 2010; Yamamoto et al., 2012). In addition to its role as a membrane source for phagophore expansion, it has been recently described the role of Atg9 as a lipid scramblase, which transfer phospholipids delivered by Atg2 from cytoplasmic to the luminal leaflet of expanding phagophore (Matoba et al., 2020). Atg9 vesicles are recruited to the PAS through direct interaction with the HORMA domain of Atg13, and Atg9 recruitment to the PAS has been reported to be crucial for the subsequent recruitment of downstream Atg proteins including Vps34 complex and Atg18 (Jao *et al.*, 2013; Papinski *et al.*, 2014; Suzuki *et al.*, 2015).

1.2.3 PAS nucleation: Autophagy-specific PtdIns3K complex I

Vps34 is the catalytic subunit of the phosphatidylinositol 3-kinase (PtdIns3K) complex which is evolutionarily conserved from yeast to humans (Reidick et al., 2017). Vps34 phosphorylates phosphatidylinositol (PtdIns) to produce phosphatidylinositol 3-phosphate (PtdIns3P), an essential lipid for autophagy and endomembrane trafficking system (Ohashi et al., 2019; Reidick *et al.*, 2017). In *Saccharomyces cerevisiae*, there are two major PtdIns3K complexes with distinct

functions: Complex I and complex II (Figure 4) (Kihara et al., 2001). Vps34 complex I is crucial for autophagy induction whereas complex II is required for endosomal trafficking and vacuolar protein sorting (Kihara *et al.*, 2001; Ohashi *et al.*, 2019; Reidick *et al.*, 2017). Both complexes contain Vps15, Vps34, and Vps30 as the common subunits. Atg14 is a specific subunit of complex I that guides the complex I to the PAS, while complex II contains Vps38 instead of Atg14, which is essential for its endosomal targeting (Obara et al., 2006). Atg38 has been identified as a fifth subunit of complex I which stabilize the complex by holding the Vps15-Vps34 and the Atg14-Vps34 subcomplexes together (Araki et al., 2013). It has been shown that PtdIns3P generated by Vps34 complex I at the PAS are crucial for the recruitment of Atg18 and Atg21, which further recruit the autophagy-related E3 complex Atg12-Atg5-Atg16 (Harada et al., 2019; Obara et al., 2008).

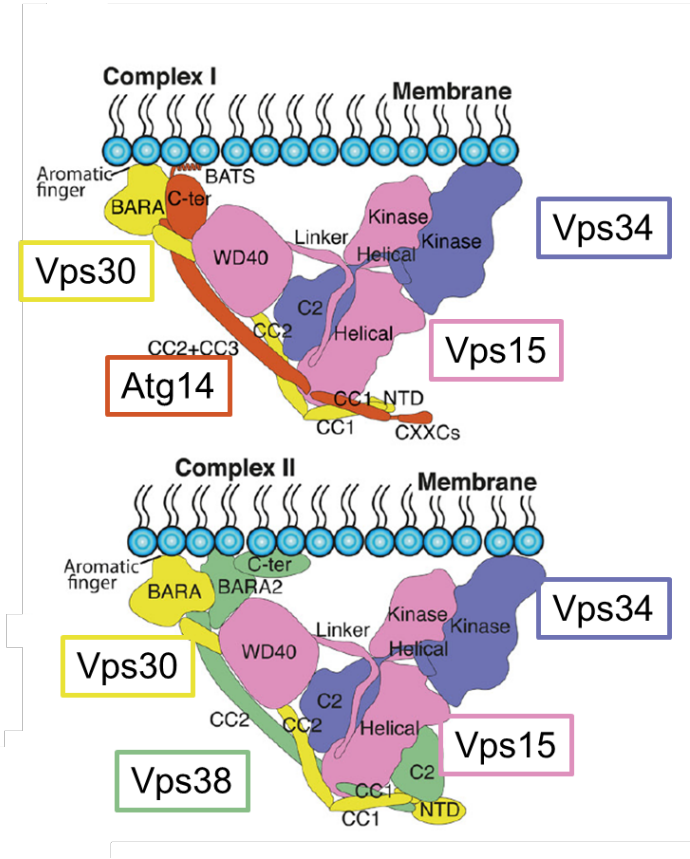

(Ohashi *et al.*, 2019)

Figure 4. The two major Vps34 complexes in yeast.

Vps34 forms two major complexes in cells, namely complex I (CI) and complex II (CII). Vps34 CI is essential for autophagy and CII is required for vacuolar protein sorting pathway. These two complex shares the common subunits Vps34, Vps15, and Vps30. Complex I specifically contains Atg14 which determines the PAS localization of Vps34 CI, while CII has Vps38 as its specific subunits. Both complexes form V- or Y-shaped structure with two arms; a catalytic arm with the kinase domain of Vps34 and an adaptor arm which consist of Vps30 and Atg14 for CI or Vps38 for CII.

1.2.4 Phagophore expansion: Atg2-Atg18 complex

Although it has been described that Atg9 vesicles provide membrane lipids for initial phagophore expansion, the amount of phospholipids supplied by Atg9 vesicles was thought to be insufficient to cover the rate of autophagosome biogenesis (Noda, 2021). Recent studies have revealed that Atg2, the largest core Atg protein, localizes at the contact site between the ER-exit site (ERES) and expanding edge of the phagophore, connecting two organelles physically and providing phospholipids required for the autophagosomal membrane expansion (Kotani et al., 2018; Osawa et al., 2019). Atg2 forms a protein complex with Atg18, a phosphoinositide-binding protein that belongs to the PROPPIN family (β-propellers that binds polyphosphoinositides) (Dove et al., 2009). Atg2-Atg18 complex is targeted to the PAS in a manner dependent on PtdIns3P binding of Atg18, and Atg9 is also required for the recruitment of this complex to the PAS (Gomez-Sanchez et al., 2018).

1.2.5 Phagophore expansion: Two ubiquitin-like conjugation systems

The most downstream groups comprising the autophagy core machinery are the two ubiquitin-like conjugation systems: The Atg12-conjugation system and the Atg8-conjugation system. Atg12 and Atg8 are conjugated to their specific target sites by mechanisms similar to the ubiquitination of proteins (Nakatogawa, 2013). Atg7 and Atg10 serve as E1 and E2 enzymes for Atg12, respectively, and Atg12 is finally conjugated to Atg5. Atg12-Atg5 conjugate further binds with Atg16 which is required for the PAS targeting of the Atg12-Atg5-Atg16 complex (Fujioka et al.,

2010). This protein complex is definitely required for the conjugation of Atg8 to the phosphatidylethanolamine (PE) of the expanding phagophore (Hanada et al., 2007). Atg8 conjugation to PE is essential for autophagosome biogenesis and the amount of Atg8 has been described to determine the size of autophagosome (Backues et al., 2012). On the other hand, a previous study has revealed that the dissociation of Atg proteins from completed autophagosomes is important for autophagosome-vacuole fusion (Cebollero et al., 2012). A protease Atg4 is involved in deconjugation of Atg8 from closed autophagosome by constitutively cleaving Atg8 from PE.

1.3 Autophagy regulation by Atg1-dependent phosphorylation

As mentioned above, Atg1 is the sole kinase among the core Atg machinery, and the pentameric Atg1 complex associates into the higher-order oligomeric structure to form an inter-complex assembly which is the molecular basis for the activation of Atg1. This leads to the autophosphorylation of T226 and S230 of Atg1, which are required for its kinase activity (Yeh et al., 2010). Activated Atg1 phosphorylates multiple substrates at the PAS. At the early stage of autophagy induction, Atg1 has been reported to phosphorylate multiple serine residues of Atg9 (Papinski *et al.*, 2014). This phosphorylation establishes the interaction between Atg9 and Atg18, which allows Atg18 to be targeted to the PAS. Atg1 also phosphorylates its regulatory subunit Atg13, enabling the Atg1 complex dissociation from the PAS (Schreiber et al., 2021). Atg4 is another Atg1 target, and Atg1-mediated phosphorylation of Atg4 restricts the protease activity of Atg4 which downregulate autophagic activity.

The mammalian PtdIns3K complex I has been reported to be regulated by extensive phosphorylation on its subunits by various kinases such as Ulk1 (Egan et al., 2015; Park et al., 2016; Park et al., 2018; Russell et al., 2013), CDK1 (Furuya et al., 2010), mTORC1 (Yuan et al., 2013), and AMPK (Kim et al., 2013; Zhang et al., 2016). Moreover, ULK1, the mammalian homolog of Atg1, has been shown to directly phosphorylate Vps34 (Egan *et al.*, 2015), the implications of which are not yet characterized. ULK1 also ATG14L and Beclin 1, mammalian homologs of Atg14 and Vps30, respectively, which promotes the autophagy-specific PtdIns3KCI activity (Park *et al.*, 2016; Park *et al.*, 2018).

1.4 Methods for monitoring autophagic activity: GFP-processing assay and Pho8Δ60 assay

Monitoring the delivery of GFP-Atg8 to the vacuole is one of the most commonly used assays to monitor bulk autophagy (Figure 5) (Nair et al., 2011). Since Atg8 is conjugated to PE of both outer and inner leaflets of the autophagosome, GFP-Atg8 fusion molecules are delivered into the vacuole upon autophagy induction where the fusion molecules are degraded by vacuolar hydrolase, leaving the protease-resistant free-GFP moiety which can be assessed by fluorescence microscopy or western blot analysis. This protease-resistant property of GFP moiety is also useful to monitor other types of autophagy. The detection of GFP accumulated in the vacuole can be applied to analyze the degradation of other proteins of interest tagged with GFP, which enables semi-quantitative analysis of selective autophagy activity (e.g. Om45-

GFP; mitophagy marker, Pex11-GFP; pexophagy marker) (Kanki et al., 2009; Motley et al., 2012).

Pho8Δ60 assay is another useful method to quantitatively measure bulk autophagic flux (Noda and Klionsky, 2008). An alkaline phosphatase (ALP) Pho8 is synthesized as a catalytically inactive precursor, which can be activated inside the vacuole. The deletion of N-terminal 60 amino acids of Pho8 protein leaves the protein in the cytoplasm and the cytoplasmic Pho8Δ60 are transported to the vacuole in a manner totally dependent on autophagy activity and the mutant proteins are activated inside the vacuole. Therefore, assessing the activity of Pho8Δ60 can be used as a sensitive readout of non-selective autophagy activity.

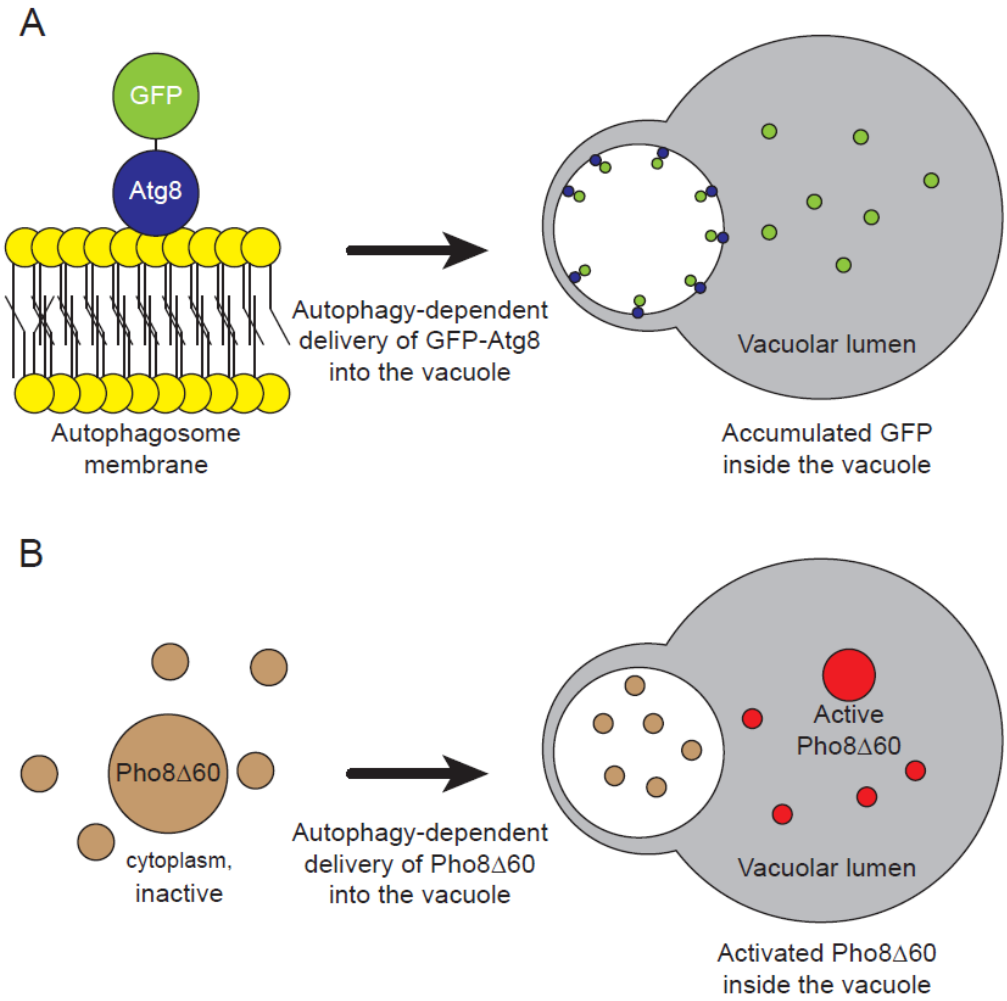
A
GFP
Atg8
Autophagosome membrane
Autophagy-dependent delivery of GFP-Atg8 into the vacuole
Vacuolar lumen
Accumulated GFP inside the vacuole
B
Pho8Δ60
cytoplasm, inactive
Autophagy-dependent delivery of Pho8Δ60 into the vacuole
Active Pho8Δ60
Vacuolar lumen
Activated Pho8Δ60 inside the vacuole

Figure 5. Assays to monitor autophagic activity.

(A) GFP-Atg8 processing assay. Since Atg8 is conjugated to PE of both outer and inner leaflets of the autophagosome, GFP-Atg8 fusion molecules are delivered into the vacuole upon autophagy induction where the fusion molecules are degraded by vacuolar hydrolase, leaving the protease-resistant free-GFP moiety which can be assessed by fluorescence microscopy or western blot analysis. (B) Pho8Δ60 assay. An alkaline phosphatase (ALP) Pho8 is synthesized as a catalytically inactive precursor, which can be activated inside the vacuole. The deletion of N-terminal 60 amino acids of Pho8 protein leaves the protein in the cytoplasm and the cytoplasmic Pho8Δ60 are transported to the vacuole in a manner dependent on autophagy activity and the mutant proteins are activated inside the vacuole. Thus the activity of Pho8Δ60 can be used as a readout of autophagy activity.

1.4 Aims of this study

As the sole kinase of the core Atg proteins, Atg1 phosphorylates a wide variety of autophagy proteins and this phosphorylation spatially and temporally modulates autophagic activity at multiple levels. Extensive studies regarding autophagy regulation via Atg1-mediated phosphorylation have broadened our understanding of the molecular basis for autophagy regulation. However, there still remain many unanswered questions. Moreover, although various phosphoregulation mechanisms of mammalian PtdIns3K complex I have been reported thus far, the physiological implications of VPS34 phosphorylation by ULK1 remain to be unveiled. In addition, our knowledge about the regulation of yeast Vps34 complex I is very limited.

Here, I show that Vps34 phosphorylation by Atg1 kinase is required for functional autophagy activity in *S. cerevisiae*. Following nitrogen starvation, the helical domain of Vps34 in autophagy-specific complex I is selectively phosphorylated, whereas Vps34 in Vps38-containing complex II is not. I discovered that this phosphorylation is necessary for robust autophagy activation and cell viability under nitrogen starvation. In vivo phosphorylation of Vps34 is entirely dependent on the kinase activity of Atg1, and Atg1 can phosphorylate part of the helical domain of Vps34 in vitro, irrespective of its associated complex type. I also provide evidence that the PAS localization of Vps34 complex I is one of the molecular basis that allows the Vps34 complex I-specific phosphorylation. This Atg1-dependent phosphorylation of Vps34 is required for the normal dynamics of downstream Atg proteins including Atg18 and Atg8 at the PAS. Collectively, these findings reveal a novel regulation

mechanism of autophagy via phosphorylation of Vps34 complex I and provide new insights into the Atg1-dependent regulation of the PAS dynamics.

2. MATERIALS AND METHODS

2.1 Yeast strains, plasmids, and growth media

Table 1 lists the *S. cerevisiae* strains and plasmids used in this study. Strains were constructed by PCR-based epitope tagging method or PCR-based gene deletion method (Wach, 1996), or plasmid integration using yeast integrative vectors (Gnugge et al., 2016). Yeast cells were grown in YPD medium (1% yeast extract, 2% peptone, and 2% glucose) or synthetic complete (SC) medium lacking amino acids as required (Sherman, 2002). For nitrogen starvation, yeast cells were grown to mid-log phase in YPD or SC medium and then washed with distilled water. The washed cells were incubated in nitrogen starvation medium (SD-N; 0.17% yeast nitrogen base without amino acids and ammonium sulfate, 2% glucose). For ammonium sulfate replenishment, $(NH_4)_2SO_4$ was directly added to the culture medium to a final concentration of 0.5% w/v. For amino acid replenishment, a 10× amino acid mixture for SC medium (Sherman, 2002) was directly added to the culture to a final concentration of 1×. For solid media, 2% agar was added. All cultures were incubated at 30°C.

The oligonucleotide primers used in this study are listed in Table 2. For the construction of pRG205-VPS34-TAP vector, the PCR product of *VPS34p-VPS34-TAP* sequence was amplified using the genomic DNA of *VPS34-TAP* strain as a template and then ligated into the *Sac*I/*Kpn*I-digested pRG205 (Gnugge et al., 2016) vector by the sequence- and ligation-independent cloning (SLIC) method (Jeong et

al., 2012). The *VPS34* promoter contains the upstream sequence (~1000 bp) of the *VPS34* start codon. For the construction of pRG205-VPS34 vector, the PCR product of *VPS34p-VPS34* sequence was amplified using the pRG205-VPS34-TAP vector as a template and then ligated into the *Sac*I/*Kpn*I-digested pRG205 (Gnugge et al., 2016) vector by the SLIC method (Jeong et al., 2012). Vps34 point mutations were introduced by the SLIC method (Jeong et al., 2012).

2.2 Western blot analysis

Yeast cells were harvested by centrifugation and washed with PBS. The washed cells were then resuspended in lysis buffer (50 mM Tris-HCl, pH 7.5, 150 mM NaCl, 0.15% NP-40, 1 mM EDTA) with protease inhibitors (10 mM PMSF, 1 mM pepstatin, 1 mM leupeptin, 1 mM benzamidine) and phosphatase inhibitors (10 mM b-glycerol phosphate, 1 mM sodium orthovanadate, 10 mM sodium fluoride, 10 mM sodium pyrophosphate) and then lysed with bead beating. Cell extracts were cleared by centrifugation at 14000 rpm for 10 min at 4ºC and the supernatant was added with 6× SDS sample buffer (375 mM Tris-HCl, pH 6.8, 9% SDS, 50 % glycerol, 9% b-mercaptoethanol, 0.03% bromophenol blue) followed by boiling at 75□C for 10 min. SDS-PAGE and western blot were performed according to standard methods using a HRP-conjugated anti-mouse IgG antibody (A9044, Sigma-Aldrich), a HRP-conjugated anti-rabbit IgG antibody (A6154, Sigma-Aldrich), a HRP-conjugated anti-GFP antibody (Rockland, 600-103-215), a HRP-conjugated anti-MYC antibody (Santa Cruz Biotechnology, SC-40 HRP), and a rabbit anti-hexokinase antibody (United States Biological, H2035-03).

2.3 Lambda phosphatase treatment

Lambda phosphatase (NEB, P0753S) was directly added to cell extracts with or without phosphatase inhibitors (1 μM sodium orthovanadate, 10 mM sodium pyrophosphate, 10 mM β-glycerol phosphate, 10 mM sodium fluoride) following manufacturer's instructions.

2.4 Co-IP assay

Cells grown in 50 ml of YPD medium to OD_{600} = 1.0 (SD-N 0 h) were shifted to SD-N medium for the indicated hours. For Atg38-Myc-expressing cells, cells grown in 150 ml of YPD (OD_{600} = 1.0) were used. Cell extracts were prepared as described above. 20 μl of IgG-Sepharose beads (GE Healthcare, 17-0969-01) were added to the lysates and incubated for overnight at 4ºC. Cells expressing no TAP-tagged proteins were used as a negative control. SDS-PAGE and western blot analyses were performed according to standard methods with an HRP-conjugated anti-MYC antibody (Santa Cruz Biotechnology, SC-40 HRP) and an HRP-conjugated anti-mouse IgG antibody (A9044, Sigma-Aldrich).

2.5 Mass spectrometry

Cells were grown in 1 L of SC medium to OD600 = 1.5 and incubated in SD-N medium for 6 h. Harvested cells were lysed as previously described 1. Cell extracts were incubated with 50 μl of IgG-Sepharose beads (GE healthcare, 17-0969-01) for overnight at 4ºC. The eluate was separated by SDS-PAGE with 6% separating gel, and proteins were visualized by Coomassie blue staining. Mass spectrometry analysis was performed by the Proteomics Core Facility at the School of Biological Sciences in Seoul National University, which is supported by the Center for RNA Research, Institute for Basic Science.

2.6 Autophagy analysis

The alkaline phosphatase activity of Pho8Δ60 was measured as previously described (Noda and Klionsky, 2008). The GFP-processing assay for GFP-Atg8, Pex11-GFP, and Om45-GFP was performed as described previously (Kim et al., 2021). Briefly, cells were grown in 10 ml of YPD medium to OD600 = 1.0 and incubated in SD-N medium for 20 h. Harvested cells were lysed as previously described (Shin and Huh, 2011). SDS-PAGE and immunoblotting were conducted using standard methods with an HRP-conjugated anti-GFP antibody (Rockland, 600-103-215), a rabbit anti-hexokinase antibody (United States Biological, H2035-03) and an HRP-conjugated anti-rabbit IgG antibody (Sigma-Aldrich, A6154).

2.7 Cell viability assay

Yeast cells were streaked onto fresh YPD agar plates for 1 day, and a single colony was grown in liquid YPD medium overnight. The overnight culture was then diluted to one-hundredth in YPD medium and grown to OD_{600} = 1.0. Cells were then shifted to SD-N medium for the indicated days. Cell viability was determined by counting colony forming units (CFUs) as previously described (Noda, 2008). For the quantification of the survival integral values, the areas under the viability curves were measured as previously described (Jung et al., 2015). Determination of cell viability by Phloxine B was performed as previously described (Medeiros et al., 2018). Cells were grown as described above and then stained with 2 μg/ml Phloxine B (sigma aldrich, P2759), followed by incubation at 30°C for 15 min. Fluorescence was examined by BD FACS Canto II flow cytometer (Becton Dickinson). The population of cells observed in a single peak with low-fluorescence (SD-N 0 day) was considered as live population. Cell population in the peaks with stronger fluorescence than day 0 sample was considered as dead population.

2.8 CPY sorting assay

CPY sorting assay was performed as previously described with some modifications 3. 10 OD600 units of cells grown in YPD medium to mid-log phase were resuspended in 1 ml of YPD medium and incubated for 2 h. Harvested cells were lysed as previously described 1. Crude lysates and supernatant media were subjected to trichloroacetic acid (TCA) precipitation. Intracellular fraction (I)

corresponding to 0.3 OD600 unit and extracellular fraction (E) corresponding to 1.5 OD600 unit were analyzed by western blotting using an anti-CPY antibody (Rockland, 200-401-135), a rabbit anti-hexokinase antibody (United States Biological, H2035-03), and an HRP-conjugated anti-rabbit IgG antibody (Sigma-Aldrich, A6154).

2.9 In vitro Vps34 activity assay

An in vitro PtdIns3K activity assay was performed as previously described with some modifications (Park *et al.*, 2016). Briefly, cells were grown in 200 ml of YPD medium to OD_{600} = 1.5 and then incubated in SD-N medium for 6 h. Cells were then disrupted as described previously (Shin and Huh, 2011). Atg14-containing Vps34 complex I was acquired by immunoprecipitation of Atg14-TAP using 20 μl of IgG-Sepharose beads (GE Healthcare, 17-0969-01). The obtained immunocomplex was washed three times with lysis buffer and additional twice with 2.5× substrate buffer (75 mM Tris-Cl, pH 7.5, 125 mM NaCl, 12.5 mM $MnCl_2$). The washed beads were then incubated with 1× substrate buffer containing 250 μg/ml phosphatidylinositol (Sigma-Aldrich, 79403) at 25°C. The PtdIns3K reactions were started by adding ATP (20 μM) and incubated for the indicated times with gentle agitation at 25°C. The reactions were then spotted on nitrocellulose membranes. The resulting membrane was blocked with 3% BSA (SERVA Electrophoresis, 11945.04) dissolved in PBS for 1 h and incubated with 0.5 μg/ml PI(3)P grip (Echelon Biosciences, G-0302) dissolved in PBS containing 3% BSA and 0.1% Tween 20 (Thermo Scientific,

J20605) overnight at 4°C. After intensive washing, the amount of PI(3)P grip on the membrane was analyzed by immunoblotting using an HRP-conjugated anti-GST antibody (Santa Cruz Biotechnology, SC-138 HRP

2.10 In vitro Atg1 kinase assay

An in vitro Atg1 kinase assay was performed as previously described with some modifications (Kira *et al.*, 2021). For the substrates, *atg1*Δ cells expressing Vps34^{D731N}-Myc (Vps34^{KD}-Myc) or Atg13-TAP were grown in 50 ml of YPD medium to OD_{600} ~ 1.0 and then incubated in SD-N medium for 6 h or 1 h, respectively. For the purification of Atg14-TAP- or Vps38-TAP-immunocomplex, 200 ml or 70 ml culture of YPD medium (OD_{600} ~ 1.0) were used, respectively. Cells were then disrupted as previously described (Shin and Huh, 2011). For isolation of Vps34^{KD}-Myc, an anti-Myc antibody (SC-40, Santa Cruz) was directly added to the lysates and incubated for 2 h at 4°C. 20 μl of Protein A-Sepharose (17-5138-01, GE healthcare) was then added and incubated for 2 h at 4°C. TAP-tagged substrates were immunoisolated using 20 μl of IgG-Sepharose beads (GE healthcare, 17-0969-01). The beads were then washed three times with lysis buffer and two times with 1× kinase buffer (50 mM Tris-Cl, pH 7.5, 75 mM NaCl, 10 mM $MgCl_2$). The washed beads were used as substrates for the Atg1 kinase assay. For purification of Atg1, cells expressing Atg1-HA or Atg1^{D211A}-HA were grown in 2 L of SC medium to OD_{600} ~ 1.5. Cells were disrupted as previously described (Shin and Huh, 2011), and cell lysates were incubated with 25 μl of an anti-HA antibody (Santa Cruz

Biotechnology, SC-7392) for 4 h at 4°C. 160 μl of Protein A-Sepharose beads (GE Healthcare, 17-5138-01) were added to the extracts and incubated overnight at 4°C. The beads were washed three times with lysis buffer and two times with 1× kinase buffer, followed by elution of the bound proteins using HA peptide (Sigma-Aldrich, I2149, 1 mg/ml) dissolved in 1× kinase buffer. The eluted proteins were added to the substrate-bound beads and reactions were performed at 30°C in the presence of 500 μM ATP. Then, the incubated beads were washed twice with ice-cooled 1× kinase buffer, and SDS-PAGE sample buffer was added. The beads were boiled at 75°C for 10 min. Phosphorylation of Atg13-TAP and Vps34-Myc was detected by western blotting using an HRP-conjugated anti-mouse IgG antibody (Sigma-Aldrich, A9044) or an HRP-conjugated anti-MYC antibody (Santa Cruz Biotechnology, SC-40 HRP), respectively.

2.11 Fluorescence microscopy

To analyze the PAS recruitment of Atg14 and Atg18 in *vps34* mutants, live cell imaging was performed using a DeltaVision system (Applied Precision) with a 100×/1.512 NA oil immersion objective lens. Cells were placed on the 8-well glass-bottom dish (Thermo Scientific, 177402) pretreated with concanavalin A (5 μg/ml) (Sigma-Aldrich, C7275) for cell immobilization. Images were acquired by collecting a z-stack of 16 pictures with 0.3 μm-distanced focal planes. The acquired images were deconvoluted and projected into one image using the softWorx software

(Applied Precision) as previously described 70. Then representative z-projected images were shown.

Live cell imaging except for Figure 25 and 29 was performed using a Nikon Eclipse E1 microscope with a Plan Fluor 100×/1.30 NA oil immersion objective lens. 96-well glass-bottomed microplates (Matrical Bioscience, MGB096) were pretreated with concanavalin A (5 μg/ml) (Sigma-Aldrich, C7275) for cell adhesion to the plates. For time-lapse microscopy, cells were placed on concanavalin A-treated 96-well glass-bottomed microplates (Matrical Bioscience, MGB096) and imaged every 45 seconds for 40 minutes at 26ºC. Unless denoted, images were acquired from a single z-section.

2.12 Statistical analysis

The values plotted are the means of three independent experiments, and the error bars indicate the standard deviations. Statistical analysis was performed by a two-tailed Student's *t*-test (***$p < 0.001$, **$p < 0.01$, *$p < 0.05$).

Table 1. Strains and plasmids used in this study

Strain	Genotype	Reference
BY4741	*MAT***a** *his3Δ1 leu2Δ0 met15Δ0 ura3Δ0*	EUROSCARF
BY4742	*MATα his3Δ1leu2Δ0 lys2Δ0 ura3Δ0*	EUROSCARF
YTS159	BY4742 *pho8Δ::pho8Δ60 pho13Δ::Kan*	Cheong et al., 2008
W303-1b	*MATα, leu2-3,112 trp1-1 can1-100 ura3-1 ade2-1 his3-11,15*	EUROSCARF
YO001	BY4741 *VPS34-TAP-His3MX6*	This study
YO002	BY4741 *VPS34-TAP-His3MX6 vps15Δ::URA3*	This study
YO003	BY4741 *VPS34-TAP-His3MX6 vps30Δ::URA3*	This study
YO004	BY4741 *VPS34-TAP-His3MX6 atg14Δ::URA3*	This study
YO005	BY4741 *VPS34-TAP-His3MX6 atg38Δ::URA3*	This study
YO006	BY4741 *VPS34-TAP-His3MX6 vps38Δ::URA3*	This study
YO007	BY4741 *VPS34-TAP-His3MX6 atg3Δ::URA3*	This study
YO008	BY4741 *VPS34-TAP-His3MX6 atg8Δ::URA3*	This study
YO009	BY4741 *VPS34-TAP-His3MX6 atg11Δ::URA3*	This study
YO010	BY4741 *VPS34-TAP-His3MX6 atg12Δ::URA3*	This study
YO011	BY4741 *VPS34-TAP-His3MX6 atg18Δ::URA3*	This study
YO012	BY4741 *VPS34-TAP-URA3*	This study
YO013	BY4741 *VPS34-TAP-URA3 atg1Δ::LEU2*	This study
YO014	BY4741 *VPS34-TAP-URA3 atg13Δ::LEU2*	This study
YO015	BY4741 *VPS34-TAP-URA3 atg17Δ::LEU2*	This study
YO016	BY4741 *VPS34-TAP-URA3 atg9Δ::LEU2*	This study
YO017	BY4741 *vps34Δ::Kan*	This study
YO018	BY4741 *vps34Δ::Kan pRS415-VPS34-TAP*	This study
YO019	BY4741 *vps34Δ::Kan pRS415-VPS34(D731N)-TAP*	This study
YO020	BY4741 *vps34Δ::Kan pRG205*	This study
YO021	BY4741 *vps34Δ::Kan pRG205-VPS34*	This study
YO022	BY4741 *vps34Δ::Kan pRG205-VPS34(12A)*	This study
YO023	BY4741 *VPS34-MYC-URA3 pRS415*	This study
YO024	BY4741 *VPS34-MYC-URA3 atg1Δ::Kan pRS415*	This study

Strain	Genotype	Reference
YO025	BY4741 *VPS34-MYC-URA3 atg1Δ::Kan pRS415-ATG1-HA*	This study
YO026	BY4741 *VPS34-MYC-URA3 atg1Δ::Kan pRS415-ATG1(D211A)-HA*	This study
YO027	BY4741 *VPS34-MYC-URA3 VPS15-TAP-His3MX6*	This study
YO028	BY4741 *VPS34-MYC-URA3 ATG14-TAP-His3MX6*	This study
YO029	BY4741 *VPS34-MYC-URA3 VPS38-TAP-His3MX6*	This study
YO030	BY4741 *vps34Δ::Kan pRG205-VPS34-TAP*	This study
YO031	BY4741 *vps34Δ::Kan pRG205-VPS34(3A-1)-TAP*	This study
YO032	BY4741 *vps34Δ::Kan pRG205-VPS34(3A-2)-TAP*	This study
YO033	BY4741 *vps34Δ::Kan pRG205-VPS34(3A-3)-TAP*	This study
YO034	BY4741 *vps34Δ::Kan pRG205-VPS34(3A-4)-TAP*	This study
YO035	BY4741 *vps34Δ::Kan pRG205-VPS34(6A-1)-TAP*	This study
YO036	BY4741 *vps34Δ::Kan pRG205-VPS34(6A-2)-TAP*	This study
YO037	BY4741 *vps34Δ::Kan pRG205-VPS34(12A)-TAP*	This study
YO038	BY4741 *vps34Δ::Kan pRG205-VPS34(6D-1)-TAP*	This study
YO039	BY4741 *vps34Δ::Kan pRG205-VPS34(6D-2)-TAP*	This study
YO040	BY4741 *vps34Δ::Kan pRG205-VPS34(12D)-TAP*	This study
YO041	BY4741 *vps34Δ::Kan pRG205-VPS34-TAP ATG14-MYC-URA3*	This study
YO042	BY4741 *vps34Δ::Kan pRG205-VPS34-TAP ATG38-MYC-URA3*	This study
YO043	BY4741 *vps34Δ::Kan pRG205-VPS34-TAP VPS15-MYC-URA3*	This study
YO044	BY4741 *vps34Δ::Kan pRG205-VPS34-TAP VPS30-MYC-URA3*	This study
YO045	BY4741 *vps34Δ::Kan pRG205-VPS34-TAP VPS38-MYC-URA3*	This study
YO046	BY4741 *vps34Δ::Kan pRG205-VPS34(12A)-TAP ATG14-MYC-URA3*	This study
YO047	BY4741 *vps34Δ::Kan pRG205-VPS34(12A)-TAP ATG38-MYC-URA3*	This study
YO048	BY4741 *vps34Δ::Kan pRG205-VPS34(12A)-TAP VPS15-MYC-URA3*	This study
YO049	BY4741 *vps34Δ::Kan pRG205-VPS34(12A)-TAP VPS30-MYC-URA3*	This study
YO050	BY4741 *vps34Δ::Kan pRG205-VPS34(12A)-TAP VPS38-MYC-URA3*	This study
YO051	YTS159 *pRG205*	This study
YO052	YTS159 *vps34Δ::URA3 pRG205*	This study

Strain	Genotype	Reference
YO053	YTS159 *vps34Δ::URA3 pRG205-VPS34*	This study
YO054	YTS159 *vps34Δ::URA3 pRG205-VPS34(3A-1)*	This study
YO055	YTS159 *vps34Δ::URA3 pRG205-VPS34(3A-2)*	This study
YO056	YTS159 *vps34Δ::URA3 pRG205-VPS34(3A-3)*	This study
YO057	YTS159 *vps34Δ::URA3 pRG205-VPS34(3A-4)*	This study
YO058	YTS159 *vps34Δ::URA3 pRG205-VPS34(6A-1)*	This study
YO059	YTS159 *vps34Δ::URA3 pRG205-VPS34(6A-2)*	This study
YO060	YTS159 *vps34Δ::URA3 pRG205-VPS34(12A)*	This study
YO061	YTS159 *vps34Δ::URA3 pRG205-VPS34(12D)*	This study
YO062	YTS159 *ATG13-2xGFP-His3MX6*	This study
YO063	YTS159 *ATG13-2xmCherry-hphMX6*	This study
YO064	YTS159 *ATG14-2xGFP-His3MX6*	This study
YO065	YTS159 *ATG18-mCherry-hphMX6*	This study
YO066	BY4741 *His3MX6-ATP8p-GFP-ATG8*	Kim et al., 2021
YO067	BY4741 *atg8Δ::kanMX6 pP$_{1K}$GFP-ATG8::URA3*	Shin and Huh, 2011
YO068	BY4741 *atg8Δ::kanMX6 pP$_{1K}$GFP-ATG8::URA3 pRG205*	This study
YO069	BY4741 *atg8Δ::kanMX6 pP$_{1K}$GFP-ATG8::URA3 vps34Δ::His3MX6 pRG205*	This study
YO070	BY4741 *atg8Δ::kanMX6 pP$_{1K}$GFP-ATG8::URA3 vps34Δ::His3MX6 pRG205-VPS34*	This study
YO071	BY4741 *atg8Δ::kanMX6 pP$_{1K}$GFP-ATG8::URA3 vps34Δ::His3MX6 pRG205-VPS34(3A-1)*	This study
YO072	BY4741 *atg8Δ::kanMX6 pP$_{1K}$GFP-ATG8::URA3 vps34Δ::His3MX6 pRG205-VPS34(3A-2)*	This study
YO073	BY4741 *atg8Δ::kanMX6 pP$_{1K}$GFP-ATG8::URA3 vps34Δ::His3MX6 pRG205-VPS34(3A-3)*	This study
YO074	BY4741 *atg8Δ::kanMX6 pP$_{1K}$GFP-ATG8::URA3 vps34Δ::His3MX6 pRG205-VPS34(3A-4)*	This study
YO075	BY4741 *atg8Δ::kanMX6 pP$_{1K}$GFP-ATG8::URA3 vps34Δ::His3MX6 pRG205-VPS34(6A-1)*	This study
YO076	BY4741 *atg8Δ::kanMX6 pP$_{1K}$GFP-ATG8::URA3 vps34Δ::His3MX6 pRG205-VPS34(6A-2)*	This study
YO077	BY4741 *atg8Δ::kanMX6 pP$_{1K}$GFP-ATG8::URA3 vps34Δ::His3MX6 pRG205-VPS34(12A)*	This study
YO078	BY4741 *atg8Δ::kanMX6 pP$_{1K}$GFP-ATG8::URA3 vps34Δ::His3MX6 pRG205-VPS34(6D-1)*	This study
YO079	BY4741 *atg8Δ::kanMX6 pP$_{1K}$GFP-ATG8::URA3 vps34Δ::His3MX6 pRG205-VPS34(6D-2)*	This study
YO080	BY4741 *atg8Δ::kanMX6 pP$_{1K}$GFP-ATG8::URA3 vps34Δ::His3MX6 pRG205-VPS34(12D)*	This study

Strain	Genotype	Reference
YO081	BY4741 *ATG14-TAP-His3MX6 vps34Δ::URA3 pRG205*	This study
YO082	BY4741 *ATG14-TAP-His3MX6 vps34Δ::URA3 pRG205-VPS34*	This study
YO083	BY4741 *ATG14-TAP-His3MX6 vps34Δ::URA3 pRG205-VPS34(12A)*	This study
YO084	BY4741 *PEX11-GFP-His3MX6 pRG205*	This study
YO085	BY4741 *PEX11-GFP-His3MX6 atg36Δ::URA3 pRG205*	This study
YO086	BY4741 *PEX11-GFP-His3MX6 vps34Δ::URA3 pRG205*	This study
YO087	BY4741 *PEX11-GFP-His3MX6 vps34Δ::URA3 pRG205-VPS34*	This study
YO088	BY4741 *PEX11-GFP-His3MX6 vps34Δ::URA3 pRG205-VPS34(12A)*	This study
YO089	BY4741 *PEX11-GFP-His3MX6 vps34Δ::URA3 pRG205-VPS34(12D)*	This study
YO090	BY4741 *OM45-GFP-His3MX6 pRG205*	This study
YO091	BY4741 *OM45-GFP-His3MX6 atg32Δ::URA3 pRG205*	This study
YO092	BY4741 *OM45-GFP-His3MX6 vps34Δ::URA3 pRG205*	This study
YO093	BY4741 *OM45-GFP-His3MX6 vps34Δ::URA3 pRG205-VPS34*	This study
YO094	BY4741 *OM45-GFP-His3MX6 vps34Δ::URA3 pRG205-VPS34(12A)*	This study
YO095	BY4741 *OM45-GFP-His3MX6 vps34Δ::URA3 pRG205-VPS34(12D)*	This study
YO096	BY4741 *atg1Δ::Kan pRS415-ATG1-HA*	This study
YO097	BY4741 *atg1Δ::Kan pRS415-ATG1(D211A)-HA*	This study
YO098	BY4741 *atg1Δ::Kan ATG13-TAP-Hix3MX6*	This study
YO099	BY4741 *atg1Δ::Kan vps34Δ::URA3 pRG205-VPS34(D731N)-MYC*	This study
YO100	BY4741 *atg1Δ::Kan vps34Δ::URA3 pRG205-VPS34(D731N)-MYC ATG14-TAP-His3MX6*	This study
YO101	BY4741 *atg1Δ::Kan vps34Δ::URA3 pRG205-VPS34(D731N+12A)-MYC ATG14-TAP-His3MX6*	This study
YO102	BY4741 *atg1Δ::Kan vps34Δ::URA3 pRG205-VPS34(D731N)-MYC VPS38-TAP-His3MX6*	This study
YO103	W303-1b *ATG14-2xGFP-His3MX6 ATG13-2xmCherry-URA3*	This study
YO104	W303-1b *ATG14-2xGFP-His3MX6 ATG13-2xmCherry-URA3 atg9Δ::LEU2*	This study
YO105	W303-1b *ATG14-2xGFP-His3MX6 ATG13-2xmCherry-hphMX6 vps30Δ::URA3 p415ADH-VPS30*	This study
YO106	W303-1b *ATG14-2xGFP-His3MX6 ATG13-2xmCherry-hphMX6 vps30Δ::URA3 p415ADH-VPS30(ΔNTD)*	This study

Strain	Genotype	Reference
YO107	W303-1b *ATG14-2xGFP-His3MX6 ATG13-2xmCherry-hphMX6 vps30Δ::URA3 p415ADH-VPS30(ΔBARA)*	This study
YO108	BY4741 *VPS34-TAP-His3MX6 vps30Δ::URA3 pRS415-VPS30-GFP*	This study
YO109	BY4741 *VPS34-TAP-His3MX6 vps30Δ::URA3 p415ADH-VPS30-GFP*	This study
YO110	BY4741 *VPS34-TAP-His3MX6 vps30Δ::URA3 p415ADH-VPS30(ΔNTD)-GFP*	This study
YO111	BY4741 *VPS34-TAP-His3MX6 vps30Δ::URA3 p415ADH-VPS30(ΔBARA)-GFP*	This study
YO112	W303-1b *ATG13-2xGFP-His3MX6 vps34Δ::URA3 pRG205-VPS34*	This study
YO113	W303-1b *ATG13-2xGFP-His3MX6 vps34Δ::URA3 pRG205-VPS34(12A)*	This study
YO114	W303-1b *ATG13-2xGFP-His3MX6 vps34Δ::URA3 pRG205-VPS34(12D)*	This study
YO115	W303-1b *ATG14-2xGFP-His3MX6 ATG13-2xmCherry-hphMX6 vps34Δ::URA3 pRG205-VPS34*	This study
YO116	W303-1b *ATG14-2xGFP-His3MX6 ATG13-2xmCherry-hphMX6 vps34Δ::URA3 pRG205-VPS34(12A)*	This study
YO117	W303-1b *ATG14-2xGFP-His3MX6 ATG13-2xmCherry-hphMX6 vps34Δ::URA3 pRG205-VPS34(12D)*	This study
YO118	W303-1b *ATG13-2xGFP-His3MX6 ATG18-mCherry-hphMX6 vps34Δ::URA3 pRG205-VPS34*	This study
YO119	W303-1b *ATG13-2xGFP-His3MX6 ATG18-mCherry-hphMX6 vps34Δ::URA3 pRG205-VPS34(12A)*	This study
YO120	W303-1b *ATG13-2xGFP-His3MX6 ATG18-mCherry-hphMX6 vps34Δ::URA3 pRG205-VPS34(12D)*	This study
YO121	W303-1b *ATG14-2xGFP-His3MX6 ATG13-2xmCherry-hphMX6 atg1Δ::URA3 p415ADH*	This study
YO122	W303-1b *ATG14-2xGFP-His3MX6 ATG13-2xmCherry-hphMX6 atg1Δ::URA3 p415ADH-ATG1*	This study
YO123	W303-1b *ATG14-2xGFP-His3MX6 ATG13-2xmCherry-hphMX6 atg1Δ::URA3 p415ADH-ATG1(D211A)*	This study
YO124	W303-1b *ATG13-2xGFP-His3MX6 ATG18-mCherry-hphMX6 atg1Δ::URA3 p415ADH*	This study
YO125	W303-1b *ATG13-2xGFP-His3MX6 ATG18-mCherry-hphMX6 atg1Δ::URA3 p415ADH-ATG1*	This study
YO126	W303-1b *ATG13-2xGFP-His3MX6 ATG18-mCherry-hphMX6 atg1Δ::URA3 p415ADH-ATG1(D211A)*	This study
YO127	BY4741 *His3MX6-ATP8p-GFP-ATG8 vps34Δ::Kan pRG205-VPS34*	This study
YO128	BY4741 *His3MX6-ATP8p-GFP-ATG8 vps34Δ::Kan pRG205-VPS34(12A)*	This study
YB001	*pRS415-VPS34-TAP*	This study

Strain	Genotype	Reference
YB002	*pRS415-VPS34(D731N)-TAP*	This study
YB003	*pRG205-VPS34-TAP*	This study
YB004	*pRG205-VPS34(3A-1)-TAP*	This study
YB005	*pRG205-VPS34(3A-2)-TAP*	This study
YB006	*pRG205-VPS34(3A-3)-TAP*	This study
YB007	*pRG205-VPS34(3A-4)-TAP*	This study
YB008	*pRG205-VPS34(6A-1)-TAP*	This study
YB009	*pRG205-VPS34(6A-2)-TAP*	This study
YB010	*pRG205-VPS34(12A)-TAP*	This study
YB011	*pRG205-VPS34(6D-1)-TAP*	This study
YB012	*pRG205-VPS34(6D-2)-TAP*	This study
YB013	*pRG205-VPS34(12D)-TAP*	This study
YB014	*pRG205-VPS34*	This study
YB015	*pRG205-VPS34(3A-1)*	This study
YB016	*pRG205-VPS34(3A-2)*	This study
YB017	*pRG205-VPS34(3A-3)*	This study
YB018	*pRG205-VPS34(3A-4)*	This study
YB019	*pRG205-VPS34(6A-1)*	This study
YB020	*pRG205-VPS34(6A-2)*	This study
YB021	*pRG205-VPS34(12A)*	This study
YB022	*pRG205-VPS34(6D-1)*	This study
YB023	*pRG205-VPS34(6D-2)*	This study
YB024	*pRG205-VPS34(12D)*	This study
YB025	*pRS415-ATG1-HA*	This study
YB026	*pRS415-ATG1(D211A)-HA*	This study
YB027	*pRG205-VPS34(D741N)-MYC*	This study
YB028	*pRG205-VPS34(D741N+12A)-MYC*	This study
YB029	*p415ADH-VPS30*	This study
YB030	*p415ADH-VPS30(ΔNTD)*	This study
YB031	*p415ADH-VPS30(ΔBARA)*	This study
YB032	*pRS415-VPS30-GFP*	This study

Strain	Genotype	Reference
YB033	*p415ADH-VPS30-GFP*	This study
YB034	*p415ADH-VPS30(ΔNTD)-GFP*	This study
YB035	*p415ADH-VPS30(ΔBARA)-GFP*	This study

Table 2. Oligonucleotide primers used in this study

Primer	Sequence (5' to 3')
VPS34-F	CATCTCCGTGAAGCATTGAGGGAAGGGTTTAACTCCAAC ACACAGGAAACAGCTATGACC
VPS34-R	ATTATCAACCAATCAGGTCCGCCAGTATTGTGCCAGATT AGTTGTAAAACGACGGCCAGT
VPS34-300	CATTTCCTTGAGAGCAGAGG
CgCHK	GGTCATAGCTGTTTCCTGTG
VPS30-F	GTCACTGTTTTCGCAAAGACTCCCAGACACGGGCATTAA A CACAGGAAACAGCTATGACC
VPS30-R	AACTACTTAGTTTCCGCTGATGGTCTTATCATTGTAATTC GTTGTAAAACGACGGCCAGT
VPS30-400	CTAGCCACTCTTCCTGATTG
ATG14-F	AACTAGAATCCTAGTATGACATGCATTGCCCAATTTGCC A CACAGGAAACAGCTATGACC
ATG14-R	GCACTCTAGCCTACCACGTACCATCGGTCATGAGGTCCT G GTTGTAAAACGACGGCCAGT
ATG14-400	TGGAATTGACTAATACTTCG
VPS38-F	TGGTTTTACCTATTAGGGATAGTAATCATAATTTAAAAAT CACAGGAAACAGCTATGACC
VPS38-R	CTATGTTGGACGGTAATTCTCCAGAATCTGTTTAAATTGC GTTGTAAAACGACGGCCAGT
VPS38-400	GAGCTCCACAACAAGTTGAG
VPS15-F	GCTGTAAGGTTATCAAAAAGGAAGGCATACAGTATAATG G CACAGGAAACAGCTATGACC
VPS15-R	GGAAGATTCCAATAAGCCCTGAGTTATCACAAGCAACCA G GTTGTAAAACGACGGCCAGT
VPS15-400	TACGTCATGAGTAGATTCAC
ATG38-F	ATAATTCAACGACAGTTATACTAATCTTGGTGATGGAATG cacaggaaacagctatgacc
ATG38-R	GATACTTCGTATCTTGAAAAGAAATTACCTTATTCGTCTA gttgtaaaacgacggccagt
ATG38-400	TAATGATGCCTTCCTTGTTC
VPS34-F2	GATTGATCATTTACATAATCTGGCACAATACTGGCGGAC CGGTCGACGGATCCCCGGGTT
VPS34-R1(URA3)	GTGACGAAATTTAAATTTTGAAGCACCAATTATCAACCAA TCTGGAGGAAGTTTGAGAGG
VPS34-CHK	TTGTCAAATCTTGTGCTGGC
ATG1-F	AGATCACACAACCTCTGTGAACCATAATCTAATGGCAAG TCACAGGAAACAGCTATGACC

Primer	Sequence (5' to 3')
ATG1-R	TCATCTTCTGCCTCAATATTTTCAACCTGTTTGCAATACT GTTGTAAAACGACGGCCAGT
ATG1-300	CGAGGTTAATTCTAGAACGC
ATG13-F	AACATACAGCCCGGTTGAATAGCATGAGTCATGCACAG GAAACAGCTATGACC
ATG13-R	GGTTCATATCACTCATGAAAAATACTAGATCATCATTCTT GGTTGTAAAACGACGGCCAGT
ATG13-400	GTGAAAGTGAAGGACAGCAC
ATG17-F	GCGAGGATATTATCAACGTATTTAACACCTATGAACGAA G CACAGGAAACAGCTATGACC
ATG17-R	TCTAAGGATTCTTCACGTTGTAATTTAAAGTGTACAGGGA GTTGTAAAACGACGGCCAGT
ATG17-400	AACACACGTGAAAGTGAAGG
ATG1(D211A)-F	GCT TTCGGGTTTGCAAGATTTTTG
ATG1(D211A)-R	TGCTATCTTTAAAATGGGTAAGTTG
ATG13-F2	AGTATTTTTCATGAGTGATATGAACCTTTCTAAAGAAGGT GGTCGACGGATCCCCGGGTT
ATG13-R1	TTTCTTTAGTTGTGCCCTTTAAAATAAAACTTTACCATTTT CGATGAATTCGAGCTCGTT
ATG13-CHK	GGGAATTCATCTACTAGTGC
ATG18-F2	CGATTGCTTAATATTGTCACAGTATTCCATCTTGATGGAT GGTCGACGGATCCCCGGGTT
ATG18-R1	CGTTGTGACGTACGGAAGGCAGCGCGAGACACTTCCGT GATCGATGAATTCGAGCTCGTT
ATG18-CHK	AACATGGAAGAAGCTGCAGC
ATG1-500F(SpeI)	AGCTACTAGTTTCGTATTCAAGCATCTG
ACT1+1684R(ApaI)	AGTCGGGCCCGATAAACATTTTTTATCAACACTATG
ATG1-F2	CAGGTTGAAAATATTGAGGCAGAAGATGAACCACCAAAA TGGTCGACGGATCCCCGGGTT
ATG1-R1	GGTCATTTGTACTTAATAAGAAAACCATATTATGCATCAC TCGATGAATTCGAGCTCGTT
ATG8-F4	GAGGGGATTGATAAGAGAATCTAATAATTGTAAAGTTGA GGAATTCGAGCTCGTTTAAAC
ATG8-R5	TTTTTTCAAATGGATATTCAGACTTAAATGTAGACTTCAT ACCACCAGAACCTTTGTATAGTTCATCCATGC
ATG8+300R	TCCTTATCCTTGTGTTCTTG
R5-CHK	AGACACAACATTGAAGATGG
VPS34-F(XbaI)SLIC	CAAGCATACAATCAACTTCTAGAATGTCACTGAACAACAT AAC

Primer	Sequence (5' to 3')
VPS34-R(ClaI)SLIC	CATGACTCGAGGTCGACGGTATCGATTCATCACTGATGATTCGCGTC
Vps34(D731N)-F	CATACATCTTAGGTGTCGGCAATAGGCATTTAGACAACTTACTAG
Vps34(D731N)-R	CTAGTAAGTTGTCTAAATGCCTATTGCCGACACCTAAGATGTATG
VPS34-1000F(SacI)SLIC	TAAAGGGAACAAAAGCTGGAGCTCGTGCGATGTTATGGAACGTC
ADH1t-R(ApaI)SLIC	TAGGGCGAATTGGGTACCGGGCCCGACGAGGCAAGCTAAACAG
Vps34-6A-F	GCTGAAGCTGCCGGGACAGAATC
VPS34-6A-R	TTCAGCCGCGATGGCCTTTAATAATTTTTGGTTG
VPS34(428,437,445A)-F	GATGCCGTAGCTTCGCAAAAGCTTTCGGGTGATGCTATGTTACTATC
VSP34(428,437,445A)-R	CACAATAGTGAATTCAGCGTTAGATTTGTCGGAAAAAGTGGACAG
VPS34S445,449A-F(SLIC)	GCAAAAGCTTTCGGGTGATGCTATGTTACTAGCTACATCGCATGCCAAC
VPS34S445,449A-R(SLIC)	GTTGGCATGCGATGTAGCTAGTAACATAGCATCACCCGAAAGCTTTTGC
VPS34-1000F_pRG205(SacI)	CCTATAGGGCGAATTGGAGCTCGTGCGATGTTATGGAACG
TAP(noAscI)R_pRG205(KpnI)	TAAATACGGCCGAAGCTGGGTACCCGTCTCACTGATGATTCG
VPS34-R_pRG205(KpnI)	TAAATACGGCCGAAGCTGGGTACCTCAGGTCCGCCAGTATTGTGC
VPS34-449.50.51 3A-F	CTATGTTACTAGCTGCAGCTCATGCCAACC
VPS34-449.50.51 3A-R	GGTTGGCATGAGCTGCAGCTAGTAACATAG
VPS34(3A-1)F	GCC ATC GCt GCT GAATCGGAAACTTCCGGGAC
VPS34(3A-1)R	TTC AGC aGC GAT GGCCTTTAATAATTTTTGGTTGGCATGC
VPS34(3A-2)F	GCt GAA GCT GCt GGGACAGAATCGCTACCAATC
VPS34(3A-2)R	CCCaGCAGCTTCaGCTTCACTCGAGATGGACTTTAATAATTTTTG

3. RESULTS

3.1. Vps34, a catalytic subunit of PtdIns3K complex, is phosphorylated upon nitrogen starvation.

In an attempt to find out whether Vps34 is regulated via post-translational modification upon autophagy activation, the mobility shift of Vps34 was examined under nitrogen starvation, one of the most well-characterized autophagy-inducing conditions. Interestingly, a slower-migrating band of Vps34 appeared upon nitrogen starvation (Figure 6A). The amount of the upshifted band of Vps34 was positively correlated with increasing autophagic activity, as confirmed by the GFP-Atg8 processing assay (Figure 6B). Since the reduced mobility of proteins in SDS-PAGE could be caused by protein phosphorylation (Lee et al., 2019), lambda phosphatase treatment was performed in order to identify whether the band shift of Vps34 resulted from phosphorylation. As shown in Figure 7, lambda phosphatase treatment clearly eliminated the upshifted band of Vps34, indicating that the mobility retardation of Vps34 under nitrogen starvation results from phosphorylation. It has been previously described that Vps34 has autophosphorylation activity (Stack and Emr, 1994). To determine whether this phosphorylation is autophosphorylation, the phosphorylation of $Vps34^{D731N}$, a kinase defective mutant of Vps34 (Stack and Emr, 1994), was measured by SDS-PAGE. Figure 8A clearly demonstrates that $Vps34^{D731N}$ can be normally phosphorylated compared to wild-type Vps34, indicating that the phosphorylation of Vps34 under nitrogen starvation is not the result of autophosphorylation. Interestingly, when nitrogen sources were replenished, Vps34

was rapidly dephosphorylated (Figure 8B). These data suggest a link between Vps34 phosphorylation and autophagy activation.

3.2. Vps34 in Atg14-containing complex I is selectively phosphorylated under nitrogen starvation.

It has been previously described that both Vps34 complex I and II could not be formed in the absence of *VPS15* or *VPS30*, a common subunit of both complexes (Kihara *et al.*, 2001). The deletion of *ATG14* specifically disrupts Vps34 complex I and the loss of *Vps38* cause exclusive disruption of complex II (Kihara *et al.*, 2001) (Obara *et al.*, 2006). Given the above results that Vps34 is phosphorylated upon autophagy induction, it is likely that Vps34 in autophagy-specific complex I is selectively phosphorylated over Vps34 complex II. To verify this possibility, the phosphorylation of Vps34 was examined in cells deleted in each gene comprising Vps34 complex, namely Vps15, Vps30, Atg14, Atg38, and Vps38. In agreement with this assumption, Figure 9A demonstrates that the phosphorylation of Vps34 was clearly eliminated when both Vps34 complexes are simultaneously disrupted (*vps15*Δ or *vps30*Δ) or complex I could not be assembled (*atg14*Δ). In contrast, the deletion of *VPS38*, a specific subunit of complex II, does not affect the phosphorylation of Vps34. Notably, Vps34 phosphorylation was significantly, but not totally, reduced in the absence of *ATG38*, another specific subunit of complex I (Figure 9B). These data indicate that Vps34 phosphorylation requires a stable complex I, not complex II, assembly.

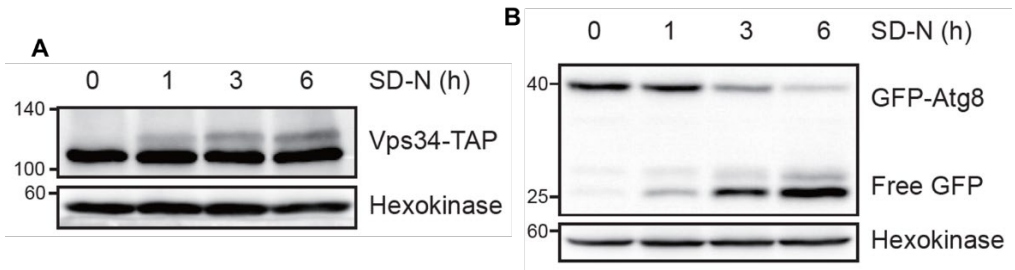

Figure 6. The emergence of the slower-migrating band of Vps34 upon autophagy induction.

(**A**) Vps34-TAP-expressing cells were grown to mid-log phase in YPD medium (SD-N 0 h) and shifted to SD-N medium for the indicated hours. Cell lysates were analyzed by immunoblotting with an anti-IgG antibody. (**B**) GFP-Atg8-expressing cells were grown and starved as in (A). GFP-Atg8 processing was examined by immunoblotting with an anti-GFP antibody. (**A** and **B**) Hexokinase was used as an internal control. The molecular weight markers (kDa) are indicated to the left of the blots. A representative data of at least three independent experiments are shown.

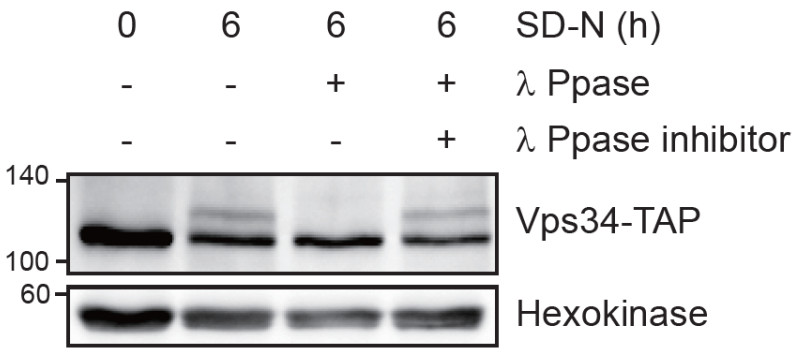

Figure 7. Vps34 is phosphorylated under nitrogen starvation

Vps34-TAP-expressing cells were grown to mid-log phase in YPD medium (SD-N 0 h) and shifted to SD-N medium for 6 hours. Cell lysates were treated with lambda phosphatase with or without phosphatase inhibitors as described in the Materials and methods. Immunoblotting was performed using an anti-IgG antibody. Hexokinase was used as an internal control. The molecular weight markers (kDa) are indicated to the left of the blots. A representative data of at least three independent experiments was shown.

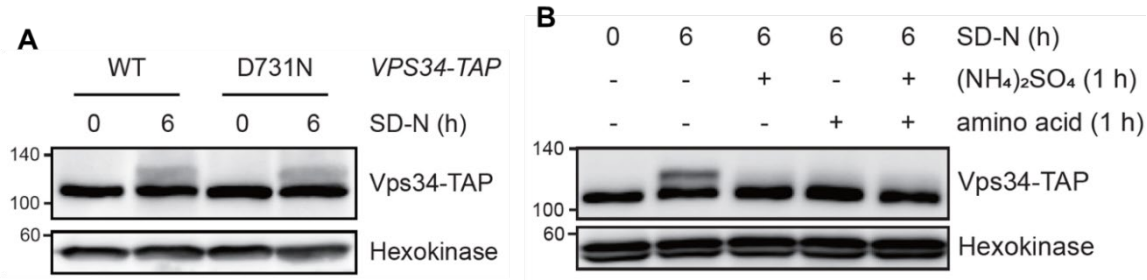

Figure 8. Characterization of Vps34 phosphorylation.

(**A**) Cells expressing either wild-type Vps34 (WT) or Vps34^{D731N} (D731N) were grown to mid-log phase in YPD medium (SD-N 0 h) and shifted to SD-N medium for 6 hours. (**B**) Vps34-TAP-expressing cells were grown to mid-log phase and then shifted to SD-N medium for 6 hours. Ammonium sulfate or amino acids were then directly added to the culture medium and incubated for additional 1 hour as indicated. (**A** and **B**) Cell lysates were analyzed by immunoblotting using an anti-IgG antibody. Hexokinase was used as an internal control. The molecular weight markers (kDa) are indicated to the left of the blots. A representative data of at least three independent experiments was shown.

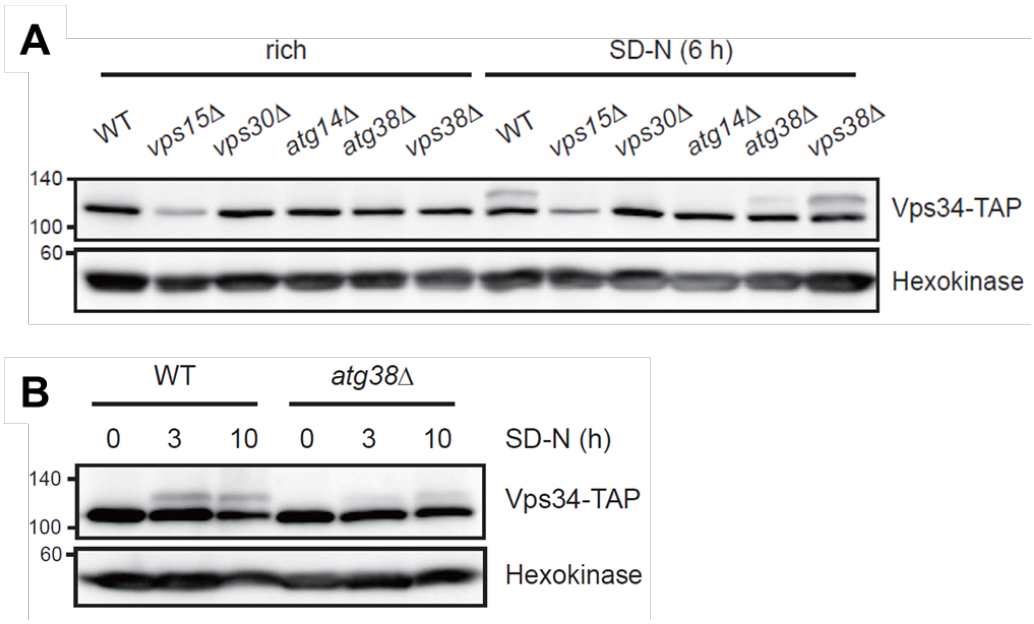

Figure 9. Complex I components are necessary for Vps34 phosphorylation.

(**A**) Cells expressing either wild-type Vps34 (WT) or Vps34^{D731N} (D731N) were grown to mid-log phase in YPD medium (SD-N 0 h) and shifted to SD-N medium for 6 hours. (**B**) Vps34-TAP-expressing cells were grown to mid-log phase and then shifted to SD-N medium for 6 hours. Ammonium sulfate or amino acids were then directly added to the culture medium and incubated for additional 1 hour as indicated. (**A** and **B**) Cell lysates were analyzed by immunoblotting using an anti-IgG antibody. Hexokinase was used as an internal control. The molecular weight markers (kDa) are indicated to the left of the blots. A representative image of at least three independent experiments was shown.

Next, a co-immunoprecipitation assay was performed in order to specifically visualize the phosphorylation status of Vps34 contained in each complex. When Vps15-TAP, a common subunit of both Vps34 complexes, was immunoprecipitated, both phosphorylated and unphosphorylated Vps34 were co-purified (Figure 10). Remarkably, the majority of Vps34 in Atg14-TAP immunoprecipitates were phosphorylated, contrary to Vps38-bound Vps34, which were mostly dephosphorylated. Collectively, these data suggest that Vps34 in complex I is selectively phosphorylated under nitrogen starvation.

3-3. The helical domain of Vps34 is phosphorylated.

To investigate the function of Vps34 phosphorylation, phosphorylated residues of Vps34 under nitrogen starvation were analyzed using immunoprecipitation followed by tandem mass spectrometry (IP-MS). Since Vps34 autophosphorylates itself (Stack and Emr, 1994), while the phosphorylation under nitrogen starvation is not an autophosphorylation (Figure 8A), the kinase-dead $Vps34^{D731N}$ was used for the IP-MS analysis to exclude signals from autophosphorylated residues. IP-MS results revealed one phosphorylated residue (S437, Figure 11A) and one phospho-peptide whose phosphorylation sites could not be precisely determined (Figure 11B, C). Table 3 lists the phospho-residues of Vps34 identified in this study and in previous studies (Hu *et al.*, 2019; Lanz et al., 2021).

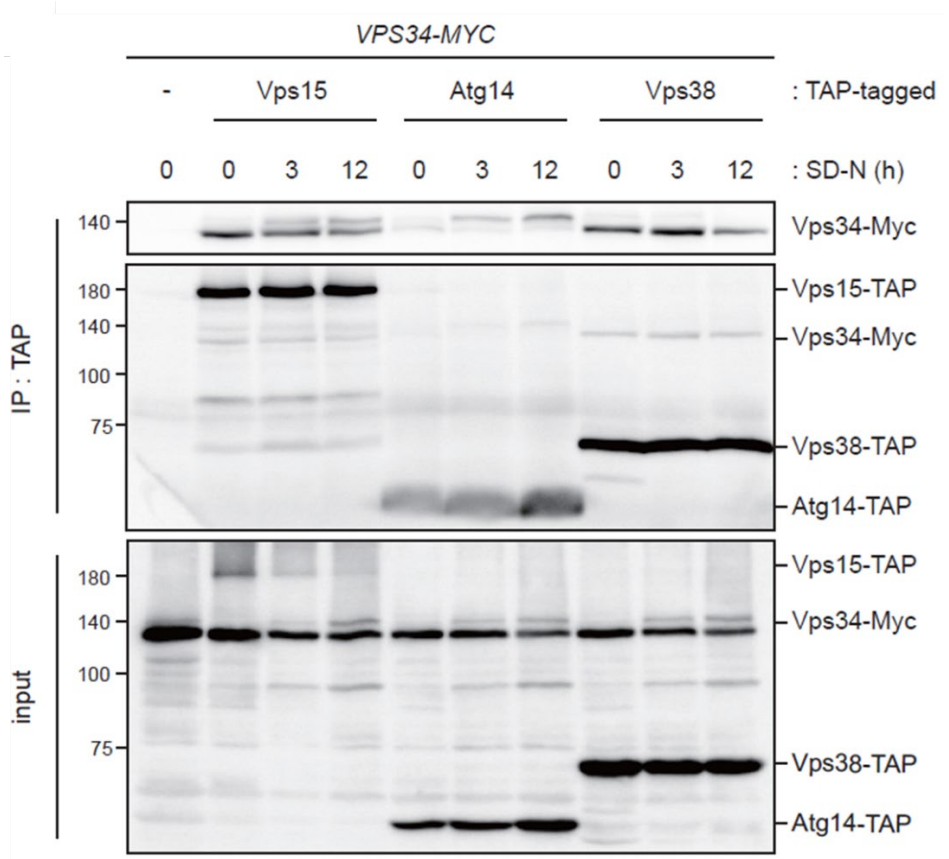

Figure 10. Vps34 in complex I is selectively phosphorylated.

Cells expressing the indicated TAP-tagged proteins and Vps34-Myc were grown to mid-log phase in YPD medium (SD-N 0 h) and then shifted to SD-N medium for the indicated hours. Coimmunoprecipitation and western blot were performed as described in the Materials and methods. The resultant membrane was first developed with an anti-Myc antibody for Vps34-Myc detection, and with an anti-IgG antibody for the detection of the TAP-tagged proteins. The molecular weight markers (kDa) are indicated to the left of the blots. A representative image of at least three independent experiments was shown.

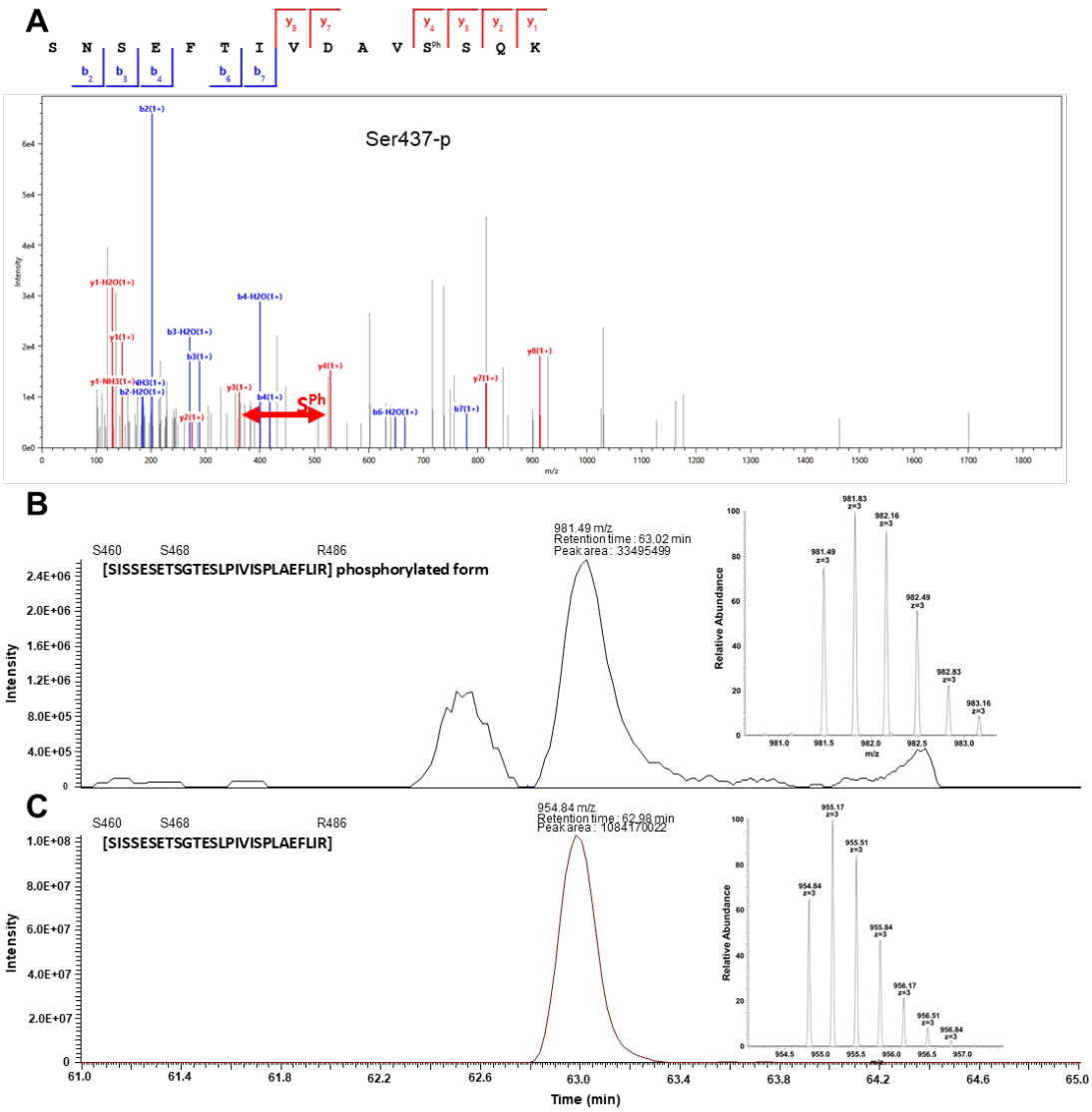
A
S N S E F T I V D A V S^Ph S Q K
Ser437-p
B
[SISSESETSGTESLPIVISPLAEFLIR] phosphorylated form
981.49 m/z
Retention time : 63.02 min
Peak area : 33495499
Intensity
Relative Abundance
m/z
C
[SISSESETSGTESLPIVISPLAEFLIR]
954.84 m/z
Retention time : 62.98 min
Peak area : 1084170022
Time (min)

Figure 11. Phosphorylated peptide spectra of Vps34^{D731N} identified in this study.

(**A**-**C**) Vps34^{D731N}-TAP-expressing cells were grown to mid-log phase in YPD medium and shifted in SD-N medium for 6 hours. Immunoprecipitation of Vps34^{D731N}-TAP was performed as described in the Materials and methods. The immunoisolated Vps34^{D731N}-TAP was subjected to mass spectrometric phosphorylation mapping. IP-MS analysis was performed as described in the Materials and methods. (**A**) Mass spectra of S437 phosphorylation. (**B** and **C**) Mass spectra for peptide spanning from S460 to R486 of Vps34^{D731N}. Spectra corresponding to phosphorylated/non-phosphorylated versions of this peptide are represented in B and C, respectively.

Table 3. List of phosphorylation sites of Vps34.

Phosphorylation site	Reference
S437	This study
SI**SS**E**S**E**TS**GTESLPIVISPLAEFLIR*	This study
S428, S449, T450, S451	(Lanz *et al.*, 2021)
S445, S449	(Hu *et al.*, 2019)

* The specific phosphorylated residues were not identified. Residues mutated in Vps34^{6A-1} are denoted in bold.

Based on the IP-MS results and previous studies (Hu *et al.*, 2019; Lanz *et al.*, 2021), seven versions of non-phosphorylatable Vps34 (Vps34^{3A-1}; Vps34[S460A, S462A, S463A], Vps34^{3A-2}; Vps34[S465A, T467A, S468A], Vps34^{6A-1}; Vps34[S460A, S462A, S463A, S465A, T467A, S468A], Vps34^{3A-3}; Vps34[S428A, S437A, S445A], Vps34^{3A-4}; Vps34[S449A, T450A, S451A], Vps34^{6A-2}; Vps34[S428A, S437A, S445A, S449A, T450A, S451A], Vps34^{12A}; all the above 12 serine/threonine residues were mutated to alanine) and three versions of phospho-mimicking Vps34 mutants (Vps34^{6D-1}; Vps34[S460D, S462D, S463D, S465D, T467D, S468D], Vps34^{6D-2}; Vps34[S428D, S437D, S445D, S449D, T450D, S451D], Vps34^{12D}; all the above 12 S/T residues were mutated to aspartic acid) were constructed. The 12 serine/threonine residues (hereafter, the 12 S/T residues) mutated in these mutants are represented in Figure 12A with respect to the domain composition of Vps34 (Rostislavleva et al., 2015). Notably, all these mutated residues above are located in the helical domain of Vps34. The expression and phosphorylation of those Vps34 mutants were then analyzed by SDS-PAGE. As shown in Figure 12B, Vps34^{3A} mutants showed similar phosphorylation to that of wild-type Vps34, although phosphorylation of Vps34^{3A-1} was slightly decreased. Remarkably, however, the phosphorylation of Vps34^{6A-1} and Vps34^{6A-2} mutants were severely compromised compared to that of wild-type Vps34, and Vps34^{12A} mutant showed nearly complete disruption in its phosphorylation. Furthermore, the mobility of phospho-mimicking Vps34^{6D-1} and Vps34^{6D-2} was slightly reduced even under nutrient-rich condition and Vps34^{12D} showed almost the same mobility with phosphorylated Vps34. These data suggest that the phosphorylation residues of Vps34 responsible for the mobility shift under nitrogen starvation are included in the

12 S/T residues. Figure 13A shows the position of the 12 S/T residues in relation to the overall Vps34 complex structure. Remarkably, 10 S/T residues out of the 12 S/T residues (except for S428 and S437) were located in a structurally uncharacterized region (SUR) of the helical domain of Vps34. A sequence alignment of the SUR with other higher eukaryotes is shown in Figure 13B.

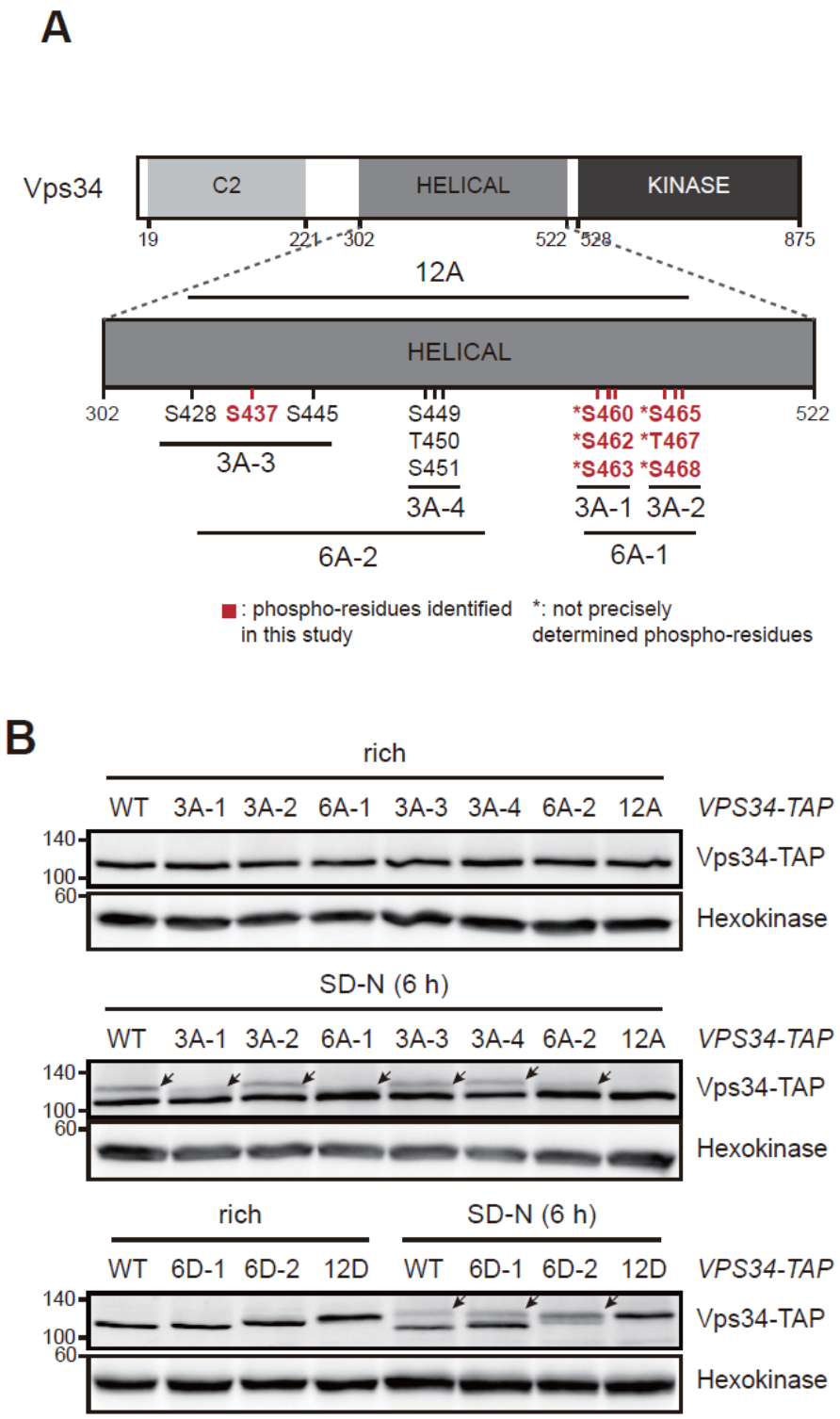
A
Vps34
C2
HELICAL
KINASE
19
221
302
522
528
875
12A
HELICAL
302
S428
S437
S445
S449
T450
S451
*S460
*S462
*S463
*S465
*T467
*S468
522
3A-3
3A-4
3A-1
3A-2
6A-2
6A-1
: phospho-residues identified in this study
*: not precisely determined phospho-residues
B
rich
WT
3A-1
3A-2
6A-1
3A-3
3A-4
6A-2
12A
VPS34-TAP
140
100
60
Vps34-TAP
Hexokinase
SD-N (6 h)
WT
3A-1
3A-2
6A-1
3A-3
3A-4
6A-2
12A
VPS34-TAP
140
100
60
Vps34-TAP
Hexokinase
rich
SD-N (6 h)
WT
6D-1
6D-2
12D
WT
6D-1
6D-2
12D
VPS34-TAP
140
100
60
Vps34-TAP
Hexokinase

Figure 12. The helical domain of Vps34 is phosphorylated under nitrogen starvation.

(**A**) A diagram depicting the phosphorylated residues of Vps34 and constructed non-phosphorylatable Vps34 mutants with respect to the domain structure of Vps34. The Vps34 domain structure was presented according to a previous study (Rostislavleva *et al.*, 2015). The phospho-residues identified in this study are denoted in red. Asterisks indicate the phospho-residues whose phosphorylation could not be precisely determined. (**B**) Cells expressing the indicated Vps34 variants were grown to mid-log phase in YPD medium (rich) and shifted to SD-N medium for 6 hours. Cell extracts were analyzed by immunoblotting with an anti-IgG antibody as described in the Materials and methods. Arrows indicate the phosphorylated Vps34. Hexokinase was used as an internal control. The molecular weight markers (kDa) are indicated to the left of the blots. A representative image of at least three independent experiments was shown.

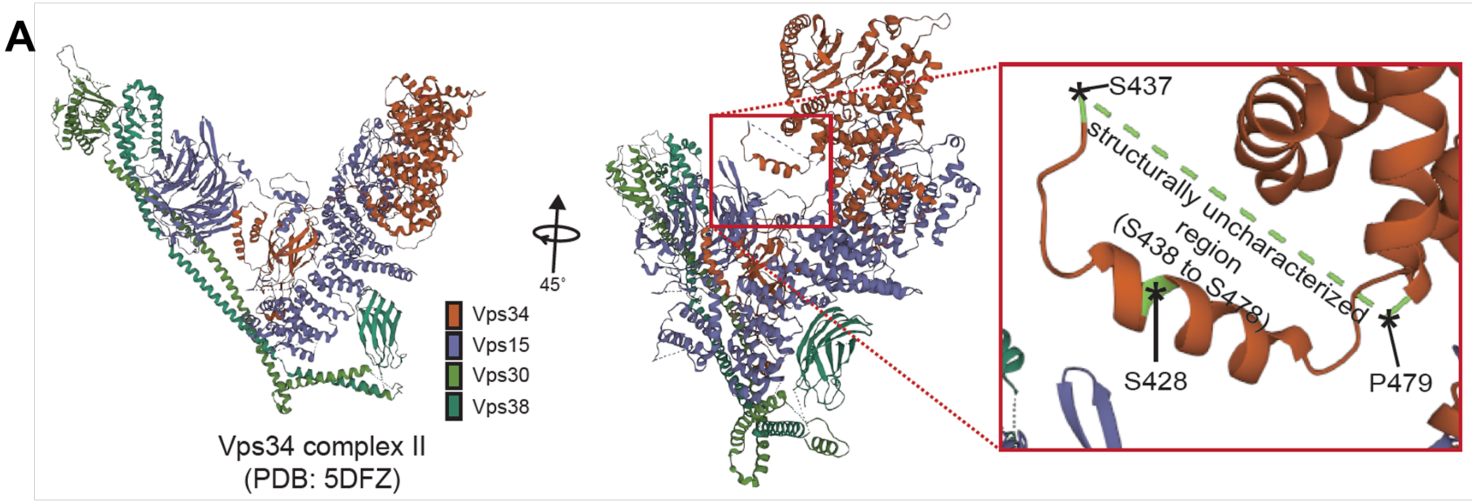

Bold : all S/T residues 🟥 the 12 S/T residues and its homologues

structurally uncharacterized region (SUR) 🟦 other homologous S/T residues

			ratio of Ser to full-length	ratio of Ser to SUR	enrichment (fold)
Vps34 *S. cerevisiae*	420	**S**TF**S**DK**S**N**S**E FTIVDAV**SS**Q KL**S**GD**S**MLL**S** **TS**HANQK...................LLK**S**.I**SS**E**S**E**TS**G			
Vps34 *H. sapiens*	409	DDIKNGLEPT KKD**S**Q**SS**V**S**E NV**S**N**S**GIN**S**. AEID**SS**Q...................IIT**S**PLP**S**V**SS**PPP			
Vps34 *D. melanogaster*	411	RHIVHLHGCI FPERDVVR**S**I LDDNG**S**LLDQ **SS**L**S**DL**S**A**TSS**GLHG**S**VIPANQRAA**S**VLAAIK**S**DK**S**V**S**PG			
Vps34 *S. cerevisiae*	470	**T**E**S**LP..IVI**S**P 479	7.5%	29.3%	3.88
Vps34 *H. sapiens*	459	A**ST**KEVPDGE.....................................NLEQD	7.1%	29.2%	4.11
Vps34 *D. melanogaster*	481	**S**AGG**S**G**S**GGQG**S**VALPNP**S**APATPG**SSS**LPCD**S**N**S**NALMLAEGI**S**FG**S**VPAN	7.6%	22.9%	3.02

Figure 13. A structurally uncharacterized region in the helical domain of Vps34 is phosphorylated under nitrogen starvation.

(**A**) The position of the 12 S/T residues with respect to overall Vps34 complex structure. The crystal structure of Vps34 complex II (PDB ID: 5DFZ (Rostislavleva *et al.*, 2015)) was used to designate the phosphorylated residues. 10 S/T residues out of 12 S/T residues (except for S428 and S437) belong to a structurally uncharacterized region (from S438 to S478) in the helical domain of Vps34. (**B**) Sequence alignment of the SUR in Vps34 from *S. cerevisiae*, *H. sapiens*, and *D. melanogaster* based on a structural analysis from a previous study (Rostislavleva et al., 2015). All S/T residues are shown in bold. Gray indicates the SUR according to the PDB entries 5DFZ for yeast (Rostislavleva et al., 2015), 7BL1 for human (Tremel et al., 2021), and 2X6H for Drosophila (Miller et al., 2010). The 12 S/T residues of yeast Vps34 and their homologous S/T residues of human and Drosophila Vps34 are shown in red. Other homologous S/T residues are indicated in blue. The ratios of serine in full-length Vps34 and the SUR are indicated to the right of each sequence. Enrichment values (the ratio of serine in the SUR divided by the ratio of serine in full-length Vps34) are also indicated.

3-4. Vps34 phosphorylation promotes autophagy and cell longevity under nitrogen starvation.

Next, the autophagic activity of each *vps34* mutant was examined by Pho8Δ60 assay and GFP-Atg8 processing assay (Figure 14). As described previously (Kihara *et al.*, 2001), autophagy was almost completely inhibited in *vps34*Δ cells. As expected, the reconstitution of wild-type *VPS34* could recover autophagic activity comparable to that of wild-type cells. Similarly, cells expressing each $Vps34^{3A}$ mutant ($Vps34^{3A-1}$ to $Vps34^{3A-4}$) showed normal autophagic flux compared with cells expressing wild-type Vps34. However, a significant defect in autophagy was observed in cells expressing $Vps34^{6A-1}$, $Vps34^{6A-2}$, or $Vps34^{12A}$ (Figure 14), while cells expressing the phospho-mimicking Vps34 mutants ($Vps34^{6D-1}$, $Vps34^{6D-2}$, and $Vps34^{12D}$) showed robust autophagic activity under nitrogen starvation (Figure 15). All of the above Vps34 variants showed similar autophagic activity under nutrient-rich condition. These data suggest that phosphorylation of Vps34 helical domain is important for autophagy activation. I also performed Pex11-GFP (pexophagy marker) and Om45-GFP (mitophagy marker) processing assay to monitor selective autophagic activity in cells expressing $Vps34^{12A}$ or $Vps34^{12D}$. The Pex11-GFP and Om45-GFP are delivered to the vacuole in a pexophagy-/mitophagy-dependent manner. Inside the vacuole, Pex11-GFP/Om45-GFP are degraded by vacuolar proteases, generating protease-resistant free-GFP molecules which can be used as an indicator of pexophagy/mitophagy activity, respectively (Kanki *et al.*, 2009; Motley *et al.*, 2012). As shown in Figure 16, the deletion of *ATG36* and *ATG32*, which are essential genes for pexophagy and mitophagy, respectively, caused complete

inhibition of corresponding selective autophagy as indicated by the inability to process Pex11-GFP or Om45-GFP into free GFP during prolonged nitrogen starvation. *vps34*Δ cells were also defective in both pexophagy and mitophagy. However, cells expressing $Vps34^{12A}$ or $Vps34^{12D}$ effectively processed Pex11-GFP and Om45-GFP to generate similar amounts of free GFP compared to wild-type cells (Figure 16), indicating that Vps34 phosphorylation is not required for mitophagy/pexophagy activity under nitrogen starvation.

Normal autophagy activity is required for extending cellular lifespan under chronic nitrogen starvation (Tsukada and Ohsumi, 1993). To better understand the physiological implications of Vps34 phosphorylation, the chronological lifespan of cells expressing wild-type Vps34 or $Vps34^{12A}$ mutants was analyzed by counting colony-forming units (CFUs/ml) and the survival integral values were obtained as previously described (Jung et al., 2015; Noda, 2008). Cells expressing $Vps34^{12A}$ mutant showed significantly impaired cell viability under prolonged nitrogen starvation, as expected (Figure 17A, B). The viability assessment by flow cytometry using Phloxine B dye, which stains dead cells (Medeiros et al., 2018), also demonstrated decreased cell survival of the $Vps34^{12A}$ mutant (Figure 17C, D). These results suggest that Vps34 phosphorylation is necessary for cell survival during prolonged nitrogen starvation.

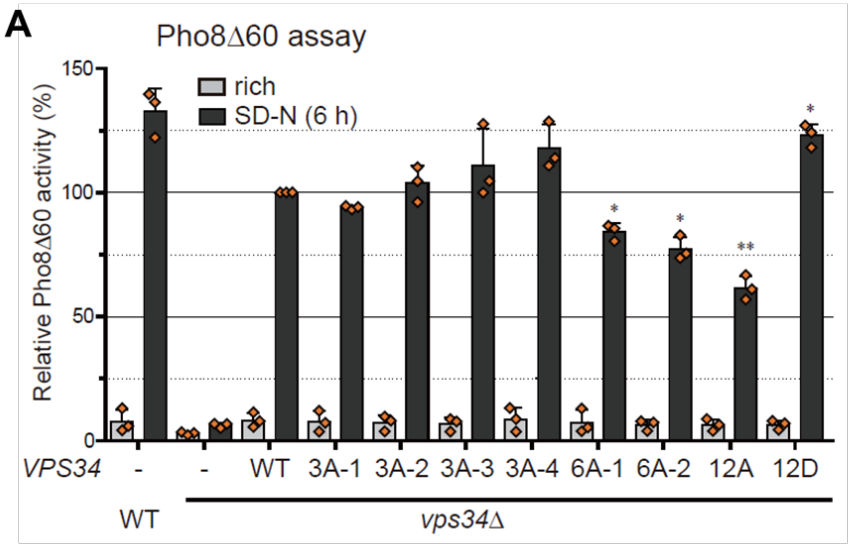
A
Pho8Δ60 assay
rich
SD-N (6 h)
Relative Pho8Δ60 activity (%)
150
100
50
0
VPS34
-
-
WT
3A-1
3A-2
3A-3
3A-4
6A-1
6A-2
12A
12D
WT
vps34Δ

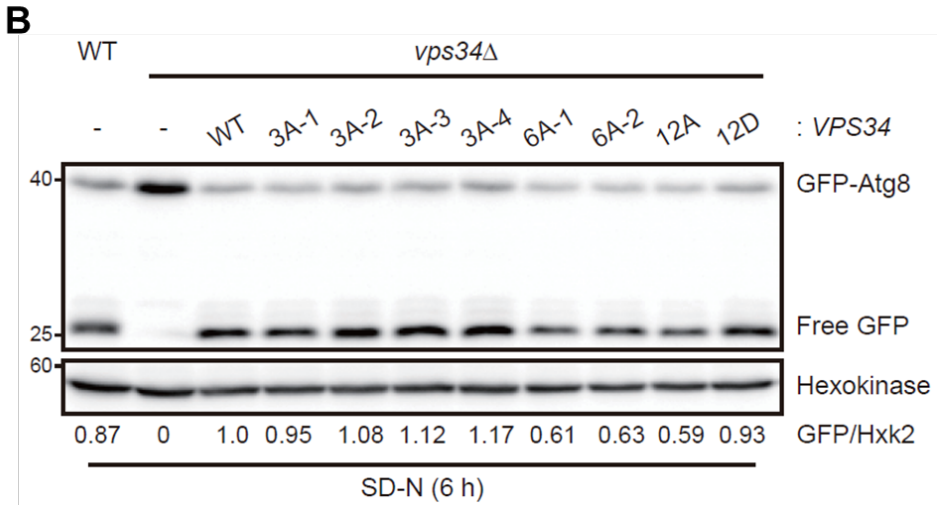
B
WT
vps34Δ
-
-
WT
3A-1
3A-2
3A-3
3A-4
6A-1
6A-2
12A
12D
: VPS34
40
25
60
GFP-Atg8
Free GFP
Hexokinase
0.87
0
1.0
0.95
1.08
1.12
1.17
0.61
0.63
0.59
0.93
GFP/Hxk2
SD-N (6 h)

Figure 14. Vps34 phosphorylation is required for normal autophagic activity.

(**A**) Wild-type cells harboring an empty vector or *vps34*Δ cells harboring an empty vector, or vectors expressing the indicated Vps34 variants were grown to mid-log phase in YPD medium (rich) and shifted to SD-N medium for 6 hours. The Pho8Δ60 assay was performed as described in the Materials and methods. The mean values of three independent experiments were normalized against that of *vps34*Δ cells expressing wild-type Vps34 in SD-N 6 h (set to 100). The error bars represent the standard deviations. Asterisks indicate the significant difference compared with *vps34*Δ cells expressing wild-type Vps34 under the corresponding conditions. (two-tailed Student's t-test): $**p < 0.01$, $*p < 0.05$. (**B**) GFP-Atg8-expressing WT cells with an empty vector, or *vps34*Δ cells with an empty vector, or with vectors expressing the indicated Vps34 variants were grown to mid-log phase in YPD medium and shifted to SD-N medium for 6 hours. Cell extracts were analyzed by immunoblotting with an anti-GFP antibody as described in the Materials and methods. Hexokinase was used as an internal control. The relative ratio of free GFP to Hxk2 from three independent experiments was normalized against that of *vps34*Δ cells expressing WT Vps34 (set to 1.0) and is shown below each lane. The molecular weight markers (kDa) are indicated to the left of the blots. A representative image of at least three independent experiments was shown.

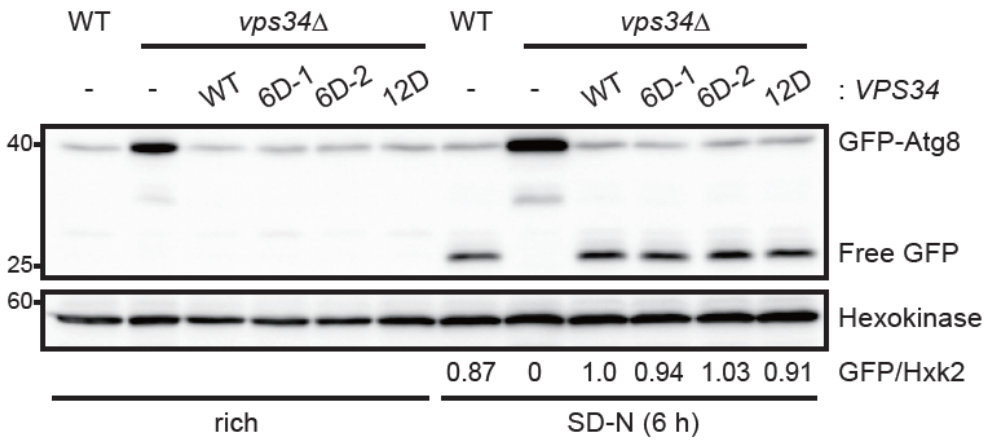

Figure 15. The phospho-mimicking Vps34 mutants showed robust autophagic activity under nitrogen starvation.

GFP-Atg8-expressing WT cells with an empty vector, or *vps34*Δ cells with an empty vector, or with vectors expressing the indicated Vps34 variants were grown to mid-log phase in YPD medium and shifted to SD-N medium for 6 hours. Cell extracts were analyzed by immunoblotting with an anti-GFP antibody as described in the Materials and methods. Hexokinase was used as an internal control. The relative ratio of free GFP to Hxk2 under nitrogen starvation from three independent experiments was normalized against that of *vps34*Δ cells expressing WT Vps34 (set to 1.0) and is shown below each lane. The molecular weight markers (kDa) are indicated to the left of the blots. A representative image of at least three independent experiments was shown.

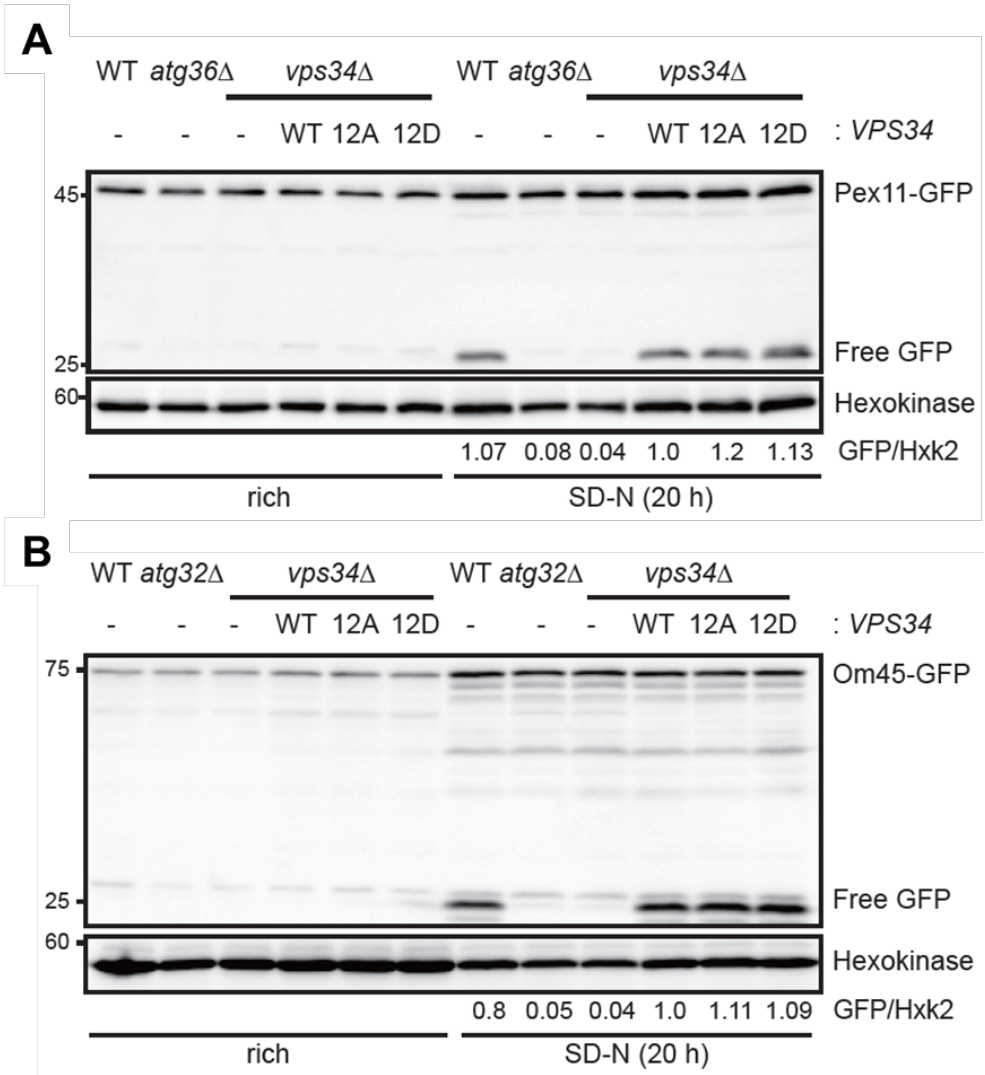
A
WT atg36Δ vps34Δ WT atg36Δ vps34Δ
- - - WT 12A 12D - - - WT 12A 12D : VPS34
45
25
60
Pex11-GFP
Free GFP
Hexokinase
1.07 0.08 0.04 1.0 1.2 1.13 GFP/Hxk2
rich
SD-N (20 h)
B
WT atg32Δ vps34Δ WT atg32Δ vps34Δ
- - - WT 12A 12D - - - WT 12A 12D : VPS34
75
25
60
Om45-GFP
Free GFP
Hexokinase
0.8 0.05 0.04 1.0 1.11 1.09 GFP/Hxk2
rich
SD-N (20 h)

Figure 16. Vps34 phosphorylation is dispensable for selective autophagy activity.

(**A**) Pex11-GFP-expressing WT cells with an empty vector, or *vps34*Δ cells with an empty vector, or with vectors expressing the indicated Vps34 variants were grown to mid-log phase in YPD medium and shifted to SD-N medium for 20 hours. (**B**) Om45-GFP-expressing WT cells with an empty vector, or *vps34*Δ cells with an empty vector, or with vectors expressing the indicated Vps34 variants were grown to mid-log phase in YPD medium and shifted to SD-N medium for 20 hours. (**A** and **B**) Cell extracts were analyzed by immunoblotting with an anti-GFP antibody as described in the Materials and methods. Hexokinase was used as an internal control. The relative ratio of free GFP to Hxk2 under nitrogen starvation from three independent experiments was normalized against that of *vps34*Δ cells expressing WT Vps34 (set to 1.0) and is shown below each lane. The molecular weight markers (kDa) are indicated to the left of the blots. A representative image of at least three independent experiments was shown.

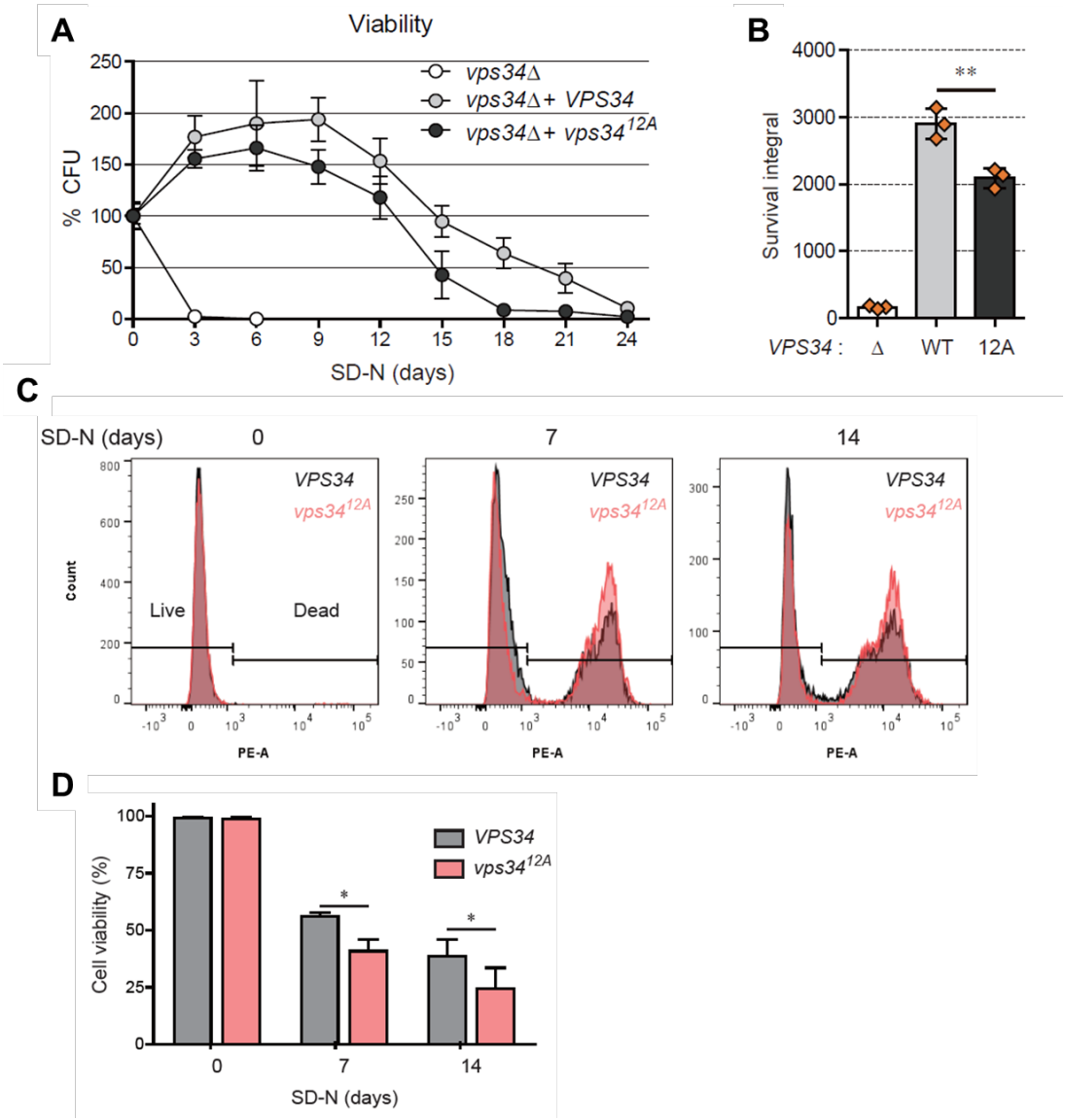
A
Viability
% CFU
SD-N (days)
vps34Δ
vps34Δ+ VPS34
vps34Δ+ vps34 12A
B
Survival integral
VPS34 :
Δ
WT
12A
**
C
SD-N (days)
0
7
14
VPS34
vps34 12A
Count
Live
Dead
PE-A
D
Cell viability (%)
SD-N (days)
VPS34
vps34 12A
*

Figure 17. Vps34 phosphorylation promotes cellular lifespan under prolonged nitrogen starvation.

(**A**) *vps34*Δ cells transformed with an empty plasmid or plasmids expressing WT Vps34 or Vps34^{12A} were grown to mid-log phase in YPD medium (Day 0) and incubated in SD-N medium for the indicated days. Survival values (CFU/ml) at each time point were normalized against the value on Day 0 of the corresponding strain, and the means of three independent experiments were plotted. The error bars indicate the standard deviations. (**B**) The survival integral values were quantified as described in the Materials and methods. The means of three independent experiments are shown, and the error bars indicate the standard deviations. Asterisks indicate significant differences compared with WT cells (two-tailed Student's t-test): $**p < 0.01$. (**C**) Cell viability was measured in cells expressing either WT Vps34 or Vps34^{12A} under nitrogen starvation by flow cytometry using Phloxine B dye as described in the Supplemental methods. Cells were grown to mid-log phase in YPD medium (Day 0) and incubated in SD-N medium for the indicated days. Fluorescence was analyzed using a BD FACS Canto II flow cytometer. A representative image of three independent experiments is shown. (**D**) The ratios of live cells shown in (C) were represented. Values are the means of three independent experiments, and the error bars indicate the standard deviations. Asterisks indicate significant differences compared with WT cells (two-tailed Student's *t*-test): $*p < 0.05$.

The cellular amount of Vps34 mutants was similar to that of wild-type Vps34 (Figure 12B) and the $Vps34^{12A}$ mutant was able to perform carboxypeptidase Y (CPY) sorting (Figure 18A), which is a reliable indicator of a functional Vps34 complex II (Kihara *et al.*, 2001). Furthermore, the binding abilities of $Vps34^{12A}$ with other complex subunits, namely, Atg14, Atg38, Vps38, Vps15, and Vps30, were comparable to those of wild-type Vps34 (Figure 18B). These results indicate that alanine substitutions of the 12 S/T residues do not affect the overall structure or stability of Vps34. In order to investigate whether Vps34 phosphorylation is necessary for the PtdIns3K activity of Vps34, I performed an in vitro PtdIns3K assay where the catalytic activity of Vps34 complex I can be measured by incubating an affinity-captured Atg14-immunocomplex with phosphatidylinositol in the presence of ATP (Park *et al.*, 2016). As shown in Figure 19, the catalytic activity of the $Vps34^{12A}$ mutant was comparable to that of wild-type Vps34, suggesting that Vps34 phosphorylation is dispensable for the enzymatic activity of Vps34 complex I. Collectively, these data indicate that alanine substitutions of the 12 S/T residues do not impair the catalytic activity of Vps34 nor perturb the overall structure of Vps34 complexes.

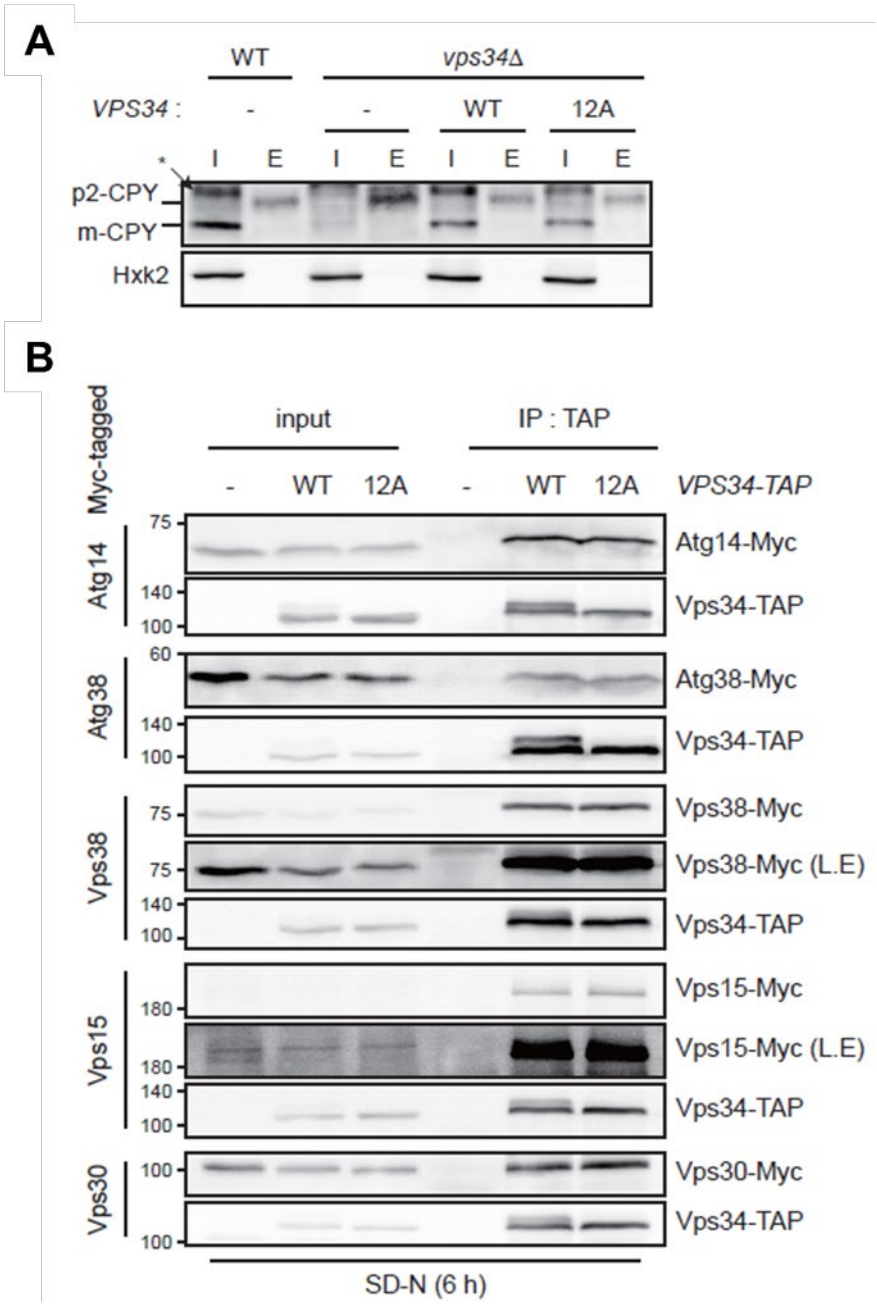
A
WT
vps34Δ
VPS34 :
-
-
WT
12A
I
E
I
E
I
E
I
E
p2-CPY
m-CPY
Hxk2
B
Myc-tagged
input
IP : TAP
-
WT
12A
-
WT
12A
VPS34-TAP
Atg14
Atg38
Vps38
Vps15
Vps30
75
140
100
60
180
Atg14-Myc
Vps34-TAP
Atg38-Myc
Vps38-Myc
Vps38-Myc (L.E)
Vps15-Myc
Vps15-Myc (L.E)
Vps30-Myc
SD-N (6 h)

Figure 18. Alanine substitution mutation does not affect the function of Vps34 complex II nor perturb the overall structure of Vps34 complexes.

(**A**) CPY sorting assay was performed in WT cells harboring an empty plasmid and *vps34*Δ cells harboring an empty plasmid or plasmids expressing WT Vps34 or $Vps34^{12A}$ as described in the Materials and methods. An asterisk indicates nonspecific bands. (**B**) Cells expressing Vps34-TAP or $Vps34^{12A}$-TAP and the indicated Myc-tagged proteins were grown to mid-log phase in YPD-medium and incubated in SD-N medium for 6 h. Co-IP assay was performed as described in the Materials and methods. WT cells expressing the indicated Myc-tagged proteins and no TAP-tagged protein were used as a negative control. As previously described (Kihara *et al.*, 2001), Vps15 was unstable in cell lysates. L.E. indicates long exposure. The molecular weight markers (kDa) are indicated to the left of the blots. (**A** and **B**) A representative image of at least three independent experiments is shown.

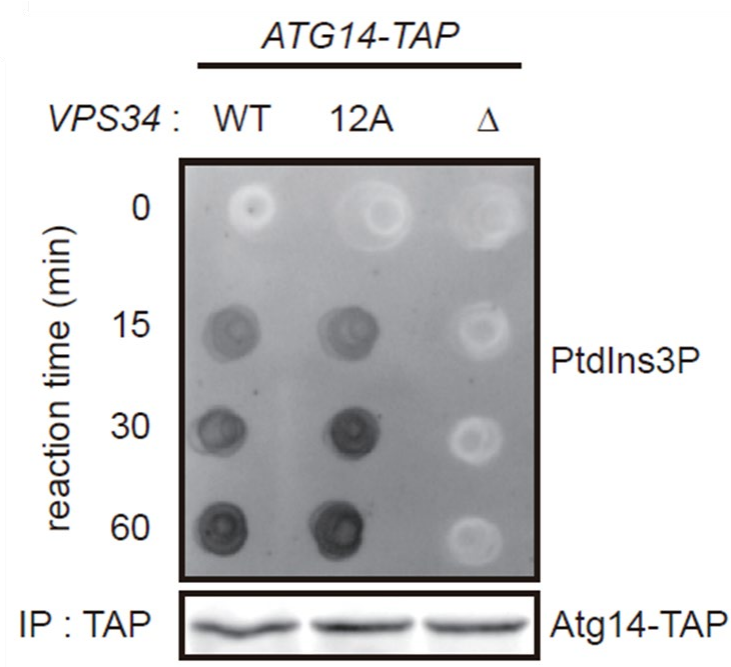

Figure 19. Vps34 phosphorylation is dispensable for its own enzymatic activity.

Atg14-TAP-expressing *vps34*Δ cells harboring an empty plasmid (Δ) or plasmids expressing WT Vps34 (WT) or $Vps34^{12A}$ (12A) were grown to mid-log phase in YPD medium and incubated in SD-N medium for 6 h. Atg14-TAP-immunoprecipitates were then obtained and incubated with PtdIns and ATP for the indicated times. The production of PtdIns3P was analyzed by dot blot analysis as described in the Materials and Methods. A representative image of at least three independent experiments is shown.

3-4. Atg1 phosphorylates Vps34 under nitrogen starvation

Atg1 is a serine/threonine kinase that phosphorylates several autophagy activators, such as Atg9 (Papinski *et al.*, 2014) and Atg19 (Pfaffenwimmer et al., 2014), at the PAS to promote autophagy. Moreover, Ulk1, the mammalian homolog of Atg1, has been reported to phosphorylate Ser249 of VPS34 directly, even though the function of this modification is not well characterized (Egan *et al.*, 2015). Therefore, it is assumable that Atg1 kinase may directly phosphorylate Vps34 under nitrogen starvation. To test this assumption, I first examined phosphorylation of Vps34 in cells with *ATG1*, *ATG13*, or *ATG17* deleted, which together comprise the Atg1 kinase complex and are necessary for Atg1 kinase activity. Deletion of *ATG1*, *ATG13*, or *ATG17* completely disrupted Vps34 phosphorylation upon nitrogen starvation (Figure 20A), as expected. On the contrary, Vps34 phosphorylation in cells deleted for other downstream *ATG* genes (*atg3*Δ, *atg8*Δ, *atg11*Δ, *atg12*Δ, and *atg18*Δ) was comparable to that of wild-type cells (Figure 20B), indicating that a functional Atg1 complex, not a functional autophagy, is necessary for Vps34 phosphorylation. In addition to its kinase activity, Atg1 has a structural role in autophagy regulation (Abeliovich et al., 2003; Stjepanovic et al., 2014), leaving the possibility that other unknown kinases recruited by Atg1 might phosphorylate Vps34. To check this hypothesis, I examined Vps34 phosphorylation in cells expressing Atg1^{D211A}, a kinase-dead variant of Atg1 (Matsuura et al., 1997). As confirmed above, deletion of *ATG1* entirely eliminated phosphorylation of Vps34 upon nitrogen starvation, and reconstitution of wild-type Atg1 recovered Vps34 phosphorylation (Figure 21). However, expression of Atg1^{D211A} could not restore this phosphorylation. This result

demonstrates that the kinase activity of Atg1, not its structural role, is required for Vps34 phosphorylation under nitrogen starvation in vivo.

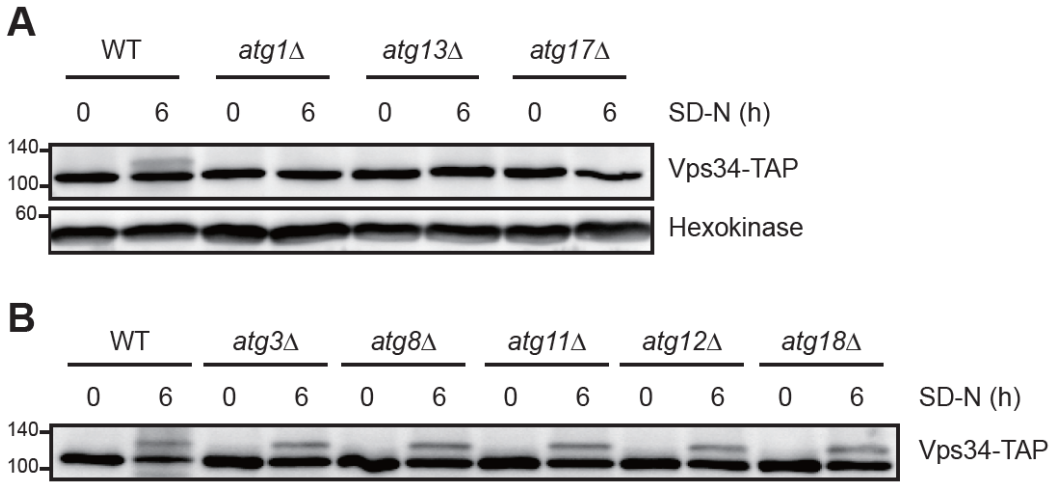

Figure 20. Functional Atg1 complex, not other downstream Atg proteins, is necessary for Vps34 phosphorylation.

(**A**) WT, *atg1*Δ, *atg13*Δ, and *atg17*Δ cells expressing Vps34-TAP were grown to mid-log phase in YPD medium (SD-N 0 h) and incubated in SD-N medium for 6 h. Cell extracts were analyzed by immunoblotting with an anti-IgG antibody as described in the Materials and methods. Hexokinase was used as an internal control. (**B**) Vps34-TAP-expressing wild-type (WT), *atg3*Δ, *atg8*Δ, *atg11*Δ, *atg12*Δ, and *atg18*Δ cells were grown to mid-log phase in YPD medium (SD-N 0 h) and incubated in SD-N medium for 6 hours. Cells extracts were analyzed by immunoblotting with an anti-IgG antibody. A representative image of at least three independent experiments is shown. (**A** and **B**) The molecular weight markers (kDa) are indicated to the left of the blots. A representative data of at least three independent experiments are shown.

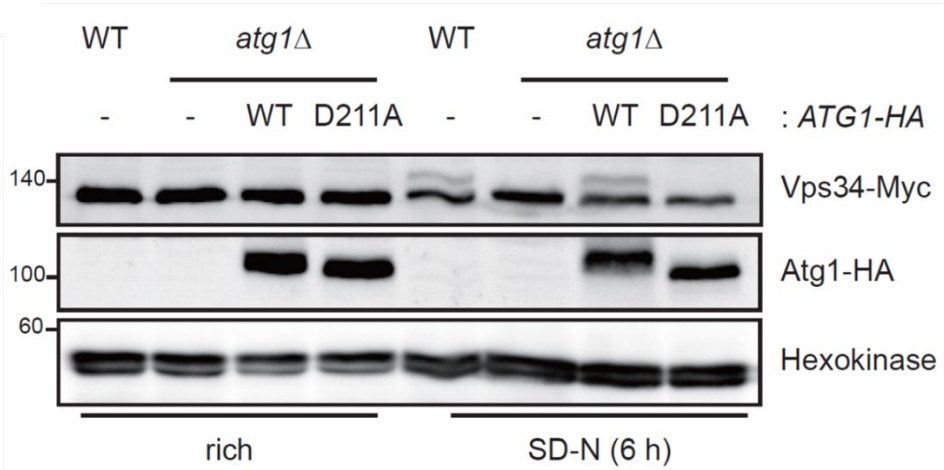

Figure 21. The kinase activity of Atg1 is required for Vps34 phosphorylation.

WT cells harboring an empty vector and *atg1*Δ cells harboring an empty vector or vectors expressing WT Atg1 or Atg1^{D211A} were grown to mid-log phase in SC medium (rich) and incubated in SD-N medium for 6 h. Cell extracts were analyzed by immunoblotting with an anti-Myc antibody or anti-HA antibody as described in the Materials and methods. Hexokinase was used as an internal control. The molecular weight markers (kDa) are indicated to the left of the blots. A representative data of at least three independent experiments are shown.

A recent study has revealed that Atg1 directly phosphorylates Vps34 in vitro, as confirmed by the incorporation of ^{32}P from [γ-^{32}P]-ATP (Schreiber *et al.*, 2021). To verify this, an in vitro Atg1 kinase assay was performed using immunoprecipitated Vps34-Myc and Atg13-TAP from *atg1*Δ cells as substrates and analyzed the mobility shifts of both proteins. In order to specifically examine Atg1-dependent phosphorylation and to exclude signals from autophosphorylation of Vps34, a kinase-dead Vps34^{D731N}-Myc (Vps34^{KD}-Myc) was used as a substrate. In accordance with previous reports (Kira *et al.*, 2021; Schreiber *et al.*, 2021), the affinity-purified Atg1 phosphorylated Atg13 but Atg1^{D211A} did not (Figure 22A, upper), as confirmed by the reduced mobility of Atg13 observed in both standard SDS-PAGE and Phos-tag SDS-PAGE, which enhances the mobility shifts of phosphorylated proteins (Kinoshita et al., 2006). Although Vps34 was already phosphorylated to some extent before Atg1 reaction, noticeable band separation of Vps34 was induced by reaction with wild-type Atg1, while Atg1^{D211A} did not induce this mobility retardation (Figure 22A, lower). This data suggests that Vps34 can be a substrate of Atg1 kinase. Notably, however, in vitro Atg1 reaction did not change the mobility of Vps34 in standard SDS-PAGE.

In order to investigate whether Atg1 can selectively phosphorylate Vps34 in complex I over Vps34 in complex II, an in vitro Atg1 kinase assay was performed using Atg14-TAP- or Vps38-TAP-immunoprecipitates from Vps34^{KD}-Myc-expressing *atg1*Δ cells as substrates. Figure 22B demonstrates that Atg1 could phosphorylate Vps34^{KD} contained in Atg14-TAP-immunoprecipitates. Remarkably, Atg1 could also phosphorylate Vps34 in Vps38-TAP-immunoprecipitates in a

similar manner to Vps34 in complex I. This result suggests that Atg1 is able to phosphorylate Vps34 in both complex I and II in vitro. Next, I examined whether Atg1 directly phosphorylates the 12 S/T residues using $Vps34^{KD}$-Myc and $Vps34^{12A+KD}$-Myc contained in Atg14-immunocomplex as substrates. In agreement with Figure 22B, Atg1 phosphorylated $Vps34^{KD}$ in complex I (Figure 22C). Interestingly, however, the Atg1-induced mobility retardation that was detectable with $Vps34^{KD}$ was not observed with $Vps34^{12A+KD}$, suggesting that the 12 S/T residues contain the Atg1 target residues. Taken together, these data suggest that Atg1 kinase activity is required for in vivo phosphorylation of Vps34 and that Atg1 can directly phosphorylate some of the 12 S/T residues of Vps34 in vitro, even though Atg1 does not phosphorylate all of the residues responsible for the mobility shift of Vps34. In addition, Atg1 does not seem to discriminate the type of Vps34 complex as a substrate in vitro.

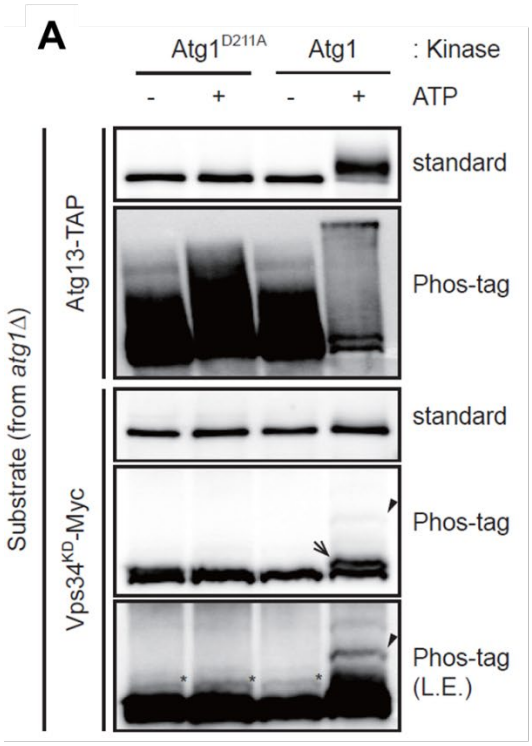
A
Atg1D211A
Atg1
: Kinase
- + - +
ATP
Substrate (from atg1Δ)
Atg13-TAP
standard
Phos-tag
Vps34KD-Myc
standard
Phos-tag
Phos-tag
(L.E.)

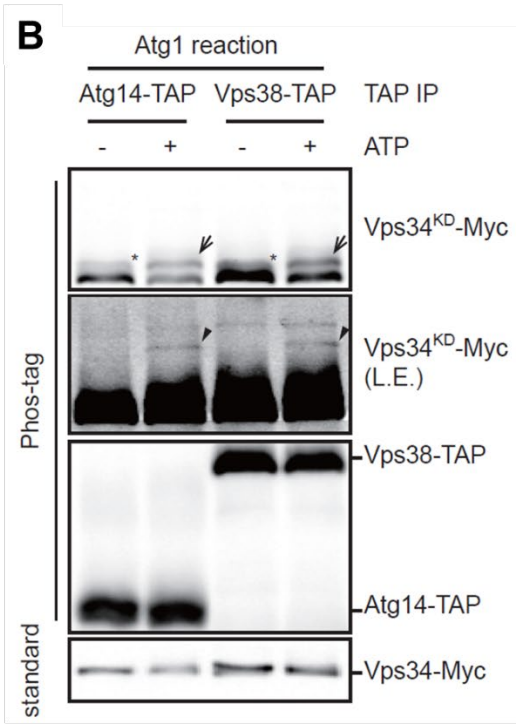
B
Atg1 reaction
Atg14-TAP
Vps38-TAP
TAP IP
- + - +
ATP
Phos-tag
Vps34KD-Myc
Vps34KD-Myc
(L.E.)
Vps38-TAP
Atg14-TAP
standard
Vps34-Myc

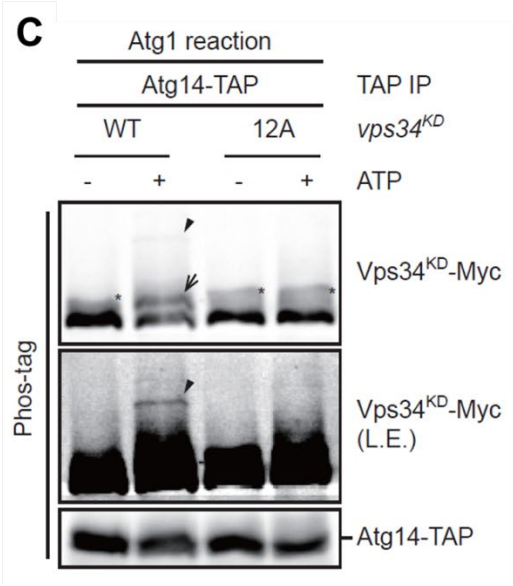
C
Atg1 reaction
Atg14-TAP
TAP IP
WT
12A
vps34KD
- + - +
ATP
Phos-tag
Vps34KD-Myc
Vps34KD-Myc
(L.E.)
Atg14-TAP

Figure 22. Atg1 phosphorylates Vps34 in vitro.

(**A**) Vps34^{KD}-Myc obtained from nitrogen-starved (SD-N 6 h) *atg1*Δ cells was incubated with HA-tagged WT Atg1 or Atg1^{D211A} isolated from nitrogen-starved (SD-N 1 h) cells in the presence of ATP. Atg13-TAP purified from *atg1*Δ cells was used as a positive control. (**B**) Atg14-TAP- or Vps38-TAP-immunocomplexes obtained from nitrogen-starved (SD-N 6 h) *atg1*Δ cells expressing Vps34^{KD}-Myc were incubated with HA-tagged WT Atg1 purified from nitrogen-starved (SD-N 1 h) cells in the presence of ATP. (**C**) Atg14-TAP-immunocomplexes obtained from *atg1*Δ cells expressing Vps34^{KD}-Myc or Vps34^{KD+12A}-Myc were incubated with HA-tagged WT Atg1 in the presence of ATP. (**A**-**C**) An in vitro kinase assay was performed as described in the Materials and methods. The results from Phos-tag SDS-PAGE and standard SDS-PAGE are indicated beside the blots. Asterisks indicate already phosphorylated protein bands of Vps34 before Atg1 reaction. Arrows and arrowheads indicate phosphorylation bands induced by Atg1. L.E. indicates long exposure. A representative image of at least three independent experiments is shown.

3-5. Specific localization of Vps34 complex I to the PAS enables the complex I-specific phosphorylation of Vps34 under nitrogen starvation

The above result that Atg1 can phosphorylate both Vps34 complexes in vitro raises a question about a molecular mechanism that allows the complex I-specific phosphorylation of Vps34. Given that Atg1 phosphorylates various substrates at the PAS and that Vps34 complex I localizes at the PAS during autophagy activation, it is likely that Atg1 phosphorylates Vps34 at the PAS; thus, the PAS localization of Vps34 might be crucial for the complex I-specific Vps34 phosphorylation. To test this possibility, Vps34 phosphorylation was examined upon deletion of *ATG9*, which substantially hinders the complex I localization to the PAS (Suzuki *et al.*, 2007; Suzuki *et al.*, 2015). As expected, phosphorylation of Vps34 was markedly decreased in *atg9*Δ cells (Figure 23A). To test whether the PAS localization of Vps34 complex I is indeed disrupted in *atg9*Δ cells, the targeting of Atg14, a specific subunit of Vps34 complex I, to the PAS was analyzed by measuring Atg14 dots colocalized with Atg13, a PAS marker protein (Yamamoto *et al.*, 2016), under nitrogen starvation. Consistent with previous reports (Suzuki *et al.*, 2007; Suzuki *et al.*, 2015), Atg14 failed to normally localize to the PAS in *atg9*Δ cells under nitrogen starvation (Figure 23B). These data suggest that Atg9 is necessary for efficient phosphorylation of Vps34 under nitrogen starvation.

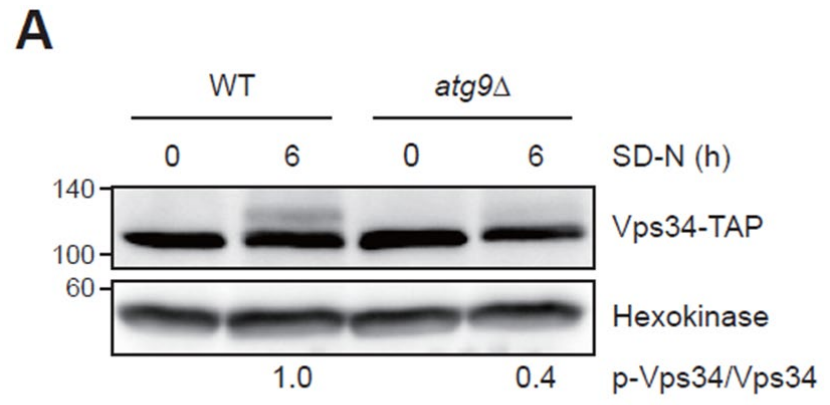
A
WT
atg9Δ
0
6
0
6
SD-N (h)
140
100
60
Vps34-TAP
Hexokinase
1.0
0.4
p-Vps34/Vps34

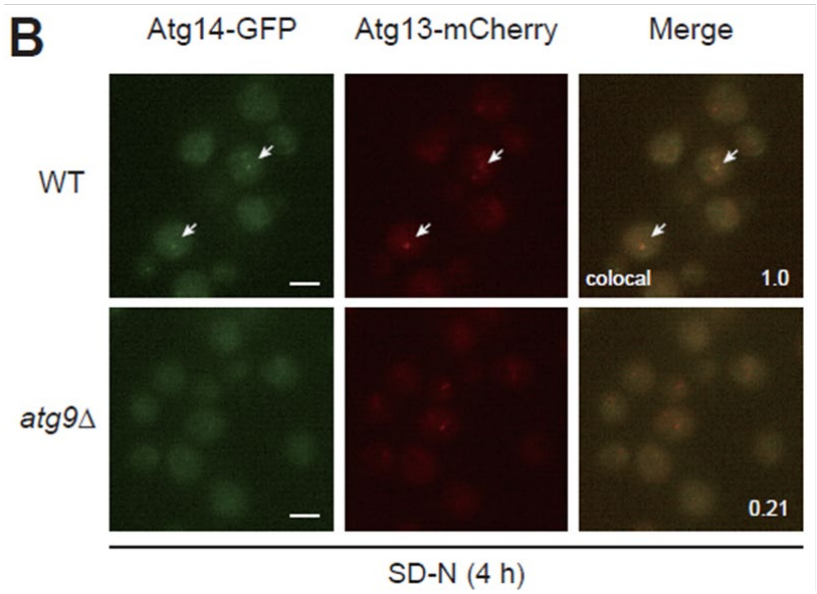
B
Atg14-GFP
Atg13-mCherry
Merge
WT
atg9Δ
colocal
1.0
0.21
SD-N (4 h)

Figure 23. Atg9 is required for Vps34 phosphorylation.

(**A**) WT and *atg9*Δ cells expressing Vps34-TAP were grown to mid-log phase in YPD medium (SD-N 0 h) and incubated in SD-N for 6 h. The relative ratio of phosphorylated Vps34 to unphosphorylated Vps34 was normalized against that of WT cells (set to 1.0) and is shown below each lane. Hexokinase was used as an internal control. The molecular weight markers (kDa) are indicated to the left of the blots. A representative data of at least three independent experiments are shown. (**B**) Colocalization of Atg14-2xGFP and Atg13-2xmCherry in WT and *atg9*Δ cells was examined after 4 h of incubation in SD-N medium. The PAS localization of Atg14 was analyzed by measuring the ratio of Atg13-2xmCherry puncta colocalized with Atg14-2xGFP. The relative colocalization value normalized against that of WT cells (set to 1.0) is shown on the lower right corner of each merged image. At least 300 Atg13-2xmCherry puncta were analyzed for each strain. Colocalized puncta are indicated by white arrows. Scale bars, 2 μm

Vps30 is composed of three domains: the N-terminal domain (NTD), the coiled-coil domain (CCD), and the β-α repeated, autophagy-specific (BARA) domain (Noda et al., 2012). It has been shown that the BARA domain of Vps30 is crucial for the recruitment of complex I to the PAS, whereas the NTD of Vps30 is not required for the PAS targeting of complex I (Noda *et al.*, 2012). To exclude the possibility that unknown functions of Atg9 might affect Vps34 phosphorylation, I made use of Vps30 truncation mutants to specifically block the PAS localization of complex I (Figure 24A). As shown in a previous report (Noda *et al.*, 2012), deletion of the BARA domain severely impaired the PAS targeting of Atg14, while *vps30*$^{\Delta NTD}$ cells showed robust, although slightly decreased, Atg14 recruitment to the PAS (Figure 24B). Next, phosphorylation of Vps34 in cells expressing Vps30 truncation mutants was measured upon nitrogen starvation. Overexpression system under the *ADH1* promoter was used to express Vps30 truncation mutants because the stability of Vps30$^{\Delta NTD}$ mutant was remarkably impaired under nitrogen starvation (Figure 24C). As demonstrated in Figure 9A, deletion of *VPS30* completely disrupted Vps34 phosphorylation under nitrogen starvation. When wild-type Vps30 was reconstituted, irrespective of the expression level, phosphorylation of Vps34 was nearly entirely recovered. Vps34 phosphorylation levels in Vps30$^{\Delta NTD}$-expressing cells were also comparable with those of wild-type cells. Remarkably, however, reintroduction of Vps30$^{\Delta BARA}$ to *vps30*Δ cells could not restore phosphorylation of Vps34 under nitrogen starvation, indicating that the BARA domain of Vps30 is necessary for the phosphorylation of Vps34. Taken together, these data suggest that recruitment of Vps34 complex I to the PAS is necessary for Vps34 phosphorylation under nitrogen starvation.

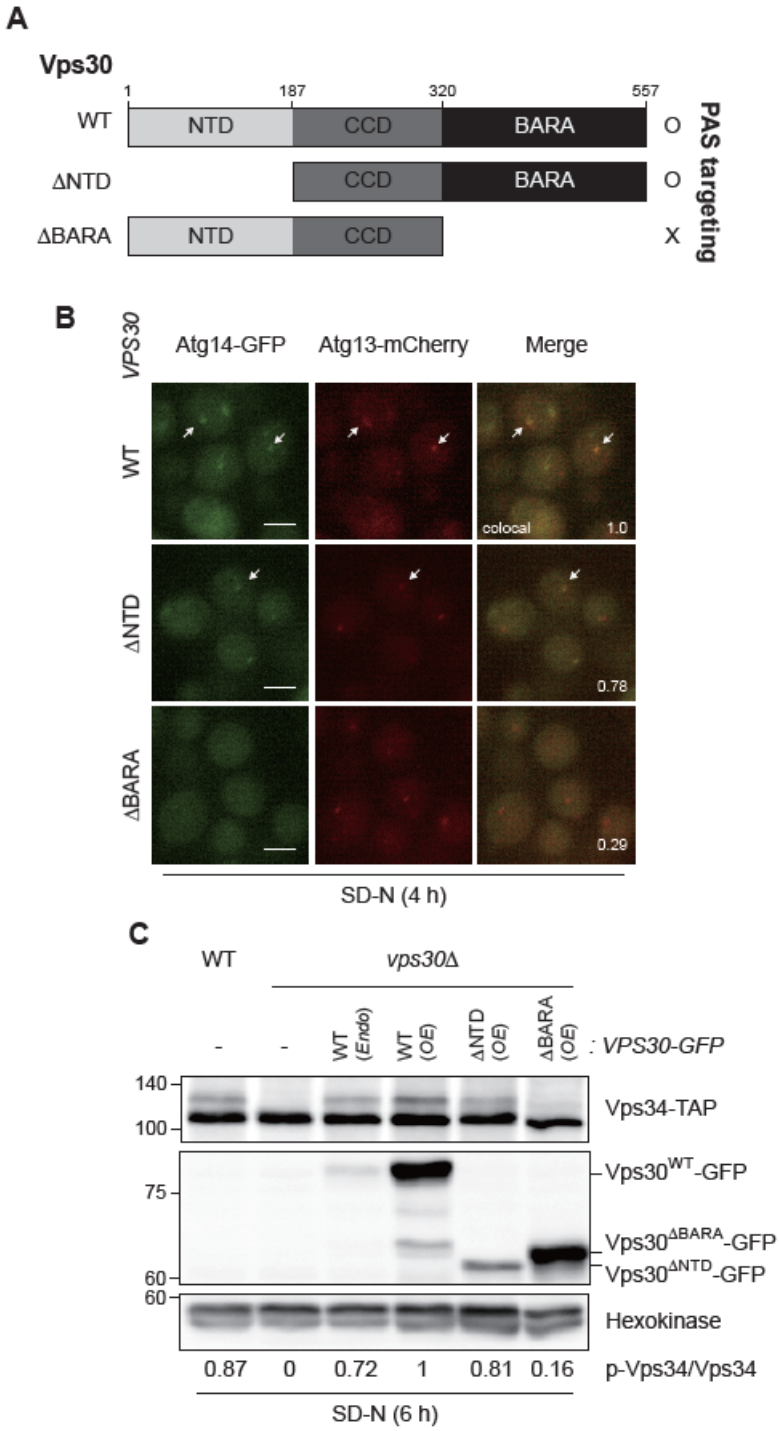
A
Vps30
1
187
320
557
WT
NTD
CCD
BARA
O
ΔNTD
CCD
BARA
O
ΔBARA
NTD
CCD
X
PAS targeting
B
VPS30
Atg14-GFP
Atg13-mCherry
Merge
WT
colocal
1.0
ΔNTD
0.78
ΔBARA
0.29
SD-N (4 h)
C
WT
vps30Δ
-
-
WT (Endo)
WT (OE)
ΔNTD (OE)
ΔBARA (OE)
: VPS30-GFP
140
100
Vps34-TAP
75
Vps30WT-GFP
Vps30ΔBARA-GFP
60
Vps30ΔNTD-GFP
60
Hexokinase
0.87
0
0.72
1
0.81
0.16
p-Vps34/Vps34
SD-N (6 h)

Figure 24. The BARA domain of Vps30 is necessary for Vps34 phosphorylation.

(**A**) Vps30 truncation mutants used in this study. ΔNTD, Vps30 deleted with the NTD. ΔBARA, Vps30 deleted with the BARA domain. (**B**) Colocalization of Atg14-2xGFP with Atg13-2xmCherry in cells expressing the indicated Vps30 variants was examined after 4 h of incubation in SD-N medium. The ratio of Atg13-2xmCherry dots colocalized with Atg14-2xGFP was examined. The relative colocalization value normalized against that of WT cells (set to 1.0) is shown on the lower right corner of each merged image. At least 300 Atg13-2xmCherry puncta were analyzed for each strain. Colocalized dots are represented by white arrows. Scale bars, 2 μm. (**C**) Vps34 phosphorylation was examined in WT cells harboring an empty vector and *vps30*Δ cells harboring an empty vector or vectors expressing WT Vps30-GFP under the endogenous promoter (WT Endo), WT Vps30-GFP under the *ADH1* promoter (WT OE), $Vps30^{\Delta NTD}$-GFP under the *ADH1* promoter (ΔNTD OE), or $Vps30^{\Delta BARA}$-GFP under the *ADH1* promoter (ΔBARA OE) after 6 h of nitrogen starvation. The relative ratio of phosphorylated Vps34 to unphosphorylated Vps34 was normalized against that of WT (OE) cells (set to 1.0) and is shown below each lane. Cell lysates were analyzed by immunoblotting as described in the Materials and methods. Hexokinase was used as a loading control. The positions of molecular-weight markers (in kDa) are indicated to the left of the blots. A representative image of at least three independent experiments is shown.

3-6. Atg1-dependent phosphorylation of Vps34 is required for normal regulation of the PAS dynamics under nitrogen starvation

It has been previously shown that Atg1 phosphorylates Atg9 and this phosphorylation promotes Atg18 recruitment to the PAS (Papinski *et al.*, 2014). Based on this observation, it has been proposed that Atg9 phosphorylation by Atg1 may recruit the Vps34 complex I to the PAS, thereby gathering Atg18, a phosphoinositide-binding protein necessary for autophagy, to the PAS (Papinski and Kraft, 2014). Given this, the above results indicating that Vps34 phosphorylation requires Atg1 kinase (Figure 20-22) but is dispensable for its own catalytic activity (Figure 19) prompted a question about whether Atg1-dependent Vps34 phosphorylation is required for the targeting of Vps34 complex I to the PAS. To answer this question, the PAS recruitment of Atg14 in *vps34* mutants was analyzed under nitrogen starvation (Figure 25). Contrary to the above assumption, the colocalization of Atg14 with Atg13 was not affected in either $vps34^{12A}$ or $vps34^{12D}$ cells, indicating that Vps34 phosphorylation is not required for the PAS recruitment of Vps34 complex I. Consistently, the localization of Atg14 to the PAS in *atg1*Δ and $atg1^{D211A}$ cells was also comparable to that of wild-type cells (Figure 26). Because the loss of Atg1 function leads to a strong accumulation of the PAS (Schreiber *et al.*, 2021), the PAS accumulation was also analyzed in cells expressing *vps34* mutants. However, I could not observe any evidence of the involvement of Vps34 phosphorylation in the PAS assembly (Figure 27). Collectively, these data indicate that Atg1-dependent phosphorylation of Vps34 is not required for the recruitment of Vps34 complex I to the PAS nor for the PAS assembly.

Because both Atg1 and Vps34 are essential for targeting Atg18 to the PAS (Obara *et al.*, 2008; Papinski *et al.*, 2014; Suzuki *et al.*, 2007), the PAS localization of Atg18 in *atg1* and *vps34* mutants were then analyzed by examining the colocalization of Atg18 with Atg13. As previously described (Papinski *et al.*, 2014), Atg18 recruitment to the PAS was severely disrupted in the absence of Atg1 or its kinase activity (Figure 28). Subsequently, I performed the same experiments in *vps34* mutant cells. In wild-type cells, approximately 26% of Atg13 puncta were colocalized with Atg18 (Figure 29). Interestingly, the ratio of Atg13 dots colocalized with Atg18 was significantly increased in $vps34^{12A}$ cells. On the other hand, the PAS targeting of Atg18 in cells expressing phospho-mimetic $Vps34^{12D}$ mutant was comparable to that of wild-type cells. These data indicate that Atg18 is more accumulated at the PAS under nitrogen starvation in the absence of Vps34 phosphorylation. The C-terminal tagging of fluorescent proteins to the Atg proteins used above does not appear to result in a severe defect in autophagy, as shown in Figure 30.

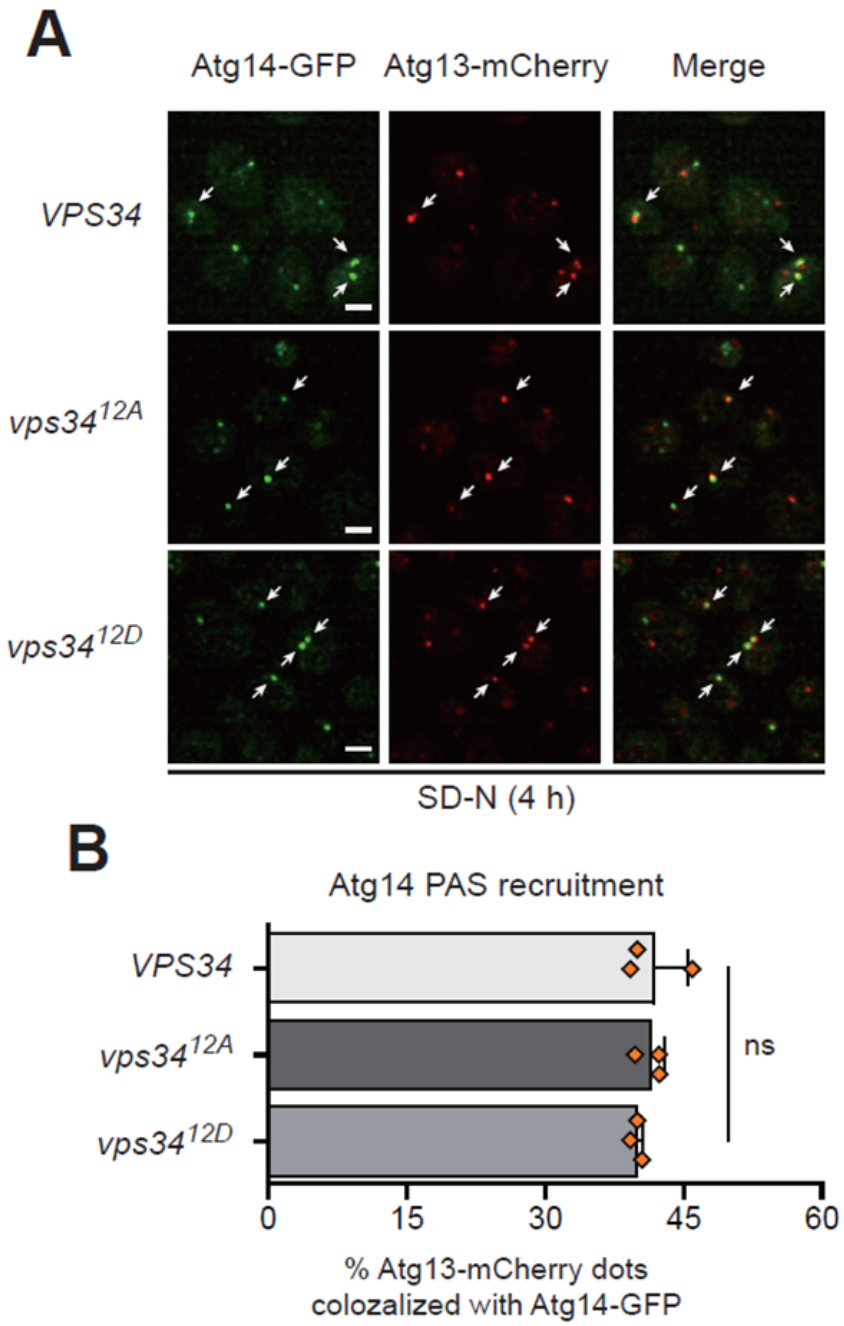
A
Atg14-GFP
Atg13-mCherry
Merge
VPS34
vps34 12A
vps34 12D
SD-N (4 h)
B
Atg14 PAS recruitment
VPS34
vps34 12A
vps34 12D
ns
0
15
30
45
60
% Atg13-mCherry dots
colozalized with Atg14-GFP

Figure 25. Vps34 phosphorylation is not necessary for the PAS recruitment of Vps34 complex I.

(**A**) Colocalization of Atg14-2xGFP with Atg13-2xmCherry in cells expressing the indicated Vps34 variants was examined after 4 hours of nitrogen starvation. Colocalized dots are indicated by white arrows. Scale bars, 2 μm. (**B**) Quantification of the ratio of Atg13-2xmCherry dots colocalized with Atg14-2xGFP in (A). At least 150 Atg13-2xmCherry puncta were counted for each measurement. The values represent the averages of three independent experiments. Error bars indicate the standard deviations. ns, not significant.

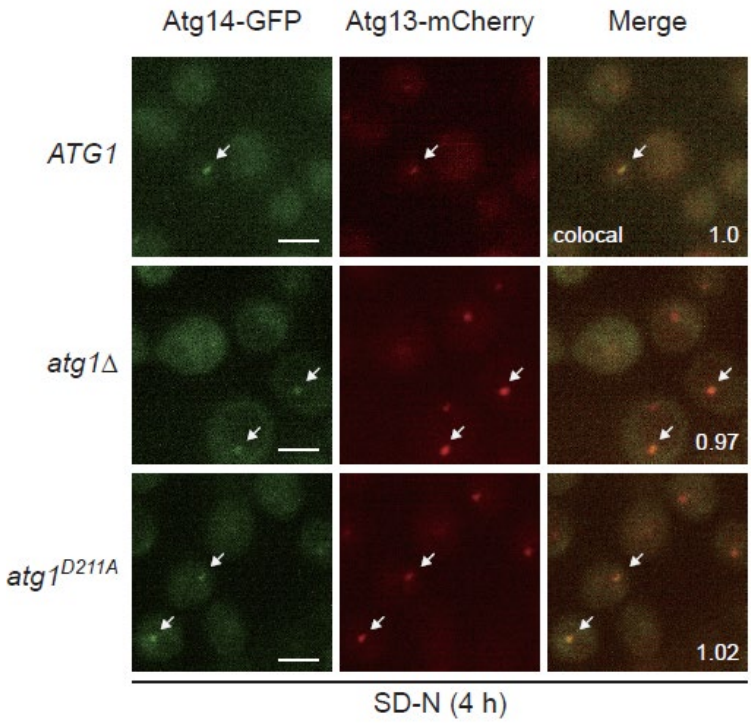

Figure 26. Atg1 is not required for the PAS recruitment of Vps34 complex I.

The PAS recruitment of Atg14 was analyzed after 4 hours of nitrogen starvation by measuring the ratio of Atg13-2xmCherry dots colocalized with Atg14-2xGFP. The relative colocalization value normalized against that of WT cells (set to 1.0) is shown on the lower right corner of each merged image. At least 300 Atg13-2xmCherry puncta were analyzed for each strain. Colocalized puncta are indicated by white arrows. Scale bars, 2 μm

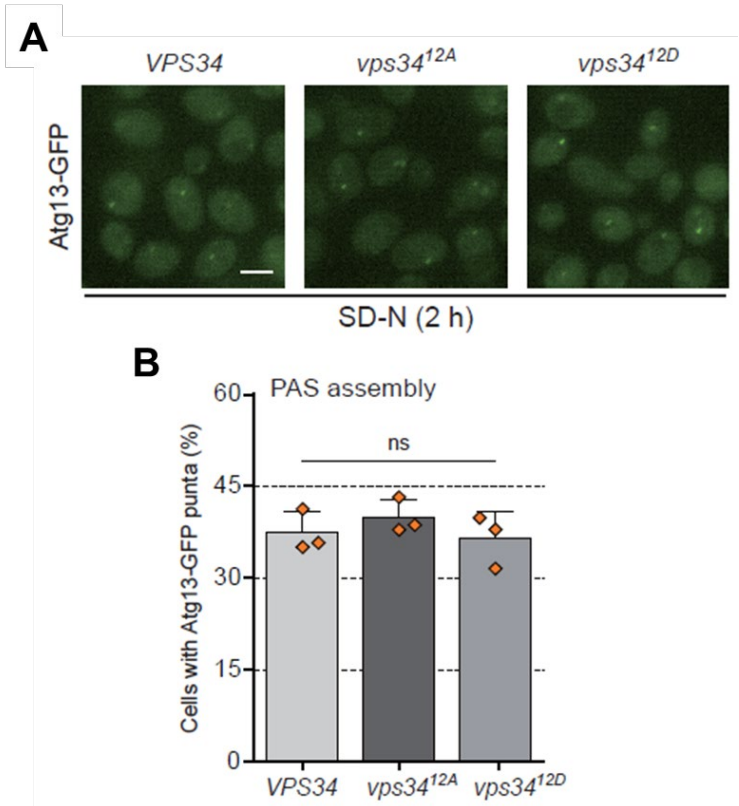

Figure 27. Vps34 phosphorylation is not required for the regulation of the PAS assembly.

(**A**) Atg13-2xGFP dot formation was analyzed in cells expressing the indicated Vps34 variants after incubation in SD-N for 2 h. (**B**) Quantification of the number of Atg13-GFP puncta per cell in (**A**). The values represent the averages of three independent experiments. Error bars indicate the standard deviations. ns, not significant.

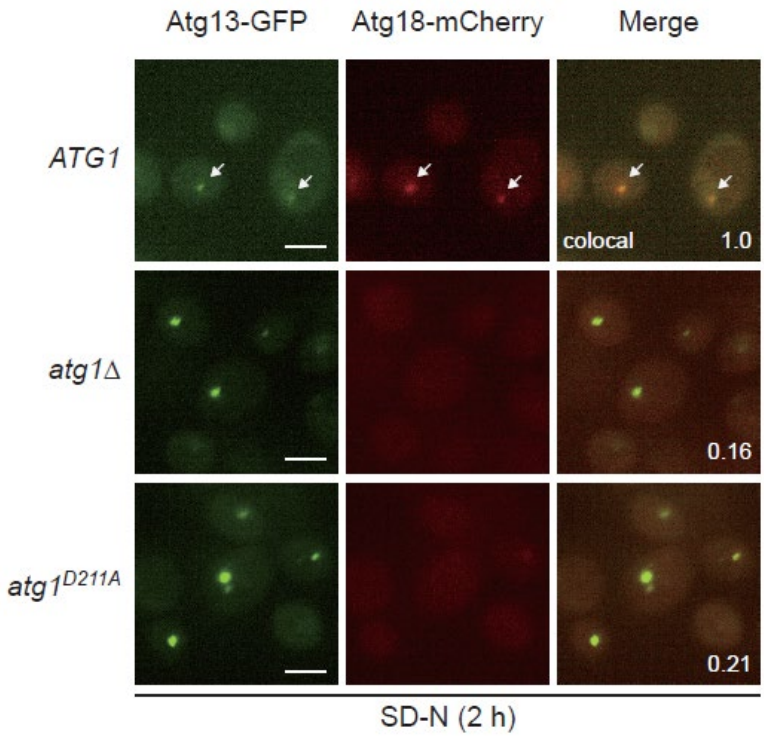

Figure 28. Atg1 is essential for Atg18 targeting to the PAS.

The PAS recruitment of Atg18 was analyzed after 2 hours of nitrogen starvation by measuring the ratio of Atg13-2xGFP dots colocalized with Atg14-2xmCherry. The relative colocalization value normalized against that of WT cells (set to 1.0) is shown on the lower right corner of each merged image. At least 300 Atg13-2xGFP dots were analyzed for each strain. Colocalized puncta are indicated by white arrows. Scale bars, 2 μm.

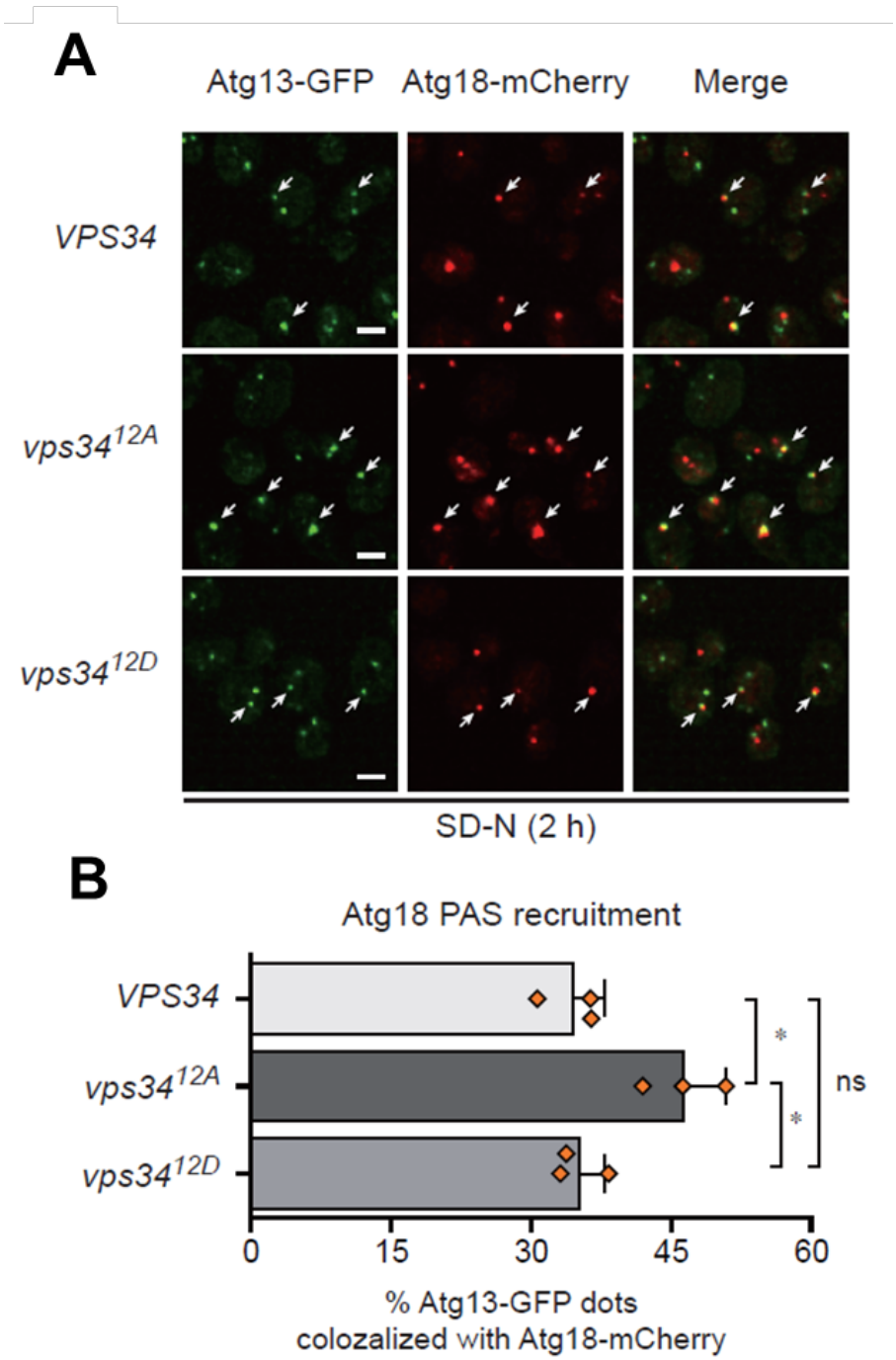
A
Atg13-GFP
Atg18-mCherry
Merge
VPS34
vps34 12A
vps34 12D
SD-N (2 h)
B
Atg18 PAS recruitment
VPS34
vps34 12A
vps34 12D
*
*
ns
0
15
30
45
60
% Atg13-GFP dots
colozalized with Atg18-mCherry

Figure 29. Atg18 is accumulated in cells expressing Vps34^{12A} mutant.

(**A**) Colocalization of Atg18-2xmCherry with Atg13-2xGFP in cells expressing the indicated Vps34 variants was examined after 2 h of nitrogen starvation. Colocalized dots are indicated by white arrows. Scale bars, 2 μm. (**B**) Quantification of the ratio of Atg13-2xmCherry dots colocalized with Atg14-2xGFP in (A). At least 150 Atg13-2xGFP puncta were counted for each measurement. The values represent the averages of three independent experiments. Error bars indicate the standard deviations. Asterisks indicate significant differences compared with WT cells (two-tailed Student's *t*-test): $*p < 0.05$; $**p < 0.01$; ns, not significant.

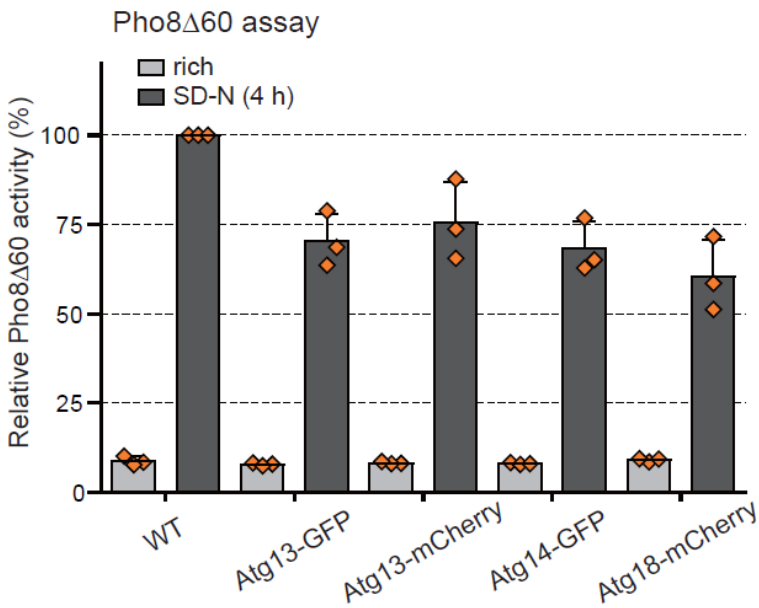

Figure 30. Functionality of the fluorescent protein-tagged Atg proteins used in this study.

The functionality of fluorescent protein-tagged Atg proteins used in this study. Cells expressing the indicated fluorescent protein-tagged Atg proteins were grown to mid-log phase in YPD medium (SD-N 0 h) and incubated in SD-N medium for 4 h. The Pho8Δ60 assay was performed as described in the Materials and methods.

It has been previously described that Atg8 recycling at the PAS is severely disrupted without Atg1 kinase activity and thus results in extended GFP-Atg8 dots lifetimes (Cheong et al., 2008; Xie et al., 2008). The prolonged GFP-Atg8 puncta lifespan has been also demonstrated in cells with defective Atg18 dynamics (Cebollero *et al.*, 2012; Steinfeld et al., 2021). Given the above results that cells expressing the nonphosphorylatable $Vps34^{12A}$ showed Atg18 accumulation at the PAS, it is possible that GFP-Atg8 puncta lifetime might be indeed affected in those cells. To test this, the lifetime of GFP-Atg8 was analyzed using time-lapse microscopy. In wild-type cells, GFP-Atg8 puncta lasted for an average of 5.44 minutes after 6 hours of nitrogen starvation (Figure 31). On the contrary, GFP-Atg8 puncta in $Vps34^{12A}$-expressing cells lasted for 6.66 minutes on average, which is approximately 22% longer than the GFP-Atg8 lifespans of wild-type cells. Remarkably, GFP-Atg8 puncta showing prominently longer lifetimes (≥12 minutes) were observed in $Vps34^{12A}$-expressing cells, whereas they were absent in cells expressing wild-type Vps34. It is likely that an extended lifetime of GFP-Atg8 dots causes accumulation of Atg8 punta in cells, resulting in an increase in the number of Atg8 puncta per cell. In agreement with this assumption, the number of GFP-Atg8 puncta was indeed increased in $Vps34^{12A}$-expressing cells (Figure 32). Collectively, these data suggest that Vps34 phosphorylation is required for normal dynamics of downstream Atg proteins including Atg18 and Atg8 at the PAS.

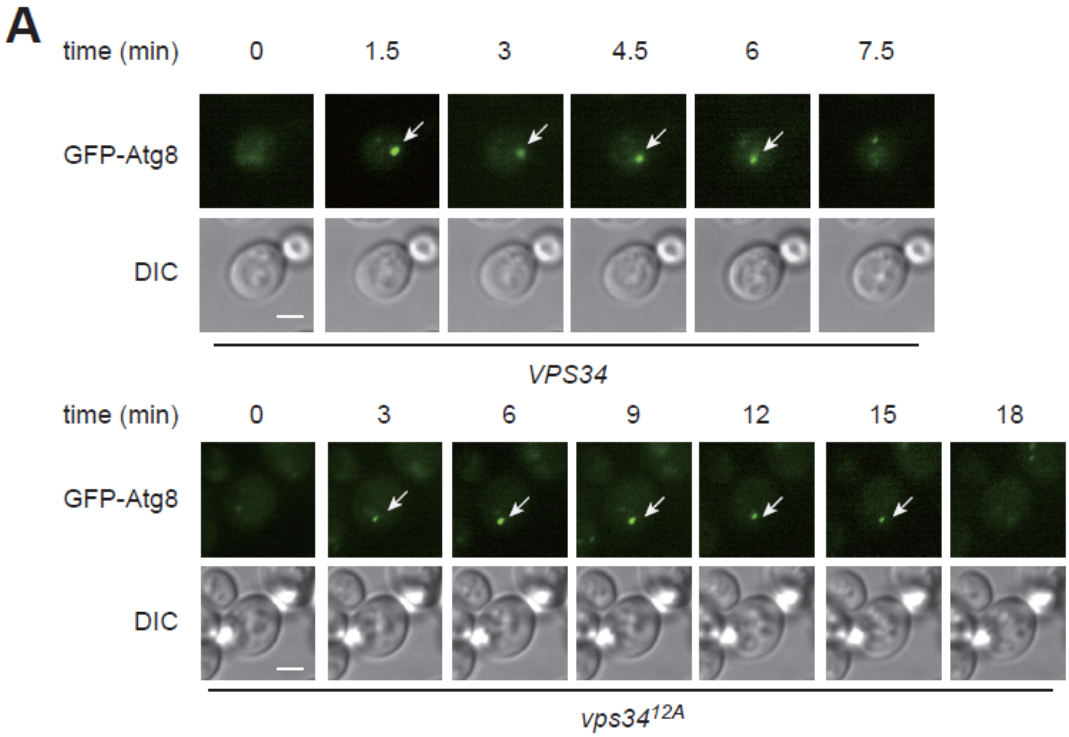
A
time (min)
0
1.5
3
4.5
6
7.5
GFP-Atg8
DIC
VPS34
time (min)
0
3
6
9
12
15
18
GFP-Atg8
DIC
vps34^12A

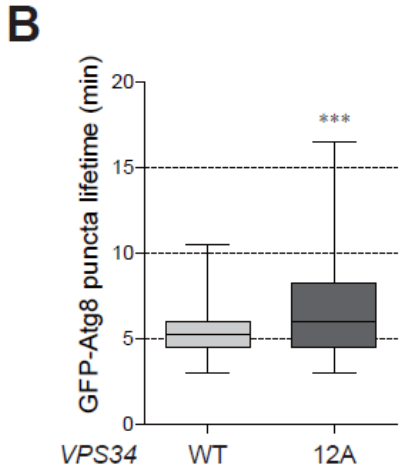
B
GFP-Atg8 puncta lifetime (min)
20
15
10
5
0
***
VPS34
WT
12A

Figure 31. Vps34 phosphorylation is required for normal regulation of the GFP-Atg8 lifespan.

(**A**) GFP-Atg8-expressing *vps34*Δ cells harboring vectors expressing WT Vps34 or Vps34^{12A} were incubated in SD-N for 6 h and then imaged every 45 seconds for 40 minutes. The GFP-Atg8 dots being traced are denoted by white arrows. Scale bars, 2 μm. (**B**) Box plot depicting the average lifetimes of GFP-Atg8 puncta shown in (A). Lifetimes of 130 puncta of GFP-Atg8 for each strain were examined. The central line represents the median, and the bottom and top edges of the box represent the interquartile range. The box plot whiskers indicate the maximum/minimum data points. Asterisks means significant differences compared with WT cells (two-tailed Student's *t*-test): $***p < 0.001$.

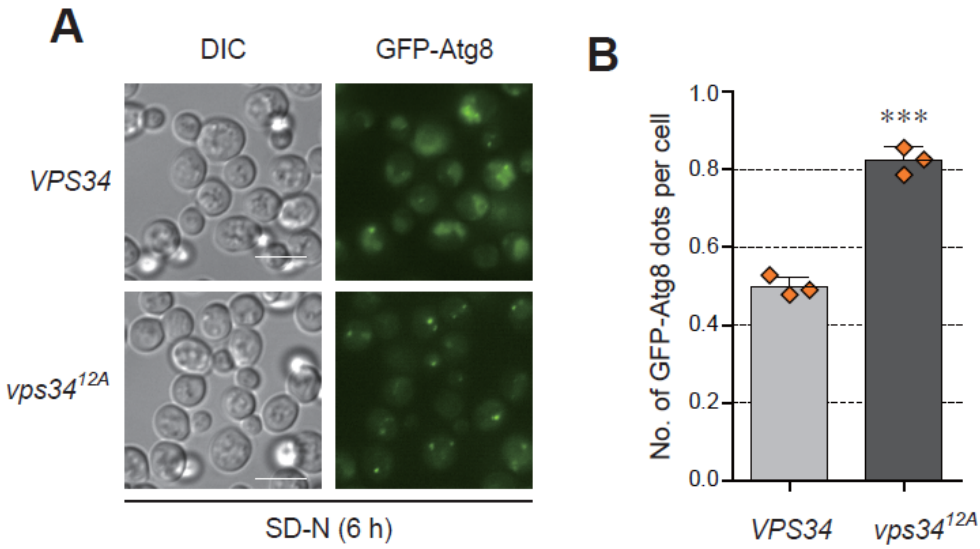

Figure 32. Atg8 is accumulated in cells expressing Vps34^{12A} mutant.

(**A**) GFP-Atg8 puncta formation was analyzed in cells expressing WT Vps34 or Vps34^{12A} after incubation in SD-N medium for 6 h. Scale bars, 5 μm. (**B**) Quantification of the numbers of GFP-Atg8 puncta per cell shown in (A). The values represent the averages of three independent experiments. Error bars indicate the standard deviations. Asterisks indicate significant differences compared with WT cells (two-tailed Student's *t*-test): $***p < 0.001$

4. DISCUSSION

In this study, I show that Vps34 is a substrate of Atg1 kinase and that phosphorylation of Vps34 is required for the robust autophagy activity. Defects in Vps34 phosphorylation lead to abnormal dynamics of Atg18 and Atg8 at the PAS, but do not affect its own PtdIns3K activity nor the PAS recruitment of Vps34 complex I itself. Notably, Vps34 with decreased mobility in SDS-PAGE has been described in both yeast and mammalian systems (Araki *et al.*, 2013; Egan *et al.*, 2015). In addition, the phosphoregulation mechanisms of the Vps34 complex by numerous kinases including AMPK and PDK, have been widely explored in mammalian systems (Eisenberg-Lerner and Kimchi, 2012; Zhang *et al.*, 2016). Nevertheless, our knowledge about the significance of direct phosphorylation of Vps34 by Atg1/ULK1 regarding autophagy regulation is still very limited in both yeast and mammalian systems. This is presumably due to the following natures of this phosphorylation: (*i*) Vps34 autophosphorylates itself, which makes it challenging to identify passively regulated phosphoresidues from autophosphorylated residues in IP-MS spectra, and (*ii*) multiple sites are simultaneously phosphorylated, making it frustrating to uncover specific combinations of residues that are important for autophagy regulation. I tried to circumvent the aforementioned issues by (*i*) using a kinase-dead variant of Vps34 in IP-MS analysis (Figure 11) and (*ii*) mutating all of the phosphoresidue candidates to alanine at once (Figure 12). Accordingly, the majority of phosphoresidue candidates identified in IP-MS analysis of wild-type Vps34 did not match with those identified using kinase-dead $Vps34^{D731N}$ (data not shown), which are most likely

autophosphorylated residues. Additionally, though all of the mutation combinations could not be examined, substitution of three consecutive S/T residues of the 12 S/T residues with alanine (Vps34^{3A-1} to Vps34^{3A-4}) had only a minor effect on the mobility shift of Vps34 in SDS-PAGE and autophagy (Figure 12B and 14), while Vps34^{12A}-expressing cells showed complete loss of mobility shift and dysfunctional autophagy. Based on this observation, it is likely that the overall phosphorylation status of the Vps34 helical domain (from S428 to S468) is important for regulating autophagy, rather than phosphorylation of particular one or two sites being essential. Although the exact phosphorylation sites or combinations of phosphorylation sites required for autophagy activation could not be determined, this study is valuable in that it reveals the functional and physiological significance of Vps34 phosphorylation in autophagy activation, which has previously been difficult to unveil.

As shown in Figure 9A, Vps34 phosphorylation was totally abolished when *VPS15*, *VPS30*, or *ATG14* was deleted. Given that deletion of *VPS15* or *VPS30* causes complete disruption of both PtdIns3K complexes and that *ATG14* deletion leads to the failure of complex I assembly (Kihara *et al.*, 2001), it is likely that Vps34 can be phosphorylated only when stable complex I is formed. Consistent with this, *VPS38* deletion, which specifically blocks complex II formation, had no effect on Vps34 phosphorylation. Substantial, but not entire, inhibition of Vps34 phosphorylation observed in *atg38*Δ cells (Figure 9B) also supports this idea because a considerable portion of complex I can be formed in the absence of Atg38 (Ohashi et al., 2016). It has been previously shown that Atg38 promotes Vps34 complex I localization to the PAS (Araki *et al.*, 2013). Given that the PAS localization of Vps34 is necessary for its phosphorylation (Figure 23, 24), it is assumable that one of the

major roles of Atg38 in autophagy activation is to facilitate phosphorylation of Vps34 in complex I by (*i*) holding Vps15-Vps34 and Atg14-Vps30 subcomplexes together, thereby stabilizing the complex I, and by (*ii*) guiding Vps34 complex I to the PAS, where Vps34 can be phosphorylated. In line with this notion, *atg38*Δ cells show a relatively mild defect in nonselective autophagic activity but normal selective autophagy activity (Araki *et al.*, 2013), a phenotype similar to that of the non-phosphorylatable $vps34^{12A}$ cells in this study (Figure 14 and Figure 16). A more detailed relationship between Atg38 and Vps34 phosphorylation remains to be investigated.

As shown in Figure 10, Vps34 in complex I is selectively phosphorylated over Vps34 in complex II under nitrogen starvation. This is consistent with the results that Vps34 phosphorylation is specifically required for autophagy regulation, which is the function of complex I, not for CPY sorting, which is the function of complex II. Because both Atg1 and Vps34 complex I localize at the PAS upon autophagy activation while Vps34 complex II does not, it is likely that specific localization to the PAS allows the complex I-specific phosphorylation of Vps34. In agreement with this assumption, Vps34 phosphorylation was disrupted when the PAS targeting of complex I was hindered either by (*i*) deletion of *ATG9* (Figure 23) or by (*ii*) deletion of the BARA domain of Vps30 (Figure 24). Structural factors between complex I and complex II do not seem to determine the complex I-specificity of this phosphorylation, as Atg1 could phosphorylate both Vps34 complexes in vitro (Figure 22B). Based on these findings, I propose that the spatiotemporal regulation of complex I at the PAS is the major determinant for the specific phosphorylation of Vps34 in complex I by Atg1.

Consistent with a previous report (Schreiber *et al.*, 2021), Atg1 could directly phosphorylate Vps34 in complex I (Figure 22). In addition, in vitro Atg1 kinase assay showed that Atg1 does not effectively phosphorylate the Vps34^{12A} mutant compared to wild-type Vps34, implying that the majority of Atg1 target residues are included in the 12 S/T residues (Figure 22C). Nonetheless, Atg1 alone could not induce mobility shift of Vps34 in standard SDS-PAGE (Figure 22A, B), suggesting that Atg1 does not phosphorylate all of the 12 S/T residues. Given that Vps34 was not phosphorylated in the absence of Atg1 kinase activity in vivo (Figure 20, 21), it is likely that, under nitrogen starvation, direct phosphorylation of the Atg1 target sites (some of the 12 S/T residues) of Vps34 is a prerequisite for the subsequent phosphorylation of the other part of the 12 S/T residues by unknown kinase(s). In this regard, phosphorylation of Vps34 under nitrogen starvation is indeed 'Atg1-dependent', and the cooperative action of Atg1 and other unknown kinase(s) seems to be necessary to complete phosphorylation of Vps34. Identification of the unknown kinase(s) responsible for Vps34 phosphorylation would be one of the intriguing issues to be addressed to understand the regulatory mechanism of autophagy.

Figure 29 demonstrates that Atg18 is accumulated at the PAS in the nonphosphorylatable Vps34^{12A}-expressing cells, although the PAS recruitment of Vps34 complex I itself is not affected (Figure 25). The increased colocalization of Atg18 punta with Atg13 could be due to either upregulation of recruitment of Atg18 to the PAS or reduced dissociation of Atg18 from the PAS in Vps34^{12A}-expressing cells. In any case, the above results are surprising in that Atg1 has been shown to promote Atg18 recruitment to the PAS by phosphorylating Atg9 (Papinski *et al.*, 2014). Given that Atg1-dependent phosphorylation of Atg9 and Vps34 function in

an opposite way in regulating Atg18 recruitment to the PAS, it appears that fine-tuning of Atg18 dynamics might be accomplished in part by spatiotemporal phosphorylation of various Atg1 substrates including Atg9 and Vps34. However, it still remains unclear how phosphorylation of Vps34 affects the dynamics of downstream Atg proteins such as Atg18 and Atg8. It has been previously reported that PtdIns3P turnover by the PtdIns3P phosphatase Ymr1 is necessary for autophagosome maturation and the recycling of various Atg proteins (Cebollero *et al.*, 2012). According to that study, Atg18 remains associated with autophagosomes in *ymr1*Δ cells, and the lifetime of Atg8 puncta in *ymr1*Δ cells is longer than that of wild-type cells. Given that Atg18 is accumulated at the PAS and the lifespan of GFP-Atg8 puncta is abnormally extended in $Vps34^{12A}$-expressing cells, it is possible that Vps34 phosphorylation might contribute to the Ymr1 recruitment to the PAS, thereby ensuring PtdIns3P clearance and the recycling of downstream Atg proteins. Alternatively, because some portion of the Atg18 pool has been described to be located in close proximity to PtdIns3K complex I at the PAS (Suzuki et al., 2013), it is also possible that phosphorylated Vps34 complex I might physically repel Atg18, promoting the dissociation of Atg18 from the PAS. A more detailed investigation of how Vps34 phosphorylation is involved in the regulation of the PAS dynamics would be helpful to expand our knowledge about the regulation of the PAS dynamics and autophagy.

It has been previously demonstrated that the release of Atg8 from autophagosome by Atg4-mediated deconjugation promotes efficient autophagosome-vacuole fusion (Yu et al., 2012). Given the extended lifetime of Atg8 punta in $vps34^{12A}$ cells, there is a possibility that, in the absence of Vps34 phosphorylation, partially impaired

release of Atg8 from autophagosome leads to an ineffective fusion between autophagosomes and the vacuole. Electron microscopic analysis would be helpful to reveal whether autophagosome fusion to the vacuole is indeed impaired in *vps34*^{12A} cells. Also, whether Vps34 phosphorylation affects Atg8 deconjugation from or conjugation to the phagophore membrane is the remaining question to be explored. It is likely that the extended Atg8 punta lifetime might be a consequence of accumulated Atg18 at the PAS. Nonetheless, the molecular linkage between Atg18 accumulation and extended Atg8 dynamics is unclear. As a binding partner of Atg18, Atg2 recruitment to the PAS might also be increased in the nonphosphorylatable *vps34* mutant. If this is the case, it is possible that phospholipid provided by Atg2 might exceed the physiological requirement for phagophore expansion, leading to abnormal lipid composition of autophagosome and Atg8 dynamics. Further efforts are needed to unveil the molecular event between Atg18 accumulation and impaired Atg8 dynamics in *vps34*^{12A} cells.

10 S/T residues of the 12 S/T residues (except for S428 and S437) belong to the serine-enriched SUR of the helical domain of Vps34 (from residue 438 to 478) (Figure 13) (Rostislavleva *et al.*, 2015), and this region has been proposed to be at the membrane binding interface of Vps34 complexes (Ma et al., 2017; Ohashi *et al.*, 2019). Furthermore, the SUR of Vps34 is predicted to be at the outermost surface of Vps34 complexes (Figure 13) (Rostislavleva *et al.*, 2015), making it accessible to other autophagy modulators. Therefore, it is assumable that phosphorylation of this region of Vps34 might affect the membrane association of Vps34 complex I and/or the physical interaction between the complex and other Atg proteins, thereby influencing protein dynamics at the PAS. Notably, the regions in human VPS34

(from S422 to E469) (Tremel *et al.*, 2021) and in *Drosophila* VPS34 (P422 to A531) (Miller *et al.*, 2010) corresponding to the SUR in yeast Vps34 are also structurally uncharacterized and similarly enriched in serine residues. Given that the SUR in yeast Vps34 is indeed phosphorylated, there is a possibility that Vps34 in other higher eukaryotes may also be similarly regulated by phosphorylation in this region. Moreover, the corresponding SUR of human VPS34 contains three serine residues (S448, S452, and S454) homologous to S460, S463, and S465, respectively, in yeast Vps34 (Rostislavleva *et al.*, 2015). It would be interesting to investigate whether the human VPS34 complex I also undergoes phosphoregulation similar to that of yeast Vps34.

REFERENCES

Abeliovich, H., Zhang, C., Dunn, W.A., Jr., Shokat, K.M., and Klionsky, D.J. (2003). Chemical genetic analysis of Apg1 reveals a non-kinase role in the induction of autophagy. Mol Biol Cell *14*, 477-490. 10.1091/mbc.e02-07-0413.

Araki, Y., Ku, W.C., Akioka, M., May, A.I., Hayashi, Y., Arisaka, F., Ishihama, Y., and Ohsumi, Y. (2013). Atg38 is required for autophagy-specific phosphatidylinositol 3-kinase complex integrity. J Cell Biol *203*, 299-313. 10.1083/jcb.201304123.

Ariosa, A.R., and Klionsky, D.J. (2016). Autophagy core machinery: overcoming spatial barriers in neurons. J Mol Med (Berl) *94*, 1217-1227. 10.1007/s00109-016-1461-9.

Backues, S.K., Lynch-Day, M.A., and Klionsky, D.J. (2012). The Ume6-Sin3-Rpd3 complex regulates ATG8 transcription to control autophagosome size. Autophagy *8*, 1835-1836. 10.4161/auto.21845.

Cebollero, E., van der Vaart, A., Zhao, M., Rieter, E., Klionsky, D.J., Helms, J.B., and Reggiori, F. (2012). Phosphatidylinositol-3-phosphate clearance plays a key role in autophagosome completion. Curr Biol *22*, 1545-1553. 10.1016/j.cub.2012.06.029.

Cheong, H., Nair, U., Geng, J.F., and Klionsky, D.J. (2008). The Atg1 kinase complex is involved in the regulation of protein recruitment to initiate sequestering vesicle formation for nonspecific autophagy in Saccharomyces cerevisiae. Mol Biol Cell *19*, 668-681. 10.1091/mbc.E07-08-0826.

Deng, Z., Dong, Y., Zhou, X., Lu, J.H., and Yue, Z. (2022). Pharmacological modulation of autophagy for Alzheimer's disease therapy: Opportunities and obstacles. Acta Pharm Sin B *12*, 1688-1706. 10.1016/j.apsb.2021.12.009.

Dou, C., Zhang, Y., Zhang, L., and Qin, C. (2022). Autophagy and autophagy-related molecules in neurodegenerative diseases. Animal Model Exp Med. 10.1002/ame2.12229.

Dove, S.K., Dong, K., Kobayashi, T., Williams, F.K., and Michell, R.H. (2009). Phosphatidylinositol 3,5-bisphosphate and Fab1p/PIKfyve underPPIn endo-lysosome function. Biochem J *419*, 1-13. 10.1042/BJ20081950.

Egan, D.F., Chun, M.G., Vamos, M., Zou, H., Rong, J., Miller, C.J., Lou, H.J., Raveendra-Panickar, D., Yang, C.C., Sheffler, D.J., et al. (2015). Small Molecule Inhibition of the Autophagy Kinase ULK1 and Identification of ULK1 Substrates. Mol Cell *59*, 285-297. 10.1016/j.molcel.2015.05.031.

Eisenberg-Lerner, A., and Kimchi, A. (2012). PKD is a kinase of Vps34 that mediates ROS-induced autophagy downstream of DAPk. Cell Death and Differentiation *19*, 788-797. 10.1038/cdd.2011.149.

Farre, J.C., and Subramani, S. (2016). Mechanistic insights into selective autophagy pathways: lessons from yeast. Nat Rev Mol Cell Bio *17*, 537-552.

10.1038/nrm.2016.74.
Feng, Y., He, D., Yao, Z., and Klionsky, D.J. (2014). The machinery of macroautophagy. Cell Res *24*, 24-41. 10.1038/cr.2013.168.
Fujioka, Y., Noda, N.N., Nakatogawa, H., Ohsumi, Y., and Inagaki, F. (2010). Dimeric coiled-coil structure of Saccharomyces cerevisiae Atg16 and its functional significance in autophagy. J Biol Chem *285*, 1508-1515. 10.1074/jbc.M109.053520.
Fujioka, Y., Suzuki, S.W., Yamamoto, H., Kondo-Kakuta, C., Kimura, Y., Hirano, H., Akada, R., Inagaki, F., Ohsumi, Y., and Noda, N.N. (2014). Structural basis of starvation-induced assembly of the autophagy initiation complex. Nat Struct Mol Biol *21*, 513-521. 10.1038/nsmb.2822.
Furuya, T., Kim, M., Lipinski, M., Li, J., Kim, D., Lu, T., Shen, Y., Rameh, L., Yankner, B., Tsai, L.H., and Yuan, J. (2010). Negative regulation of Vps34 by Cdk mediated phosphorylation. Mol Cell *38*, 500-511. 10.1016/j.molcel.2010.05.009.
Gnugge, R., Liphardt, T., and Rudolf, F. (2016). A shuttle vector series for precise genetic engineering of Saccharomyces cerevisiae. Yeast *33*, 83-98. 10.1002/yea.3144.
Gomez-Sanchez, R., Rose, J., Guimaraes, R., Mari, M., Papinski, D., Rieter, E., Geerts, W.J., Hardenberg, R., Kraft, C., Ungermann, C., and Reggiori, F. (2018). Atg9 establishes Atg2-dependent contact sites between the endoplasmic reticulum and phagophores. Journal of Cell Biology *217*, 2743-2763. 10.1083/jcb.201710116.
Hanada, T., Noda, N.N., Satomi, Y., Ichimura, Y., Fujioka, Y., Takao, T., Inagaki, F., and Ohsumi, Y. (2007). The Atg12-Atg5 conjugate has a novel E3-like activity for protein lipidation in autophagy. J Biol Chem *282*, 37298-37302. 10.1074/jbc.C700195200.
Harada, K., Kotani, T., Kirisako, H., Sakoh-Nakatogawa, M., Oikawa, Y., Kimura, Y., Hirano, H., Yamamoto, H., Ohsumi, Y., and Nakatogawa, H. (2019). Two distinct mechanisms target the autophagy-related E3 complex to the pre-autophagosomal structure. Elife *8*. 10.7554/eLife.43088.
Hu, Z., Raucci, S., Jaquenoud, M., Hatakeyama, R., Stumpe, M., Rohr, R., Reggiori, F., De Virgilio, C., and Dengjel, J. (2019). Multilayered Control of Protein Turnover by TORC1 and Atg1. Cell Rep *28*, 3486-3496 e3486. 10.1016/j.celrep.2019.08.069.
Ichimiya, T., Yamakawa, T., Hirano, T., Yokoyama, Y., Hayashi, Y., Hirayama, D., Wagatsuma, K., Itoi, T., and Nakase, H. (2020). Autophagy and Autophagy-Related Diseases: A Review. Int J Mol Sci *21*. 10.3390/ijms21238974.
Jao, C.C., Ragusa, M.J., Stanley, R.E., and Hurley, J.H. (2013). A HORMA domain in Atg13 mediates PI 3-kinase recruitment in autophagy. Proc Natl Acad Sci U S A *110*, 5486-5491. 10.1073/pnas.1220306110.
Jeong, J.Y., Yim, H.S., Ryu, J.Y., Lee, H.S., Lee, J.H., Seen, D.S., and Kang, S.G. (2012). One-step sequence- and ligation-independent cloning as a rapid and versatile cloning method for functional genomics studies. Appl Environ Microbiol *78*, 5440-5443. 10.1128/AEM.00844-12.

Jung, P.P., Christian, N., Kay, D.P., Skupin, A., and Linster, C.L. (2015). Protocols and programs for high-throughput growth and aging phenotyping in yeast. PLoS One *10*, e0119807. 10.1371/journal.pone.0119807.
Kamada, Y., Yoshino, K., Kondo, C., Kawamata, T., Oshiro, N., Yonezawa, K., and Ohsumi, Y. (2010). Tor directly controls the Atg1 kinase complex to regulate autophagy. Mol Cell Biol *30*, 1049-1058. 10.1128/MCB.01344-09.
Kanki, T., Kang, D., and Klionsky, D.J. (2009). Monitoring mitophagy in yeast: the Om45-GFP processing assay. Autophagy *5*, 1186-1189. 10.4161/auto.5.8.9854.
Kihara, A., Noda, T., Ishihara, N., and Ohsumi, Y. (2001). Two distinct Vps34 phosphatidylinositol 3-kinase complexes function in autophagy and carboxypeptidase Y sorting in Saccharomyces cerevisiae. J Cell Biol *152*, 519-530. 10.1083/jcb.152.3.519.
Kim, B., Lee, Y., Choi, H., and Huh, W.K. (2021). The trehalose-6-phosphate phosphatase Tps2 regulates ATG8 transcription and autophagy in Saccharomyces cerevisiae. Autophagy *17*, 1013-1027. 10.1080/15548627.2020.1746592.
Kim, J., Kim, Y.C., Fang, C., Russell, R.C., Kim, J.H., Fan, W., Liu, R., Zhong, Q., and Guan, K.L. (2013). Differential regulation of distinct Vps34 complexes by AMPK in nutrient stress and autophagy. Cell *152*, 290-303. 10.1016/j.cell.2012.12.016.
Kinoshita, E., Kinoshita-Kikuta, E., Takiyama, K., and Koike, T. (2006). Phosphate-binding tag, a new tool to visualize phosphorylated proteins. Mol Cell Proteomics *5*, 749-757. 10.1074/mcp.T500024-MCP200.
Kira, S., Noguchi, M., Araki, Y., Oikawa, Y., Yoshimori, T., Miyahara, A., and Noda, T. (2021). Vacuolar protein Tag1 and Atg1-Atg13 regulate autophagy termination during persistent starvation in S. cerevisiae. J Cell Sci *134*. 10.1242/jcs.253682.
Kotani, T., Kirisako, H., Koizumi, M., Ohsumi, Y., and Nakatogawa, H. (2018). The Atg2-Atg18 complex tethers pre-autophagosomal membranes to the endoplasmic reticulum for autophagosome formation. Proc Natl Acad Sci U S A *115*, 10363-10368. 10.1073/pnas.1806727115.
Ktistakis, N.T., and Tooze, S.A. (2016). Digesting the Expanding Mechanisms of Autophagy. Trends Cell Biol *26*, 624-635. 10.1016/j.tcb.2016.03.006.
Lanz, M.C., Yugandhar, K., Gupta, S., Sanford, E.J., Faca, V.M., Vega, S., Joiner, A.M.N., Fromme, J.C., Yu, H.Y., and Smolka, M.B. (2021). In-depth and 3-dimensional exploration of the budding yeast phosphoproteome. Embo Rep *22*. ARTN e51121

10.15252/embr.202051121.
Lee, C.R., Park, Y.H., Min, H., Kim, Y.R., and Seok, Y.J. (2019). Determination of protein phosphorylation by polyacrylamide gel electrophoresis. J Microbiol *57*, 93-100. 10.1007/s12275-019-9021-y.
Licheva, M., Raman, B., Kraft, C., and Reggiori, F. (2022). Phosphoregulation of the autophagy machinery by kinases and phosphatases. Autophagy *18*, 104-123.

10.1080/15548627.2021.1909407.
Ma, M., Liu, J.J., Li, Y., Huang, Y., Ta, N., Chen, Y., Fu, H., Ye, M.D., Ding, Y., Huang, W., et al. (2017). Cryo-EM structure and biochemical analysis reveal the basis of the functional difference between human PI3KC3-C1 and -C2. Cell Res *27*, 989-1001. 10.1038/cr.2017.94.
Mari, M., Griffith, J., Rieter, E., Krishnappa, L., Klionsky, D.J., and Reggiori, F. (2010). An Atg9-containing compartment that functions in the early steps of autophagosome biogenesis. Journal of Cell Biology *190*, 1005-1022. 10.1083/jcb.200912089.
Matoba, K., Kotani, T., Tsutsumi, A., Tsuji, T., Mori, T., Noshiro, D., Sugita, Y., Nomura, N., Iwata, S., Ohsumi, Y., et al. (2020). Atg9 is a lipid scramblase that mediates autophagosomal membrane expansion (October, 10.1038/s41594-020-00518-w, 2020). Nat Struct Mol Biol *27*, 1210-1210. 10.1038/s41594-020-00538-6.
Matsuura, A., Tsukada, M., Wada, Y., and Ohsumi, Y. (1997). Apg1p, a novel protein kinase required for the autophagic process in Saccharomyces cerevisiae. Gene *192*, 245-250. 10.1016/s0378-1119(97)00084-x.
Medeiros, T.C., Thomas, R.L., Ghillebert, R., and Graef, M. (2018). Autophagy balances mtDNA synthesis and degradation by DNA polymerase POLG during starvation. J Cell Biol *217*, 1601-1611. 10.1083/jcb.201801168.
Miller, S., Tavshanjian, B., Oleksy, A., Perisic, O., Houseman, B.T., Shokat, K.M., and Williams, R.L. (2010). Shaping development of autophagy inhibitors with the structure of the lipid kinase Vps34. Science *327*, 1638-1642. 10.1126/science.1184429.
Mizushima, N., Yoshimori, T., and Ohsumi, Y. (2011). The role of Atg proteins in autophagosome formation. Annu Rev Cell Dev Biol *27*, 107-132. 10.1146/annurev-cellbio-092910-154005.
Motley, A.M., Nuttall, J.M., and Hettema, E.H. (2012). Pex3-anchored Atg36 tags peroxisomes for degradation in Saccharomyces cerevisiae. EMBO J *31*, 2852-2868. 10.1038/emboj.2012.151.
Nair, U., Thumm, M., Klionsky, D.J., and Krick, R. (2011). GFP-Atg8 protease protection as a tool to monitor autophagosome biogenesis. Autophagy *7*, 1546-1550. 10.4161/auto.7.12.18424.
Nakatogawa, H. (2013). Two ubiquitin-like conjugation systems that mediate membrane formation during autophagy. Essays Biochem *55*, 39-50. 10.1042/Bse0550039.
Nakatogawa, H., Suzuki, K., Kamada, Y., and Ohsumi, Y. (2009). Dynamics and diversity in autophagy mechanisms: lessons from yeast. Nat Rev Mol Cell Biol *10*, 458-467. 10.1038/nrm2708.
Nishimura, T., and Tooze, S.A. (2020). Emerging roles of ATG proteins and membrane lipids in autophagosome formation. Cell Discov *6*, 32. 10.1038/s41421-020-0161-3.

Noda, N.N. (2021). Atg2 and Atg9: Intermembrane and interleaflet lipid transporters driving autophagy. Biochim Biophys Acta Mol Cell Biol Lipids *1866*, 158956. 10.1016/j.bbalip.2021.158956.
Noda, N.N., and Fujioka, Y. (2015). Atg1 family kinases in autophagy initiation. Cell Mol Life Sci *72*, 3083-3096. 10.1007/s00018-015-1917-z.
Noda, N.N., Kobayashi, T., Adachi, W., Fujioka, Y., Ohsumi, Y., and Inagaki, F. (2012). Structure of the novel C-terminal domain of vacuolar protein sorting 30/autophagy-related protein 6 and its specific role in autophagy. J Biol Chem *287*, 16256-16266. 10.1074/jbc.M112.348250.
Noda, T. (2008). Viability assays to monitor yeast autophagy. Methods Enzymol *451*, 27-32. 10.1016/S0076-6879(08)03202-3.
Noda, T., and Klionsky, D.J. (2008). The quantitative Pho8Delta60 assay of nonspecific autophagy. Methods Enzymol *451*, 33-42. 10.1016/S0076-6879(08)03203-5.
Obara, K., Sekito, T., Niimi, K., and Ohsumi, Y. (2008). The Atg18-Atg2 complex is recruited to autophagic membranes via phosphatidylinositol 3-phosphate and exerts an essential function. J Biol Chem *283*, 23972-23980. 10.1074/jbc.M803180200.
Obara, K., Sekito, T., and Ohsumi, Y. (2006). Assortment of phosphatidylinositol 3-kinase complexes--Atg14p directs association of complex I to the pre-autophagosomal structure in Saccharomyces cerevisiae. Mol Biol Cell *17*, 1527-1539. 10.1091/mbc.e05-09-0841.
Ohashi, Y., Soler, N., Garcia Ortegon, M., Zhang, L., Kirsten, M.L., Perisic, O., Masson, G.R., Burke, J.E., Jakobi, A.J., Apostolakis, A.A., et al. (2016). Characterization of Atg38 and NRBF2, a fifth subunit of the autophagic Vps34/PIK3C3 complex. Autophagy *12*, 2129-2144. 10.1080/15548627.2016.1226736.
Ohashi, Y., Tremel, S., and Williams, R.L. (2019). VPS34 complexes from a structural perspective. J Lipid Res *60*, 229-241. 10.1194/jlr.R089490.
Osawa, T., Kotani, T., Kawaoka, T., Hirata, E., Suzuki, K., Nakatogawa, H., Ohsumi, Y., and Noda, N.N. (2019). Atg2 mediates direct lipid transfer between membranes for autophagosome formation. Nat Struct Mol Biol *26*, 281-+. 10.1038/s41594-019-0203-4.
Papinski, D., and Kraft, C. (2014). Atg1 kinase organizes autophagosome formation by phosphorylating Atg9. Autophagy *10*, 1338-1340. 10.4161/auto.28971.
Papinski, D., Schuschnig, M., Reiter, W., Wilhelm, L., Barnes, C.A., Maiolica, A., Hansmann, I., Pfaffenwimmer, T., Kijanska, M., Stoffel, I., et al. (2014). Early steps in autophagy depend on direct phosphorylation of Atg9 by the Atg1 kinase. Mol Cell *53*, 471-483. 10.1016/j.molcel.2013.12.011.
Park, J.M., Jung, C.H., Seo, M., Otto, N.M., Grunwald, D., Kim, K.H., Moriarity, B., Kim, Y.M., Starker, C., Nho, R.S., et al. (2016). The ULK1 complex mediates MTORC1 signaling to the autophagy initiation machinery via binding and

phosphorylating ATG14. Autophagy *12*, 547-564. 10.1080/15548627.2016.1140293.
Park, J.M., Seo, M., Jung, C.H., Grunwald, D., Stone, M., Otto, N.M., Toso, E., Ahn, Y., Kyba, M., Griffin, T.J., et al. (2018). ULK1 phosphorylates Ser30 of BECN1 in association with ATG14 to stimulate autophagy induction. Autophagy *14*, 584-597. 10.1080/15548627.2017.1422851.
Pfaffenwimmer, T., Reiter, W., Brach, T., Nogellova, V., Papinski, D., Schuschnig, M., Abert, C., Ammerer, G., Martens, S., and Kraft, C. (2014). Hrr25 kinase promotes selective autophagy by phosphorylating the cargo receptor Atg19. Embo Rep *15*, 862-870. 10.15252/embr.201438932.
Reggiori, F., and Klionsky, D.J. (2013). Autophagic processes in yeast: mechanism, machinery and regulation. Genetics *194*, 341-361. 10.1534/genetics.112.149013.
Reidick, C., Boutouja, F., and Platta, H.W. (2017). The class III phosphatidylinositol 3-kinase Vps34 in Saccharomyces cerevisiae. Biol Chem *398*, 677-685. 10.1515/hsz-2016-0288.
Rostislavleva, K., Soler, N., Ohashi, Y., Zhang, L., Pardon, E., Burke, J.E., Masson, G.R., Johnson, C., Steyaert, J., Ktistakis, N.T., and Williams, R.L. (2015). Structure and flexibility of the endosomal Vps34 complex reveals the basis of its function on membranes. Science *350*, aac7365. 10.1126/science.aac7365.
Rubinsztein, D.C., Shpilka, T., and Elazar, Z. (2012). Mechanisms of autophagosome biogenesis. Curr Biol *22*, R29-34. 10.1016/j.cub.2011.11.034.
Ruocco, N., Costantini, S., and Costantini, M. (2016). Blue-Print Autophagy: Potential for Cancer Treatment. Mar Drugs *14*. 10.3390/md14070138.
Russell, R.C., Tian, Y., Yuan, H., Park, H.W., Chang, Y.Y., Kim, J., Kim, H., Neufeld, T.P., Dillin, A., and Guan, K.L. (2013). ULK1 induces autophagy by phosphorylating Beclin-1 and activating VPS34 lipid kinase. Nat Cell Biol *15*, 741-750. 10.1038/ncb2757.
Sanchez-Wandelmer, J., Kriegenburg, F., Rohringer, S., Schuschnig, M., Gomez-Sanchez, R., Zens, B., Abreu, S., Hardenberg, R., Hollenstein, D., Gao, J.Q., et al. (2017). Atg4 proteolytic activity can be inhibited by Atg1 phosphorylation. Nature Commun *8*. ARTN 295

10.1038/s41467-017-00302-3.
Schreiber, A., Collins, B.C., Davis, C., Enchev, R.I., Sedra, A., D'Antuono, R., Aebersold, R., and Peter, M. (2021). Multilayered regulation of autophagy by the Atg1 kinase orchestrates spatial and temporal control of autophagosome formation. Mol Cell *81*, 5066-5081 e5010. 10.1016/j.molcel.2021.10.024.
Sherman, F. (2002). Getting started with yeast. Methods Enzymol *350*, 3-41.
Shin, C.S., and Huh, W.K. (2011). Bidirectional regulation between TORC1 and autophagy in Saccharomyces cerevisiae. Autophagy *7*, 854-862.
Stack, J.H., and Emr, S.D. (1994). Vps34p Required for Yeast Vacuolar Protein Sorting Is a Multiple Specificity Kinase That Exhibits Both Protein-Kinase and Phosphatidylinositol-Specific Pi-3-Kinase Activities. J Biol Chem *269*, 31552-

31562.
Steinfeld, N., Lahiri, V., Morrison, A., Metur, S.P., Klionsky, D.J., and Weisman, L.S. (2021). Elevating PI3P drives select downstream membrane trafficking pathways. Mol Biol Cell *32*, 143-156. 10.1091/mbc.E20-03-0191.
Stjepanovic, G., Davies, C.W., Stanley, R.E., Ragusa, M.J., Kim, D.J., and Hurley, J.H. (2014). Assembly and dynamics of the autophagy-initiating Atg1 complex. Proc Natl Acad Sci U S A *111*, 12793-12798. 10.1073/pnas.1407214111.
Suzuki, H., Osawa, T., Fujioka, Y., and Noda, N.N. (2017). Structural biology of the core autophagy machinery. Curr Opin Struct Biol *43*, 10-17. 10.1016/j.sbi.2016.09.010.
Suzuki, K., Akioka, M., Kondo-Kakuta, C., Yamamoto, H., and Ohsumi, Y. (2013). Fine mapping of autophagy-related proteins during autophagosome formation in Saccharomyces cerevisiae. J Cell Sci *126*, 2534-2544. 10.1242/jcs.122960.
Suzuki, K., Kubota, Y., Sekito, T., and Ohsumi, Y. (2007). Hierarchy of Atg proteins in pre-autophagosomal structure organization. Genes Cells *12*, 209-218. 10.1111/j.1365-2443.2007.01050.x.
Suzuki, S.W., Yamamoto, H., Oikawa, Y., Kondo-Kakuta, C., Kimura, Y., Hirano, H., and Ohsumi, Y. (2015). Atg13 HORMA domain recruits Atg9 vesicles during autophagosome formation. Proc Natl Acad Sci U S A *112*, 3350-3355. 10.1073/pnas.1421092112.
Tremel, S., Ohashi, Y., Morado, D.R., Bertram, J., Perisic, O., Brandt, L.T.L., von Wrisberg, M.K., Chen, Z.A., Maslen, S.L., Kovtun, O., et al. (2021). Structural basis for VPS34 kinase activation by Rab1 and Rab5 on membranes. Nat Commun *12*, 1564. 10.1038/s41467-021-21695-2.
Tsukada, M., and Ohsumi, Y. (1993). Isolation and characterization of autophagy-defective mutants of Saccharomyces cerevisiae. FEBS Lett *333*, 169-174. 10.1016/0014-5793(93)80398-e.
Wach, A. (1996). PCR-synthesis of marker cassettes with long flanking homology regions for gene disruptions in S. cerevisiae. Yeast *12*, 259-265. 10.1002/(SICI)1097-0061(19960315)12:3%3C259::AID-YEA901%3E3.0.CO;2-C.
Xie, Z., Nair, U., and Klionsky, D.J. (2008). Atg8 controls phagophore expansion during autophagosome formation. Mol Biol Cell *19*, 3290-3298. 10.1091/mbc.E07-12-1292.
Yamamoto, H., Fujioka, Y., Suzuki, S.W., Noshiro, D., Suzuki, H., Kondo-Kakuta, C., Kimura, Y., Hirano, H., Ando, T., Noda, N.N., and Ohsumi, Y. (2016). The Intrinsically Disordered Protein Atg13 Mediates Supramolecular Assembly of Autophagy Initiation Complexes. Dev Cell *38*, 86-99. 10.1016/j.devcel.2016.06.015.
Yamamoto, H., Kakuta, S., Watanabe, T.M., Kitamura, A., Sekito, T., Kondo-Kakuta, C., Ichikawa, R., Kinjo, M., and Ohsumi, Y. (2012). Atg9 vesicles are an important membrane source during early steps of autophagosome formation. J Cell Biol *198*, 219-233. 10.1083/jcb.201202061.

Yang, Z., and Klionsky, D.J. (2009). An overview of the molecular mechanism of autophagy. Curr Top Microbiol Immunol *335*, 1-32. 10.1007/978-3-642-00302-8_1.
Yeh, Y.Y., Wrasman, K., and Herman, P.K. (2010). Autophosphorylation Within the Atg1 Activation Loop Is Required for Both Kinase Activity and the Induction of Autophagy in Saccharomyces cerevisiae. Genetics *185*, 871-882. 10.1534/genetics.110.116566.
Yu, Z.Q., Ni, T., Hong, B., Wang, H.Y., Jiang, F.J., Zou, S., Chen, Y., Zheng, X.L., Klionsky, D.J., Liang, Y., and Xie, Z. (2012). Dual roles of Atg8-PE deconjugation by Atg4 in autophagy. Autophagy *8*, 883-892. 10.4161/auto.19652.
Yuan, H.X., Russell, R.C., and Guan, K.L. (2013). Regulation of PIK3C3/VPS34 complexes by MTOR in nutrient stress-induced autophagy. Autophagy *9*, 1983-1995. 10.4161/auto.26058.
Zhang, D., Wang, W., Sun, X., Xu, D., Wang, C., Zhang, Q., Wang, H., Luo, W., Chen, Y., Chen, H., and Liu, Z. (2016). AMPK regulates autophagy by phosphorylating BECN1 at threonine 388. Autophagy *12*, 1447-1459. 10.1080/15548627.2016.1185576.

국 문 초 록

효모에서 Vps34의 인산화를 통한 자가포식 활성 조절

자가포식은 진핵 생물 전반에 걸쳐 잘 보존된 세포 내 물질 분해 기전이다. 다양한 외부 스트레스에 대해 세포는 자가포식 작용을 통해 세포 내 여러 고분자 물질 및 비정상적인 세포 소기관 등을 분해함으로써 세포 내 재구성을 위한 영양분을 재생산함과 동시에 세포 독성 물질을 효과적으로 제거할 수 있다. 자가포식 유도 시 Phagophore assembly site (PAS) 에 자가포식 연관 (Atg) 단백질들이 결집하게 되고 이들 단백질 군의 상호 협력적인 작용을 통해 자가포식 소체 (autophagosome) 가 생성된다. Vps34 는 제 3 군 포스파티딜이노시톨 3-인산화 효소 (class III phosphatidylinositol 3-kinase) 로서 Vps34 1 형 복합체 (Vps34 complex I) 는 PAS 에서 autophagosome 형성에 핵심적인 역할을 수행하지만 Vps34 1 형 복합체의 분자적 조절 기전에 대해 알려진 바는 제한적이다. 본 연구에서는 출아 효모 (*Saccharomyces cerevisiae*) 에서 Vps34 1 형 복합체의 인산화를 통한 자가포식 조절 기전을 분석하였다. 자가포식 유도 조건인 질소 결핍 시 Atg1 의존적으로 Vps34 인산화가

일어나고 이 인산화가 자가포식을 활성화 하고 질소 기아 조건에서 세포 생존을 유지하는 데 중요하다는 것을 확인했다. 이러한 Vps34 의 인산화는 1 형 복합체 특이적으로 발생하며 Atg1 인산화 효소 유전자가 결실 될 시 완전히 저해되었다. 시험관 내 인산화 효소 반응 (in vitro kinase assay) 을 통해 Atg1 인산화 효소가 Vps34 복합체 유형에 관계 없이 직접적으로 Vps34 를 인산화 시킬 수 있음을 확인했으며 Vps34 1 형 복합체-특이적인 인산화가 1 형 복합체만이 PAS 로 이동할 수 있기 때문임을 밝혔다. 나아가 Vps34의 인산화가 PAS에서의 Atg18 및 Atg8를 포함한 하위 Atg 단백질들의 역학 조절에 중요하다는 것을 확인했다. Vps34 의 인산화 조절에 관한 본 연구는 현재까지 미비했던 Vps34 1 형 복합체의 인산화 조절에 대한 새로운 분자적 조절 기전을 밝혀내었고 또한 Atg1-의존적인 PAS 역학 조절에 대한 추가적인 지식을 제공함으로써 향후 자가포식 연구에 중요한 과학적 기반으로 활용될 수 있을 것이다.

주요어 : 자가포식, Vps34, Atg1, 질소 기아,
Saccharomyces cerevisiae, Atg8, Atg18

학 번 : 2016-24695